ACKNOWLEDGEMENTS

The author would like to express his gratitude to the following :

Professor T. Mulvey, Department of Physics, University of Aston in Birmingham for his helpful advice and encouragement and for assistance in editing the final draft.

Dr. S.P.S. Andrew and P. Davies, Catalysts and Chemicals Group, Agricultural Division, Imperial Chemical Industries Ltd., for invaluable discussions on the "state of the art", for suggestions as to the course of the research and for provision of samples and surface area determinations.

Dr. S. Murphy, Department of Metallurgy and Materials Science, University of Aston in Birmingham, for help and guidance on electron-optical techniques.

Dr. B.J. Tighe, Department of Chemistry, University of Aston in Birmingham, for discussions on the chemical aspects of automotive pollution control.

Dr. J. Weaving and D.C. Haynes, B L Technology Ltd., for their help and guidance, especially on air pollution in general and engineering aspects of automotive catalysis.

Acknowledgements contd...

J.S. O'Neil, B.L. Technology Ltd., for advice, particularly in the early stages of the project and for suggestions leading to the development of the coating technique.

M.K. Hussey and G.A. Montgomerie, IHD Department, University of Aston in Birmingham for valuable help and encouragement.

K.L. Stephens , Mrs. P. Winfield, M. Vas, Miss A. Sayed and J. May for help with various aspects of the experimental work.

The author would also like to thank the Science Research Council, Advanced Technology, B L Cars Ltd. and the Catalysts and Chemicals Group, Agricultural Division, Imperial Chemical Industries Ltd. for financial support during the project.

A Study in the reduction of efficiency of nitrogen oxide removal catalysts for automobiles

John Raymond Dyhouse

Ph.D. Thesis - 1980

SUMMARY

Automotive catalysts are the most effective short-term answer to air pollution from automobiles. Since strict control of exhaust emissions is, or will be, covered by legislation in most developed countries in the world, catalytic devices will be increasingly fitted to cars. There is consequently an urgent need for the development of catalysts that will not compete for scarce precious metal resources. A number of problems have already been identified in connection with base metal catalysts but quantitative investigations are lacking.

The base metal reduction catalysts developed by Imperial Chemical Industries Limited, Catalysts and Chemicals Group, in collaboration with the Air Pollution Control Laboratory, B L Cars Limited, for automotive emission control, are susceptible to de-activation by three major mechanisms. These are : physical loss of the wash-coat (a high surface area coating which supports the active species), aggregation of the active species and poisoning by fuel and engine oil additives. This thesis is especially concerned with the first two of these and attempts to indicate the relative magnitude of their effect on the activity of the catalysts.

Aggregation of the active species, or sintering, as it is loosely called, was studied by using impregnated granules to overcome effects due to the loss of the wash-coat. Samples were aged in a synthetic exhaust gas, free from poisons, and metal crystallite sizes were measured by scanning-electron microscopy. The increase in particle size was correlated with the loss in catalytic activity.

In order to maintain a link with the real conditions of service, a number of monolithic catalysts were tested in an engine-dynamometer and several previously tested endurance catalysts were examined. A mechanism is proposed for the break-up and subsequent loss of the wash-coat and suggestions for improved resistance to loss of the coating and active species are proposed.

KEY WORDS : AUTOMOTIVE-EMISSIONS ; CATALYSTS ; SCANNING-ELECTRON MICROSCOPY ; SINTERING ; PARTICLE SIZE.

(i) CONTENTS

LIST OF SYMBOLS USED

a	order of reaction, reduction of NO
d	diameter subtended at the base of crystallite
D	crystallite diameter at time t
$\overline{D}$	average crystallite diameter
D_c	coefficient of diffusion for the gas into catalyst pores
E_A	activation energy, crystallite aggregation
E_N	activation energy, reduction of NO
F	flow rate of exhaust gas
G	material loss coefficient
H	gas hourly space velocity
k_1	rate constant, particle aggregation
k_2	reaction rate constant, reduction of NO
L	fractional loss of wash-coat and active species
M	concentration of active species in catalyst wash-coat
n	order of reaction, particle aggregation
P	partial pressure of NO
r	rate of reaction, reduction of NO
R	gas constant
s	specific surface area
t	time
T	absolute temperature
V	volume of catalyst bed
W	wash-coat loading, i.e. the weight fraction of wash-coat on matrix catalysts
x	fractional conversion of NO
X_{net}	fractional conversion of NO to nitrogen
X_o	initial concentration of NO in the exhaust gas
y	thickness of the wash-coat at the centre of the cell walls

GREEK LETTERS

γ	(gamma)	surface tension
θ	(theta)	contact angle
ρ	(rho)	density
η	(eta)	catalyst effectiveness factor

LIST OF TABLES

List of tables contd....

List of tables contd....

LIST OF FIGURES

List of Figures contd....

List of Figures contd....

List of Figures contd....

List of Figures contd....

List of Figures contd....

List of Figures contd....

1. A SURVEY OF AUTOMOTIVE AIR POLLUTION

1.1. Air Pollution and the Automobile

In the United Kingdom, air pollution caused by a combination of fog and smoke from coal fires has been a familiar part of life for town dwellers for centuries, but in the supposedly more healthy, sunlit American west coast, the severe air pollution suffered is of a different nature[1]. In the United Kingdom, sulphur dioxide from domestic and industrial coal fires gave rise to a "smog" which was of a reducing nature, but in Los Angeles, the smog was shown to be oxidising due to a high ozone content. This is caused by reactions between nitrogen oxides and hydrocarbons in the presence of sunlight. A related problem is the very high concentrations of carbon monoxide found in cities with large automobile populations. It has been shown[2] that in urban areas the concentrations of carbon monoxide, hydrocarbons and nitric oxide in the atmosphere followed a pattern which closely reflected the cycle of peak-period traffic build-up, and that ozone and other oxidants approached maximum concentrations several hours later. Natural processes account for greater than 50% of all atmospheric pollutants, more than all man-made sources put together, but they do not contribute significantly to air pollution because of their dispersion[3]. It is the concentration of man-made sources in heavily industrialised areas that leads to the problem of air pollution ; this is often aggravated by geographical and meteorological conditions which prevent the dispersion of these pollutants[4]. Automobiles account for more than 50% of all man-made emissions of carbon monoxide, hydrocarbons and nitric oxide, and also for smaller

amounts of lead, sulphur oxides and particulate matter[2], so the control of automotive emissions is a significant step towards combating air pollution.

This thesis is especially concerned with the control of nitric oxides from internal combustion engines and so attention will be concentrated on the behaviour of this particular pollutant, its effects on the environment, and how it may be controlled. A promising method of control is to fit a suitable catalyst at source. In the following pages, the characteristics of such catalysts are investigated in some detail. In practice, catalysts have a limited life, the reasons for which are not yet clearly understood. It is the object of the present investigation to devise analytical techniques for the micro-examination of catalysts with a view to accounting for their performance in vehicles.

1.2. The Formation of Nitrogen Oxides

Nitrogen oxides are formed within the combustion zone at a rate dependent on the reaction temperature ; once formed, their concentration is not significantly changed during the expansion and exhaust strokes of the engine. The simple molecular reaction between oxygen and nitrogen described by :

$$N_2 + O_2 \rightarrow 2NO \quad \ldots\ldots\ldots\ldots 1.1$$

is acknowledged to be too slow at the temperature and pressures encountered in the normal working of the internal combustion engine, to account for the concentrations of nitric oxides in the exhaust[5]. According to Zeldovich[6] this mechanism for the formation of nitric oxide is initiated by the dissociation of oxygen molecules during combustion when the temperature is above 1000°C ; this results

in the further reactions :

$$O_2 \rightarrow 2O \quad \ldots\ldots\ldots 1.2$$

$$N_2 + O \rightarrow NO + N \quad \ldots\ldots\ldots 1.3$$

$$N + O_2 \rightarrow NO + O \quad \ldots\ldots\ldots 1.4$$

It can be seen that this mechanism suggests a chain reaction in which the presence of atomic oxygen causes the concentration of nitric oxide to increase rapidly. The oxygen atoms are assumed to initiate the process because of their relatively high equilibrium concentration compared to that of nitrogen atoms during combustion under these conditions. The equilibrium concentrations of atomic oxygen and nitric oxide increase with temperature and air-fuel ratio up to the stoichiometric value (=14.7). Further increase in the air-fuel ratio results in a lowering of the temperature of combustion ; nevertheless, sufficient oxygen is present to ensure that at an air-fuel ratio of 16, the rate of formation of nitric oxides is at a maximum[7].

Fennimore[8] studied nitric oxide formation in flames of different fuels such as carbon monoxide, hydrogen and various hydrocarbons. He concluded that the rate-determining step was the reaction of carbon or hydrocarbon radicals on nitrogen molecules. This contradicts the Zeldovich mechanism which has been supported by experimental work carried out by others including Schuck and Stephens[6]. Newhall and Shahed[9] directly measured the rate of formation of nitric oxide at the flame-front of a hydrocarbon-air mixture in a high-pressure combustion vessel, and found good agreement at several different air-fuel ratios with values calculated with the Zeldovich mechanism.

An extension to the Zeldovich mechanism proposed by Lavoie, Heywood and Keck[10] incorporated several other reactants :

$$N + OH \rightarrow NO + H \quad \ldots\ldots\ldots\ldots\ldots 1.5$$

$$H + N_2O \rightarrow N_2 + OH \quad \ldots\ldots\ldots\ldots\ldots 1.6$$

$$O + N_2O \rightarrow N_2 + O_2 \quad \ldots\ldots\ldots\ldots\ldots 1.7$$

$$O + N_2O \rightarrow 2NO \quad \ldots\ldots\ldots\ldots\ldots 1.8$$

This scheme was used to calculate the concentrations of nitric oxide in internal combustion engines and it was found that under equilibrium conditions, much of the nitric oxide formed is converted back to its elements as the gas is cooled. However, in practice, the gas is cooled rapidly as the thermal energy is converted into useful work and the concentration of nitric oxide remains very close to its maximum under the given conditions. This was shown experimentally by Newhall and Starkman[11] who showed that no decomposition of the nitric oxide formed at the maximum cycle temperature occurred during the expansion stroke. Obert[12] compared the measured concentration of nitric oxide in the exhaust with the initial and final states of expansion equilibrium and found that the observed values were similar to those calculated for the start of the expansion stroke, thereby confirming that negligible decomposition of nitric oxide occurs during expansion and exhaust.

1.3. Formation of Photochemical "Smog"

The most serious environmental aspect of nitrogen oxide atmospheric pollution is its role in the formation of photochemical "smog", identified in the early 1950's by Haagen-Smit[1] as a complex

photochemical reaction. The formation of "smog" is initiated by the dissociation of nitrogen dioxide which is present in very small concentrations in automobile exhaust gases, the proportion of nitric oxide to nitrogen dioxide being typically 10 to 1. The nitric oxide is oxidised by ozone, which is formed in the upper atmosphere and diffuses down, according to the reaction :

$$NO + O_3 \rightarrow NO_2 + O_2 \quad \ldots\ldots\ldots 1.9$$

rather than by reaction with oxygen[3] according to the reaction :

$$2NO + O_2 \rightarrow 2NO_2 \quad \ldots\ldots\ldots 1.10$$

This reaction occurs very slowly, for example, the rate of oxidation in burnt gases (1000 ppm NO and 5% O_2) is only 0.8 ppm.s^{-1} and is proportional to the square of the concentrations. Even in urban areas the level of nitrogen oxide may be only 0.1 ppm so that the rate of oxidation by the mechanism of equation 1.10 would be negligible. Nitrogen dioxide absorbs solar radiation of between 0.38 and 0.6 μm which causes molecular dissociation described by the overall reaction:

$$NO_2 + \text{Energy} \rightarrow NO + O \quad \ldots\ldots\ldots 1.11$$

This reaction is relatively fast in full sunlight. Because of the relatively high oxygen concentration in the atmosphere, the atomic oxygen rapidly reacts with molecular oxygen and any molecule able to carry off excess energy according to the reaction :

$$O + O_2 + M_e \rightarrow O_3 + M_e \quad \ldots\ldots\ldots 1.12$$

resulting in the formation of ozone. This ozone may then react with unreacted nitric oxide and thus a closed cycle is set up which would be expected to proceed until equilibrium occurs. However, calculations for the expected concentrations of ozone did not account for the

large concentrations measured in the photochemical "smogs" of Los Angeles. For example, with an initial nitrogen dioxide concentration of 0.1 ppm the predicted ozone concentration was 0.3 ppm, but in fact, the observed ambient concentration was an order of magnitude higher[14].

These observations can be explained by the participation in the reactions of organic molecules which compete for the atomic oxygen and ozone. The resulting oxidised hydrocarbons react with nitric oxide and nitrogen dioxide to form nitrates including peroxyalkyl nitrates (PAN) which eventually remove both the hydrocarbons and the nitrogen oxides from the closed loop[15]. The overall result is a build-up of ozone, nitrogen dioxide and other oxidants such as PAN at the expense of the nitric oxide and hydrocarbons. This type of "smog" is, therefore, strongly oxidising and the PAN group is thought to be responsible for many of the adverse effects[16] such as plant damage, material damage, colouration of the atmosphere, eye irritation, odour and toxic effects as reviewed by several investigators[17][18].

Caplan[16], Romanovsky[20], and Agnew[21] showed independently by "smog"-chamber experiments that by reducing the level of nitric oxide at relatively low hydrocarbon levels, the yield of ozone initially increases, thereby intensifying "smog" effects. Despite this, most authorities feel that the control of nitric oxide from vehicle exhausts is necessary in order to combat the problem of photochemical "smog".

1.4. Methods of Control

In the United States, the Clean Air Amendments Act of 1970[22] gave a great impetus to research into the control of automobile emissions, although the first steps at cleaning up exhaust systems had been taken in 1949 when Houdry[23] developed mufflers for fork-lift trucks used in confined spaces such as mines and warehouses. In 1959, California enacted laws on air quality and automotive emission standards and during the 1960's the automotive, petroleum and chemical industries together with the federal government set up an inter-industry commission to monitor research into emission control. This research led to engine modifications such as "lean" carburation, secondary air injection and the control of evaporative hydrocarbon losses. By 1970, total hydrocarbon losses from new cars had been lowered to 15% of the amount reported for 1960 figures, with a similar reduction in carbon monoxide emissions.

The Clean Air Amendments Act[22] called for a further reduction of hydrocarbons and carbon monoxide to 10% of the 1970 value by 1975, and nitric oxide removal was also included in this legislation. Initially, nitric oxide was required to be reduced to the level of an uncontrolled pre-1960 car, since measures taken after this date to reduce carbon monoxide and hydrocarbons had increased nitric oxide emissions ; a further decrease to 10% of this value to a level of 0.25 $g.km^{-1}$ (0.41g.$mile^{-1}$) was required by 1976. However, due to lack of a suitable technology and to an increased awareness of the need for conservation of fossil fuel stocks, the introduction of the more stringent requirements has been repeatedly delayed until after

1985, as seen in Table 1.1[24]. California imposes its own regulations which still propose that by 1985 NOx should be less than 0.25 g.km^{-1} (0.41 g.mile^{-1}).

Table 1.1. : US Federal Emissions Control Requirements (for light duty vehicles)

Year	Emissions g.mile^{-1} (g.km^{-1} in brackets)		
	Hydro-carbons	Carbon monoxide	Nitrogen oxide
1978	1.5 (.93)	15 (9.3)	2.0 (1.2)
1979	1.5 (.93)	15 (9.3)	2.0 (1.2)
1980	0.41 (.25)	7 (4.3)	2.0 (1.2)
1981/82	0.41 (.25)	3.4 (2.1)	1.0 (0.6)
1983/85	0.41 (.25)	3.4 (2.1)	1.0 (0.6)

The regulations of the Economic Commission for Europe (ECE), Table 1.2 are less severe than the American requirements, especially for heavy vehicles, since they make allowance for the weight, and hence the engine size of the car[25].

Table 1.2. : European Emission Regulations (ECE15) for a Vehicle with a Kerb Weight of 1130 kg.

Year	Emissions g.km^{-1}		
	Hydro-carbons	Carbon monoxide	Nitrogen oxide
1978	5.1	68	7.7
1979	4.3	55	6.4
1980	2.8	43	5.4
1981	1.9	28	5.4
1982	1.2	17.2	1.5

1.4.1. Alternative Power Sources

The uniform charge (uc) Otto engine is, at present, almost universally employed in automobiles. In order to comply with emission regulations, catalysts will be necessary to reduce all three major pollutants in standard engines. Modifications of this type of engine are, however, currently under development ; these include the stratified charge engine in which combustion is initiated in a side chamber in a fuel-rich zone (low oxygen content) and spreads through the main combustion chamber where the mixture is lean (high oxygen content). This decreases the rate of NO formation ; in the side chamber, the fuel burns with a low oxygen availability, whilst the bulk of the fuel is burnt at relatively low temperatures in the main chamber.

A recent review and evaluation of alternative engines for automotive use has been carried out at the Jet Propulsion Laboratory, California Institute of Technology, which compared various power sources and their likely developments over the next decade. It was concluded that, in the long term, on grounds of efficiency and cleanliness of the exhaust, the most likely choice of engine would employ continuous combustion ; examples of these are the gas turbine and the Stirling engines [26].

Because of the long lead times in the automotive industry, and the need to develop new technology, the introduction of these clean engines is still one or two decades away. In the short term, therefore, catalysts will be required to meet the proposed emission legislation in countries such as the United States of America, Russia, Europe including the United Kingdom, Japan and Australia.

1.4.2. Mechanical Devices

As mentioned in Section 1.2, the rate of formation of nitrogen oxides is proportional to the temperature in the combustion zone, and the oxygen availability. Mixtures with greater than the stoichiometric concentration of oxygen which minimise hydrocarbon and carbon monoxide emissions therefore tend to maximise nitric oxide formation. In spite of this, present trends are to more economical engines which run on lean, high oxygen content mixtures. The most practical way to reduce the formation of nitric oxide is to reduce the peak combustion temperature. This can be achieved, for example, by diluting the incoming air-fuel mixture by injecting an inert fluid such as water, or recirculating a portion of the exhaust gas. Water injection has been shown to be effective experimentally[27], a 60% reduction in nitric oxide emissions was achieved with a 1 : 1 mixture of fuel and water at stoichiometric air-fuel ratio, but this system suffers from several practical difficulties, not least of which is the need for a large water tank. Exhaust gas recirculation is a more rewarding approach at the stoichiometric air-fuel ratio, a decrease in nitric oxide emissions of 70% may be obtained with 20% of the exhaust gas recycled.

Thermal reactors are designed to permit the completion of combustion by the addition of excess air to the exhaust to promote combustion and so remove residual hydrocarbons and carbom monoxide. Under these oxidising conditions, no reduction of nitric oxide can take place. They are, however, used in conjunction with nitric oxide reducing catalysts as described below.

1.4.3. Catalytic Devices

Many workers have shown that the decomposition of nitric oxide to its elements is possible. Rudham and Saunders[29] and Winters[30] found this to occur over many transition metal oxides and Winters postulated the adsorption of nitric oxide molecules on a doublet oxygen vacancy with simultaneous release of nitrogen into the gas phase. The desorption of an oxygen molecule restores the original reaction centre. Amirazmi and co-workers[31] studied the kinetics of the decomposition of nitric oxide over platinum and base-metal oxides, but found that even at temperatures of 900°C, oxygen had an inhibiting effect on the reaction rate which was two or three orders of magnitude too slow to be considered as practical for automotive use.

The reduction of nitric oxide by a reducing agent such as carbon monoxide or hydrogen proceeds at a sufficiently attractive rate over a number of catalysts, however, which leads to the possibility of using catalysts to control nitric oxide emissions[32][33]. The use of catalysts to promote oxidation of carbon monoxide and hydrocarbons depends on the presence of excess oxygen ; however, it has been shown[34][35] that oxygen strongly inhibited catalysts for the reduction of nitric oxide by carbon monoxide. This led Sourirajan and Blumenthal[36] to suggest a dual bed approach.

Figure 1.1 : The "dual-bed" approach to exhaust emission control by catalysts

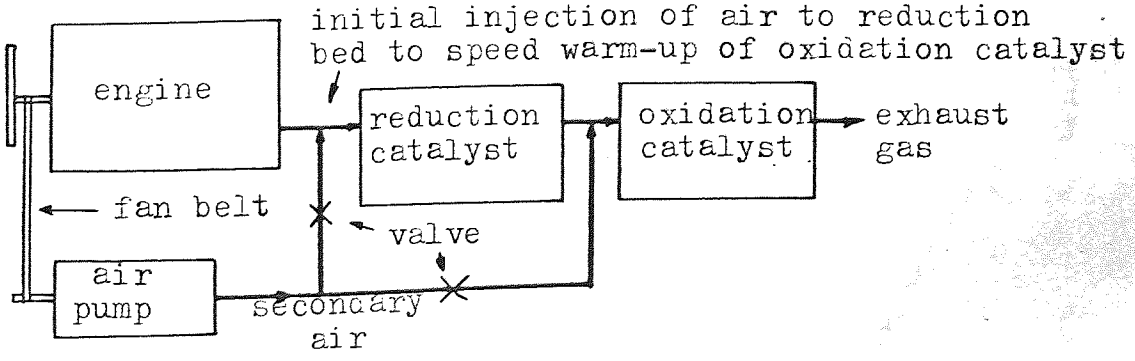

This consisted essentially of operating the engine with a rich mixture at less than the stoichiometric amount of oxygen to produce the net reducing conditions required by the nitric oxide reduction catalyst. Secondary air is then added to the gases between the two catalysts to provide oxidising conditions over the second catalyst necessary for the removal of carbon monoxide and hydrocarbons. This is not a satisfactory solution for several reasons. During the warming-up period before the engine has reached its normal operating temperature, nitric oxide emissions are low but carbon monoxide and hydrocarbon emissions are very high. This is because the thermal mass of the reduction catalyst prevents the rapid warm-up of the oxidation catalyst. To overcome this, excess air is added before the first catalyst so that it acts as an oxidation catalyst to help remove carbon monoxide and hydrocarbons during this period. This provides additional heat from the exothermic reactions to bring the oxidation catalyst more quickly to the operating temperature. The reduction catalyst is therefore subjected to a cycle of severe oxidising and reducing conditions which is detrimental to its durability.

Ammonia is produced by many catalysts as a by-product of nitric oxide reduction ; this is an unacceptable constituent of automotive exhaust gases since it is itself an unpleasant pollutant. However, in a dual-bed catalyst system this ammonia is reconverted to nitric oxide by the second catalyst[37]. This formation and reconversion of ammonia precludes the use of many otherwise acceptable reduction catalysts such as platinum.

A variation of the dual-bed scheme is the combination of thermal reactors with reduction catalysts. The Questor Company Ltd. has developed a reactor with three zones : first is a thermal reactor with limited air to raise the temperature of the exhaust gas ; the second is a catalytic bed of metallic screens to chemically reduce the nitric oxide, and the third is another thermal reactor where further air is admitted to complete the combustion processes[38].

A further proposed variation makes use of the production of ammonia by having a third catalyst bed between the oxidation and reduction catalysts to reduce the ammonia formed by unconverted nitric oxide :

$$6NO + 4NH_3 \longrightarrow 5N_2 + 6H_2O \quad \ldots\ldots\ldots 1.13$$

The sizes of the catalysts are carefully chosen so that the ammonia produced over the first reduction catalyst is just sufficient to reduce the remaining nitric oxide in the second reduction catalyst[39]. The major difficulties with these latter variations are the complicated engineering and hence high cost of the system, and the size, since little space is available in most British vehicles.

1.4.4. The Three-Way Catalyst

Simultaneous oxidation and reduction can take place in a single catalytic bed, provided that the air-fuel ratio is maintained at precisely the stoichiometric air-fuel ratio (14.7 ± 0.1). The precise metering required for the "redox" (or three-way catalyst) is difficult to achieve and much work is being carried out to discover catalysts with an increased "window" where more than 80% conversion can be obtained on all three major pollutants as shown in Figure 1.2.

Figure 1.2 : Conversion of the three major pollutants as a function of the air-fuel ratio, showing the concept of the "window" of a three-way catalyst

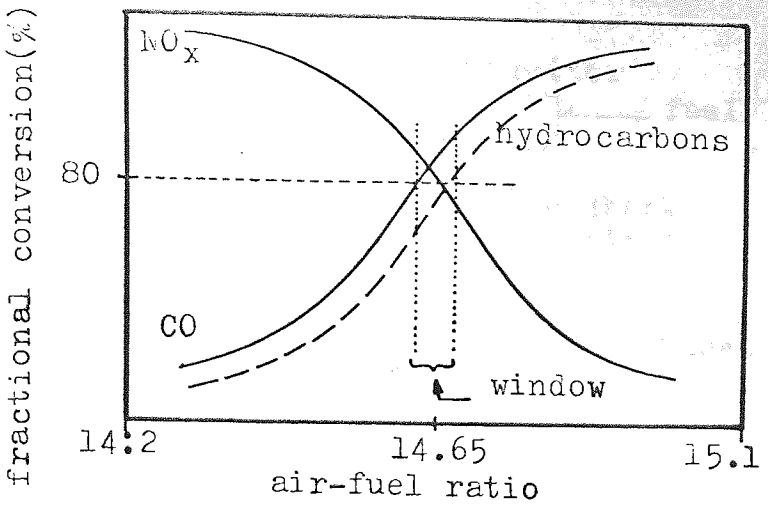

The air-fuel ratio of conventional carburettors can vary by $\pm$ 1.0, and in order to maintain the required air-fuel ratio, the system must include a feedback control mechanism equipped with an oxygen sensor. Such sensors based on the change of electrical resistance with oxygen partial pressure are under development using titania[42] or zirconia[43]. Other sensors have been based on oxygen cells. The three-way system has the advantage of good fuel economy compared with the dual-bed approach, but the system as a whole is relatively expensive.

1.4.5. Physical Characteristics of Catalysts

Whichever system is used, the active species must be presented to the exhaust gas in such a manner that the required efficiency is achieved over a wide range of operating conditions. The temperature and gas-flow rate vary over wide limits, depending upon driving conditions, and the catalyst must maintain its efficiency at space velocities of up to 200 000hrs^{-1} or residence times of 18ms.

Figure 1.3. : Schematic diagram of a three-way catalyst system including the oxygen sensor and feedback control loop to the carburettor

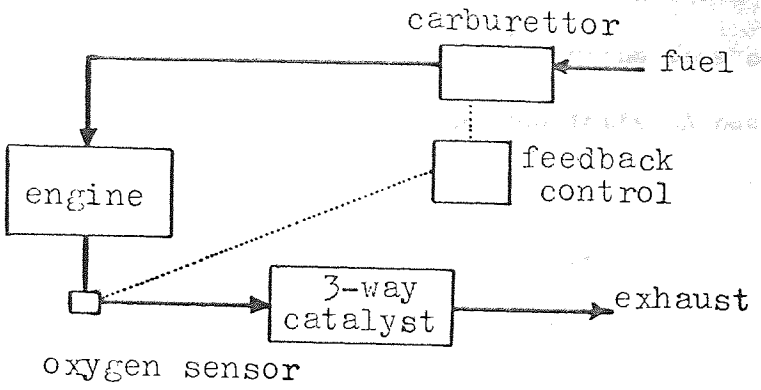

Except for metal catalysts, the active species is usually dispersed in the form of fine crystallites on a ceramic substrate. The support may take one of several different forms and may be either granular or monolithic but must have a high thermal stability, low thermal expansion, a high surface area, a relatively low density and be unreactive toward the catalytically active species. Where the support is in the form of a "monolith" it is usual to extend the specific surface area by means of a 'wash-coat' which should also have all of the above properties. Harned and Montgomery[44] have compared conversion efficiency and hydraulic factors for several catalyst substrates and found that monolithic substrates provide the best compromise for vehicle installation when catalyst volume and back pressure requirements are considered. An additional consideration is that in a 3mm (0.125in) pellet under typical conditions in an automotive catalytic reactor, only a few per cent of the internal surface area is effective because of mass transfer limitations to the rate of reaction. Monolithic structures offer the possibility of

faster heating because of their lower thermal mass, and do not suffer from the attrition caused by vibration as do pellets[46]. Several proprietary catalysts are manufactured from alloys, including "monel" and stainless steel coated with Monel[38]: in the form of woven screens, saddles or perforated and expanded foils. A new copper-chromium-nickel alloy[40] developed by the International Nickel Company Ltd. is said to offer resistance to oxidation whilst maintaining adequate catalytic efficiency, by forming a multi-layer oxide at the surface. The outer part of this is catalytically active and is backed by a coherent layer preventing further oxidation.

1.5. The Chemistry of Nitric Oxide Removal from Automotive Exhausts

1.5.1. Reduction of Nitric Oxide by Hydrogen

As previously indicated, the removal of nitric oxide from automobile exhaust gases occurs by reduction. Although the rates of reaction of nitric oxide and hydrogen, and nitric oxide and carbon monoxide are comparable at temperatures above 425°C there is evidence to suggest that the reduction by carbon monoxide according to the reaction

$$NO + CO \rightarrow \tfrac{1}{2}N_2 + CO_2 \quad \text{.....1.14.}$$

is not a major reaction path when both carbon monoxide and hydrogen are present together. There are two ways in which hydrogen can reduce nitric oxide, either without defixation as indicated by

$$NO + 5/2\ H_2 \rightarrow NH_3 + H_2O \quad \text{.....1.15.}$$

or with defixation

$$NO + H_2 \rightarrow \tfrac{1}{2}N_2 + H_2O \quad \text{.....1.16.}$$

Both are thermodynamically favoured at temperatures above 200°C[49]

The selectivity for nitrogen is dependent both on the type of catalyst and reaction temperature. Since ammonia is thermodynamically unstable with respect to its elements above 400°C, a maximum occurs in the rate of formation of ammonia with respect to temperature. The temperature at which this maximum occurs depends on the catalyst, and varies from 700-750°C for copper-chromite[50], to 400°C for nickel-based catalysts[51].

There are three sources of hydrogen in automobile exhaust gas. Molecular hydrogen which is present at a concentration of a quarter to one half that of carbon monoxide. Water vapour, which is converted to hydrogen in the water-gas shift reaction by the same catalysts that reduce nitric oxide, and finally the hydrocarbons which can themselves react directly with nitric oxide. There is evidence to suggest that hydrogen from the water-gas shift reaction is the major component. In general, the proportion of nitric oxide converted to ammonia decreases monotonically with nitric oxide concentration while the absolute amount formed passes through a maximum which varies widely for different catalysts[50]. Conversely, an increase in hydrogen concentration promotes formation of ammonia. Water vapour, which is present at about 15% in automotive exhausts, reacts with carbon monoxide in the water-gas shift reaction :

$$H_2O + CO \longrightarrow H_2 + CO_2 \quad \ldots\ldots\ldots 1.17.$$

It has been shown that the activity of a catalyst to promote this reaction is directly related to its activity for the reduction of nitric oxide[52][53]. Many catalysts which are active for the shift reaction produce more ammonia when the source of hydrogen is water

than when the source is molecular hydrogen[54]. In laboratory experiments, therefore, product distributions from the same catalyst can vary depending on whether water is present or not. In general, the behaviour of catalysts under test in wet and dry systems is similar, but some catalysts such as chromia are deactivated in the presence of water due to the formation of a hydroxyl layer[55]. The overall behavior of nitric oxide reduction by hydrogen holds for base-metal oxide catalysts[50] and noble metal catalysts[56].

1.5.2. The Mechanism of Ammonia Formation

Nitric oxide and hydrogen are dissociatively absorbed onto the surface of the catalyst[49] which gives rise to two possible products according to the reactions shown by equations 1.15 and 1.16. Anything that lowers the surface coverage of nitric oxide such as a layer of carbon monoxide or oxygen will lower the probability of interaction of two N-containing species and conversely increase the probability of hydrogenation to form ammonia. There are three ways by which the pairing of two N-containing species can occur more rapidly at higher temperatures to explain the maximum in the formation of ammonia. These are the reaction of two ammonia molecules in the gas phase to form nitrogen and hydrogen. Secondly, the increased mobility of the partially hydrogenated N-containing species leading to an increased rate of reaction for the formation of nitrogen molecules. Finally, the direct reaction of ammonia with unconverted nitric oxide in the gas phase.

The first may be rejected since the effect of space velocity on selectivity in a nitric oxide-hydrogen system and on the decomposition of ammonia[50][57] showed that on some catalysts the

decomposition rate of ammonia was very slow and should have been the rate limiting step in the overall reaction which was not the case. Similar results were obtained in a nitric oxide-water system. However, it was observed that catalysts with a high activity for ammonia decomposition had a good selectivity for nitrogen, showing that pairing of N-containing species was faster on these catalysts.

The last explanation may be rejected since the use of labelled reactants in a detailed study[58] showed no evidence of ammonia released to the gas phase being responsible for the main defixation path. If this was not the case, then catalysts such as copper and platinum would be expected to be very selective for nitrogen since they are active for the nitric oxide-ammonia reaction. However, both produce large quantities of ammonia[59][60]. It was therefore concluded that the main defixation path was the pairing of partially hydrogenated fragments. These have a high mobility on catalysts active in ammonia decomposition such as ruthenium and nickel which are also highly selective for nitrogen. This pairing occurs more rapidly that full hydrogenation and desorption of ammonia on these catalysts. For catalysts with high selectivity for ammonia, the reverse was true.

1.5.3. Miscellaneous Nitric Oxide Reactions

The addition of carbon monoxide to a dry nitric oxide-hydrogen system over base-metal oxide catalysts was found not to decrease ammonia formation by direct reduction according to equation 1.4, Rather, ammonia formation[50], was enhanced by decreasing the surface coverage of nitric oxide and lowering the probability of pairing of N-containing species before full hydrogenation. On platinum and palladium there was a small decrease in the rate of ammonia formation[57] caused by the very strong carbon monoxide absorption

on the noble metals, so that the nitric oxide could not participate in the reaction until the temperature was increased. In this instance, ruthenium behaved as a base metal. The presence of oxygen in an overall reducing atmosphere shifted the reduction reaction on base-metal oxides to higher temperature[49] due to the increased average oxidation state of the surface which had a lower catalytic activity. The presence of oxygen at less than the stoichiometric amount had no effect on the selectivity or activity of the noble metals and in this instance, ruthenium behaved as a noble metal.

Infra-red spectroscopy studies[61][62] on noble metal catalysts have shown the existence of isocyanate radicals, the hydrolysis of these radicals was proposed as an alternative mechanism for the formation of ammonia. Hydrogen cyanide has also been reported as being formed over monel and perovskite catalysts[63].

1.6. Practical Reduction Catalysts

1.6.1. Noble Metal Catalysts

With the exception of ruthenium, noble metal catalysts are not selective enough for nitrogen to be of practical value and the use of metallic ruthenium is precluded because of the volatility of the higher ruthenium oxides[64]. To overcome this difficulty, the acidic ruthenium oxides were mixed with a basic oxide such as that of barium[65][66] to form a more stable double oxide. This and many ruthenates of the alkaline earth metals tend to crystallize with the perovskite structure[67] of which several have been claimed to be useful catalysts for the reduction of nitric oxide in automotive exhaust gases[68]. This stabilised form is not completely satisfactory

since some loss of the ruthenium still occurs. In the repeated cycling from oxidising to reducing conditions in the exhaust, the ruthenium tends to form a separate phase which is then susceptible to volatilization[69].

A further improvement in stability is achieved by diluting the ruthenium in the B positions of the ABO_3 perovskite structure by other metals[65] although this is accompanied by some loss of selectivity[70].

1.6.2. Metal Oxide Compounds

Of this group, the most widely acclaimed as catalysts are the perovskites, first proposed for use in automobiles by Libby[71] after work by Meadowcroft[72] had shown that they had similar activity to platinum as oxygen electrode materials. Later work has shown that the presence of a noble metal or a metal capable of reduction to the metallic form is necessary to impart catalytic properties which the perovskite crystals do not possess intrinsically[49][73]. Under cyclic conditions, the perovskites tend to revert to a mixture of the more easily reducible metal and of the more refractory metal oxide as seen above for ruthenium oxide-barium oxide mixtures. Other compounds such as spinels[74][75] and crysolites[76] have been investigated as automotive catalysts but generally to a lesser extent than the perovskites. Activity is found to be lower for the mixed oxides than for the simple oxides, as in the case of the perovskites, but judicious choice of composition should tend to minimise thermal sintering and support interaction. The addition of nickel and ruthenium to these compounds generally imparted some of the metal's selectivity for the reduction of nitric oxide to nitrogen.

1.6.3. Base Metal Oxides

Large numbers of base-metal oxides and various combinations of oxides have been investigated by many workers including Bauerle at al.[74], Shelef and Kummer[78] and Meguerian et al.[79]. Many potential reduction catalysts were investigated, including large numbers of nickel-containing formulations which tend to retain, to a large extent, the high selectivity for nitrogen of nickel itself. In nearly all cases the active catalyst is the reduced metal rather than the oxide, and therefore it requires some form of activation treatment, although this may be left until the catalyst is installed in the vehicle exhaust where it is activated in situ by the exhaust gases. A potential problem with nickel catalysts is the formation of its carbonyl, although this has been shown to be negligible[80] in the case of monel metal. The carbonyl is unstable above 200°C[81] and conditions in the exhaust are seldom favourable for its formation except during initial heating.

Reduced nickel and copper oxide mixtures were indicated as being useful catalysts because of the use of monel[82] as a reduction catalyst. Bauerle et al.[83][84] have investigated nickel and copper oxide catalysts for the reduction of nitric oxide by both carbon monoxide and hydrogen. They found that the activity of these catalysts was dependent on the activation procedure, i.e. for the reduction of nitric oxide by carbon monoxide they found that activating the catalysts in carbon monoxide at 350°C resulted in better catalytic properties than when activated at 500°C. This proved to be reversible after recalcination, indicating that the observed differences in activity were not due to differences in surface area.

For the reduction of nitric oxide by hydrogen, it was found[84] that addition of copper reduced activity but did not significantly affect ammonia formation. Nickel-chromium oxide mixtures were found to be less active but to be more selective for nitrogen formation. It was found that addition of oxygen caused a shift in the activity and ammonia production curves to higher temperatures. Davies[85] has shown that increase of copper content in a nickel-copper oxide catalyst increased the activity in a simulated exhaust environment especially at low temperatures where the nickel is more susceptible to oxygen poisoning. It was reported that the addition of copper did not markedly affect the formation of ammonia and that the effect of the copper was to improve activity in the presence of oxygen. An addition of 0.1% platinum also enhanced this effect[86]. The effect of copper when alloyed with nickel is strongly dependent on the nature of the reaction and on the side reactions possible. Ponec[87] has recently reviewed the question of catalysis by alloys and cites numerous examples of reactions affected by alloying copper with nickel.

1.7. Deactivation of Catalysts

The subject of the durability of catalysts is vital to their future use in automobiles, and much work had been carried out to evaluate their durability in vehicles. However, much less has been undertaken to determine the underlying failure mechanisms. Furthermore, whilst the deactivation mechanisms have been evaluated qualitatively, few quantitative studies have been carried out and published.

The experimentally observed activity of a catalyst is attributable to three factors which may be conveniently expressed in terms of the reaction rate constant :

$$K_{obs} = K_{int} \eta S \qquad \ldots\ldots\ldots 1.18.$$

1. The intrinsic activity, K_{int}, is affected by the promoters added to the catalyst during preparation or by any chemical changes that occur to the active species such as the separation of ruthenium from its stabilised form.
2. The specific surface area, S, of the active species is affected by aggregation (or sintering) of the active species which decreases the specific surface area. This can also occur by poisoning which limits the number of active sites available to the reactants, or by reaction of the active species with the substrate to form an inactive compound.
3. The efficiency factor, η , is a measure of the proportion of active sites available due to diffusional effects and may be reduced by blocking of the pores by deposition of poisons or dust or other solid matter.

Some mechanisms by which catalytic deactivation can occur are : (i) sintering or crystal growth of the active component, (ii) sintering of the support, (iii) poisoning of the active species, (iv) blocking of the pores by particulate materials, (v) volatilisation of the active species, (vi) reaction of the active species with the support, (vii) loss of the coating/active species due to thermal and mechanical stresses and erosion, (viii) melting of the support. The major factors in the deactivation of the catalysts considered in this dissertation are dicussed below in Chapter 2.

1.7.1. Catalyst poisoning

Lead is probably the most harmful element in the exhaust gases and is present in petrol as tetraethyl (or tetramethyl) lead which decomposes during combustion and combines with ethylene dibromide and ethylene dichloride to form a mixture of halides and oxides with a melting point around 900°C. Lead is then emitted partly as gaseous and partly as particulate matter ranging in size from 0.3 μm. to 10 μm. ; this can block pores and cover the active surfaces. It is envisaged[88] that lead should be present at a level of no more than 0.013g.L^{-1} of lead (0.05g. per gallon) ; even so, this amounts to a consumption of about 100g of lead per 80 000 km (50 000 miles) at a fuel consumption of 8.9 km.L^{-1} (25 mpg). In the catalytic bed, lead tends to deposit at the inlet face of the catalyst[89][90]. In an oxidation catalyst, lead, sulphur and phosphorus were detected within the wash-coat by electron probe micro-analysis, suggesting these were deposited from the gas phase[89]. In the same sample zinc and iron were found not to penetrate the wash-coat, suggesting deposition as particulates. The combined effect of lead and sulphur is said to be more detrimental than the sum of the separate effects[91]. With increasing temperature, the poisoning effect of sulphur is lessened[79] and the effect is also minimised at high carbon monoxide contents possibly due to diminished sulphur retention on the catalysts. Shelef[49] investigated the established durability of a stabilised ruthenium catalyst in vehicles run on fuels containing 0.013g.L^{-1} (0.05gm.gal^{-1}) lead, 0.0125 $^{W}/_{O}$ sulphur ; 0.013g.L^{-1} (0.05gm.gal^{-1}) lead plus 0.0125 $^{w}/_{o}$ sulphur, and 0.016gm.gal^{-1} of phosphorus. The harmful effects of lead and sulphur were clearly evident ; the effect of phosphorus was less harmful to the catalyst although analysis showed a higher retention of this

poison. Sulphur poisoning has been shown to be reversible, the activity of a sulphur poisoned catalyst being restored after running in a sterile atmosphere[92]. One significant effect of halogens in the exhaust gas was to provide a path for the volatilization of copper leading to depletion of copper in surface layers[93] of a copper-chromite catalyst.

1.7.2. Thermal Ageing of Catalysts

The catalyst is subject to continual cycling of both temperature and the reducing potential of the exhaust gas. The exhaust gases also contain about 15% water vapour which has been shown to accelerate the sintering of some supports. After 100 hours at 900°C in a water-free atmosphere a reduction of the surface area of gamma-alumina from 120 to about $40 m^2 gm.^{-1}$ was measured[94], whereas the same time at 800°C in the presence of water vapour[95] reduced the surface area to less than $10 m.gm.^{-1}$. This behaviour is typical of an evaporative/condensation sintering process. The presence of water vapour also increased the aggregation of supported nickel, as mentioned below.

One of the most spectacular failures of catalysts is the melting of the substrate material[96] which for alumina occurs at temperatures in excess of 2,000°C. This is obviously far above normal operating temperatures, but 1% CO in the exhaust can raise the gas temperature by 110°C and 2% of petrol in the exhaust, arising from severe misfire, would provide an adiabatic flame temperature of 2,250°C which is quite sufficient to melt the support.

Liedermann[97] examined thermally aged and engine-tested platinum-based oxidation catalysts by scanning-electron microscopy and came to

the conclusion that the majority of the deactivation was caused by growth of the metal crystallites. Later work by Dalla Betta[98] made use of both surface area measurements and electron microscopy to show that for a supported metal catalyst, 95% of the original metal surface area was lost due to aggregation after service under severe conditions, and that 95% of the remaining surface area was not available because of poisoning.

1.7.3. Crystal Growth in Catalysts

Much of the data on the effect of thermal treatment on crystallite size of supported metal catalysts has arisen as a by-product from investigations on the effect of particle size on activity, and furthermore, much of the available data concerns the highly dispersed noble metals. This data was recently reviewed in depth by Flynn and Wanke[99] who found that very little data on crystallite aggregation in supported metal catalysts has been published. However, they drew a number of general conclusions from the available data. They found the most important factors were temperature and the composition of the atmosphere. The type of support and the degree of metal loading appeared to be of secondary importance.

The rate of crystallite aggregation increased with increasing temperature except in an oxygen containing atmosphere where many investigators have observed redispersion or increase in metal surface area at temperatures in the range 400-620^{o}C. The rate of aggregation except where this redispersion occurred, was proportional to the oxygen partial pressure. Oxygen was found to have a greater effect on the rate of aggregation than hydrogen or nitrogen, and the rate of aggregation in vacuum was, in general, lower than when a gas phase was present. Baker and France[100] found that some hydrocarbons

accelerated crystallite aggregation at lower temperatures than did oxygen. Huang and Li[101] showed that on single crystals of alumina the orientation of the support affected the rate of platinum crystal growth, but Flynn and Wanke[99] could not determine the effect of the support on the aggregation rate with the available data.

Gruber[102][103] found that with platinum-on-alumina catalysts, the metal loading affected the rate of aggregation but not as a monotonic function of the metal loading. This apparent anomaly may have been due to different initial particle size distributions since it has been shown[104] that catalysts with a bi-modal size distribution sinter more rapidly than catalysts with narrow size distributions.

The data on supported nickel catalysts is much more limited and falls into two distinct categories : low ($<15\%$) and high ($>40\%$) metal loading, the published data is shown in Tables 1.3 and 1.4. The lack of data on aggregation of supported nickel catalysts is clearly apparent, but it is possible to see that rapid aggregation occurs even with low metal loadings (Table 1.3). All the data for high metal loadings is given in the form of metal surface areas, and in many cases, the final surface area was not measureable. The importance of the pressure of water vapour in any synthetic gas used for ageing is shown by the results in Table 1.4.

Robertson[110] showed that the metal crystallite size for a nickel-copper supported catalyst was inversely proportional to the metal loading and also proportional to the surface area of the support,

TABLE 1.3. : Increase in metal crystallite size as a function of time and temperature[105][106][107]

Catalyst,	Temperature(°C)	Time (hrs)	Crystallite size(nm)	
			Initial	Final
3% $Ni-Al_2O_3$	900	72	24	252
6.7% $Ni-SiO_2$	450	16	3.5	5.5
10% $Ni-Al_2O_3-SiO_2$	370	1	3.0	4.5
"	450	1	3.0	7.7
"	500	1	3.0	9.9
"	580	1	3.0	13.0
"	700	1	3.0	18.0

TABLE 1.4. : Decrease in surface area as a function of time, temperature and the presence of water vapour[108][109]

Catalyst	Temperature(°C)	Time (hrs)	Surface area(m^2g^{-1})	
			Initial	Final
75% $Ni-Al_2O_3$	600 ($+H_2O$)	100	35	5
	800 (dry)	50	35	28
	800 ($+H_2O$)	10	35	none detected
75% $Ni-Al_2O_3$	340 ($+H_2O$)	16	56	none detected

1.7.4. Mathematical Evaluation of Loss of Catalyst Surface Area

1.7.4.1. The Emprical Approach

Many investigators have used an empirical approach in correlating sintering data. This was based on a power-law rate function of the form[111][112] :

$$dD/dt = k/D^2 \qquad \text{.....1.19.}$$

which, on integration, gives :

$$D^n - D_o^n = k_1 t \qquad \ldots\ldots\ldots\ldots 1.20.$$

and on taking logarithms :

$$\log (D/D_o) = \frac{1}{n} \log k_1 + \frac{1}{n} \log t \qquad \ldots\ldots 1.21.$$

A plot of $\log (D/D_o)$ versus log(t) would enable the evaluation of the power-law order and the reaction rate constant, k_1. The latter was assumed to follow an Arrhenius law :

$$k_1 = A\exp(-E_A/RT) \qquad \ldots\ldots 1.22$$

Thus, n = 1 for viscous flow, 2 for evaporation, 3 for volume diffusion and 4 for surface migration. However, it was often found that n was greater than 4 and this was probably to some unfavourable aspect of growth such as nucleation barriers giving rise to growth along certain crystallographic planes. More recently, this same empirical relationship has been applied to growth of supported metal catalyst particles and it has been suggested that growth occurs by diffusion of metal species (atoms or oxide molecules) across the surface of the support material, since the growth rate of platinum on alumina was found to be dependent on surface orientation of the alumina[113]. Further evidence for this is that an increase in the partial pressure of oxygen was shown to increase the rate of growth of platinum particles on polycrystalline alumina[114]. Furthermore, Baker and France[100] observed that in the presence of oxygen, palladium crystallites on graphite were relatively mobile, and growth occurred by aggregation, and that in the presence of both acetylene and hydrogen, rates of particle growth were accelerated.

An attempt by Flynn and Wanke[99] to correlate published data on sintering of supported metals with this simple power-law rate function met with only partial success, although many authors have found that their experimental results were adequately described by this relationship.

1.7.4.2. The Mechanistic Approach

Two mechanistic models are currently proposed in the literature for the aggregation of metal crystallites on supported metal catalysts. The first is due to Ruckenstein and Pulvermacher[115][116] who have described a process which occurs by the migration of metal crystallites over the surface of the support, and the subsequent collision and coalescence of the crystallites. The second is due to Flynn and Wanke[117][118] who consider aggregation to occur by migration of atomic or molecular species from the metal crystallite so that the smaller crystallites disappear while the larger crystallites grow by capturing the migrated species. There is little direct evidence for the Brownian-type motion of metal crystallites as suggested in the crystallite migration theory, and it is suggested by Flynn and Wanke[99] that its use is restricted to the early stages of aggregation when crystallites are of the order of 5nm or less. Metal crystallites have been observed to exceed the size of the support particles[104] and under these circumstances, this theory would be inapplicable. The atomic migration theory[117][118] envisages aggregation to occur by three distinct steps :

(i) escape of metal atoms (or molecules such as metal oxides) from the metal crystallites to the support surface ;

(ii) migration of these atoms along the support surface, and

(iii) capture of the migrating atoms by metal crystallites.

The rate of capture controls the process which can be either dependent or independent of metal loading. If the rate of capture was large, the concentration of migrating atoms at any time would be small, and the aggregation rate would be dependent on the concentration of migrating atoms, that is the metal loading. If the rate of capture is small, the number of migrating species at any time is large, and the process is less dependent on the metal loading. This model, however, has a basic deficiency in that the activation energy for the escape of metal atoms has to be about 80Kcal.g-atom^{-1}, whereas the heat of the sublimation of platinum, for example, is 135kcal.g.atom^{-1}, hence the metal support interaction has to be of the order of 55 kcal.g.atom^{-1}, which is larger than can presently be justified[99]. Although no direct experimental evidence is yet available, Flynn and Wanke[99] list five areas to which their model is applicable :

(i) Redispersion of the metal crystallites under some conditions, although Ruckenstein and Malhotra[119] have proposed an alternative explanation based on a Pt-alumina compound which is stable between 200 and 600^{o}C ;

(ii) The formation of a bimodal particle size distribution. This is predicted by the atomic migration theory and observed in a number of investigations ;

(iii) The absence of appreciable aggregation in vacuum ;

(iv) The increase in rate of aggregation due to an initial bimodal particle size distribution ;

(v) The observation of crystallite growth in excess of the size of the crystals of the support.

Granquist and Burhmann[120] have formulated a simple statistical model which regards the growth of the metal crystallites as a series of discrete events and have shown that increase in particle size due to coalescence leads to a log-normal distribution with a sharp cut-off on the small particle side and a long tail on the large particle side. They contrast this[121] with the distribution predicted by Flynn and Wanke[117] which has a long tail on the small particle side and compare data from six references all of which compare favourably with the distribution predicted by the model due to crystallite migration and coalescence. It is claimed that this is strong evidence that the predominant growth mechanism for supported metal crystallites is due to crystallite migration.

Wanke[122] in reply to this criticism has shown that by choice of constants the theory due to atomic migration may be used to predict log-normal distributions with long tails on either the small or large particle side.

1.7.4.3. Implications of the Aggregation Mechanism to Catalyst Development

The rate of aggregation of metal crystallites has been shown to be increased in the presence of oxygen and to be strongly dependent on temperature although it was found that the Arrhenius law applied to a simple power-law rate function did not adequately correlate with the available sintering data.

The identification of the aggregation mechanism would allow the development of catalysts more resistant to aggregation, although this would have to be with regard to the catalytic properties required. The

use of alloying, for instance, to increase the metal-metal interaction and decrease the metal support interaction would result in a more stable catalyst according to the atomic migration model, but the crystallite migration theory predicts a less stable catalyst. The two models also predict different dependences on the initial particle size distribution and metal-support-atmosphere interactions. The crystallite migration model predicts that the rate of aggregation is relatively unaffected by the initial particle size distribution and that large metal support interactions would result in a more stable catalyst due to the decreased mobility of the crystallites. The atomic migration model predicts a strong dependence on initial particle size, and that small metal support interactions would give a more stable catalyst.

1.8. Future Prospects for Nitric Oxide Reduction Catalysts

At present, there is a controversy in the United States over what many experts call the unnecessarily stringent requirements of $0.25 g.km^{-1}$ ($0.4 g.mile^{-1}$) for nitrogen oxide emissions ; any relaxing of this standard would, of course, have profound effects on automotive catalysts. Present engines with correct tuning and exhaust gas recirculation would be able to maintain the nitrogen oxide emissions below $0.9 g.km^{-1}$ ($0.4 g.mile^{-1}$) and the need for a reduction catalyst or a three-way catalyst would be lessened. Assuming the figure of $0.25 g.km^{-1}$ ($0.4 g.mile^{-1}$) is allowed to stand, then in the short term, catalysts must be employed to keep emissions to the legally permitted amounts, in this case it is likely that the three-way system would be preferred since it has many advantages

over the dual-bed approach. In the longer term, however, the need for NO reduction catalysts will depend on the development of continuous-combustion engines, such as the Stirling engine, which is thought to be capable of operating with nitrogen oxide emissions below $0.12 g.km^{-1}$ ($0.2 g.mile^{-1}$).

2. PHYSICAL EXAMINATION OF SOME ENDURANCE TESTED CATALYSTS

Between 1971 and 1975, the Catalysts and Chemicals Group, Imperial Chemical Industries Ltd. and the Air Pollution Control Laboratories, B L Cars Ltd., collaborated in the development of catalyst systems for automotive use. As a result of this work, a nickel-copper-platinum catalyst was found to be the most satisfactory active component. However, the traditional wash-coat of gamma-alumina was found to react chemically with the base metal oxide to form inert spinels and was therefore unsatisfactory. Further investigations led to the use of gehlenite (a calcium alumino-silicate) as the secondary support, it was found that the addition of basic calcium oxide to the aluminium-silicate rendered the material inert to nickel and copper oxides at the temperatures under consideration.

In the period 1971-75 several of these catalysts were endurance tested in vehicles by B.L. Cars and since one of the main objectives of these tests was to obtain operating experience over long catalyst lives, spark retardation, secondary air and manifold lagging were introduced to maintain nitric oxide removal efficiency over this period. The catalysts themselves were constantly improved so that at the end of this period catalyst lives of 8 000-32 000 km (5-20 000 miles). During 1975-76, two further tests were carried out, the sample was just within the limit for NOx emissions of 0.6g. km^{-1} (0.4g.$mile^{-1}$) for a distance of 22 400 km (14 000 miles) but outside this limit by a factor of 2 at 32 000 km (20 000 miles). The second was tested to 80 000 km (50 000 miles)[124] and was still within the limit at the end of the test. U.S. Federal legislation[24] required that the emission limits given in Table 1.1 be maintained for

80 000 km (50 000 miles) with one allowable change of catalyst so that although the target had been shown to be within reach, the life of the present available catalyst had to be improved by a factor of 2 to comply with the proposed legislation.

The object of the present investigation was to study in depth the reasons for the deterioration of the performance of the catalyst and to suggest, if possible, ways of preventing or retarding the deterioration so that a catalyst could be manufactured to achieve 80 500 km (50 000 miles) on the road and still be within the very stringent U.S. emission requirements for NOx of 0.6g.km^{-1} (0.4g.$mile^{-1}$) when tested on a chassis dynamometer under specified running conditions. As a start in assessing the task to be performed, catalysts that had run for up to 20 000 km (12 000 miles) were selected for microscopic examination and analysis.

2.1. Description of the ICI/BL Catalyst

The catalyst developed by ICI in collaboration with BL Cars consisted of three components. There was a monolithic primary support, a secondary support and finally the active species itself. The primary support was usually an extruded cordierite monolith with ducts of square cross-section at a density of 225 cells per square inch. This item was manufactured by Corning Glass Ltd. and designated by them EX 20. The specific surface area of this material is about 0.16$m^2 g^{-1}$. The matrix of a 48 000 km (30 000 miles) catalyst referred to above, was constructed from alternate layers of flat and corrugated cordierite sheet material and the 80 000 km (50 000 miles) one was an extruded square section monolith catalyst but had 296 cells per square inch.

ICI practice was to apply a wash-coat of gehlenite ($2CaO.Al_2O_3.SiO_2$) to the primary support to extend the surface area. Gehlenite powder was wet-ground to give a slurry containing particles no bigger than 20μm in size and with the majority of particles less than 7μm. During the wet comminution process some hydration takes place ; minor amounts of hydrated calcium aluminates (mainly $3CaO.Al_2O_3.6H_2O$) and about 15% of a hydrated gehlenite ($2CaO.Al_2O_3.SiO_2.8H_2O$) were usually found to be present[125]. Major metallic impurities were Fe_2O_3 (0.8%) and MgO (0.6%). The coating was usually fired at a temperature of 1100°C to give a specific surface area of about 1.0$m^2g.^{-1}$ of catalyst. The choice of gehlenite arose from ICI's experience in catalyst technology ; later surveys[126][127] of possible support materials have, in fact, confirmed that gehlenite is a prime contender on the grounds of its chemical compatibility with nickel and copper oxides.

The active species was a mixture of nickel and copper. These metals were impregnated from a solution of nitrates with a pH of about 2 ; a lower pH was said to lead to to excessive leaching of calcium from the gehlenite with the formation of calcium oxide on the catalyst during calcination. Increasing the pH further by addition of ammonia was said to lower the concentration of metal in the solution so that an excessive number of impregnations were required. The metal loading of about 60% (as a percentage of the total coating) was the maximum which could be reasonably and economically obtained. The nickel-copper ratio was optimised during work on granules ; it was found[85] that 10% of copper increased the activity of the catalyst although no work was carried out specifically to assess the effect of copper on deactivation. In later catalysts, 0.1% platinum was added to confer resistance to oxygen poisoning[51].

2.2. Examination of Endurance Tested Catalysts

ICI also carried out examinations of some of the catalysts tested by B L Cars. They found that up to 60% of the coating and active material had been lost after 32 000km (20 000 miles) in service and that sintering of the active species occurred giving crystallite sizes of up to 10μm. The catalysts were also found to be contaminated with sulphur and phosphorus which were distributed evenly throughout the catalyst, and with lead, which was present as a glassy silicate phase concentrated mainly at the inlet face and localised in the outer 5-10μm of the coating[88]. It was concluded that there were three main causes of deactivation :

(i) Physical loss of the wash-coat ;

(ii) Sintering of the active species accompanied by segregation of the nickel and copper due to the cyclic oxidising and reducing conditions ;

(iii) poisoning of the active species by impurities and additives from the fuel and lubricants.

Only three of these endurance tested catalysts were available at the start of the project and a fourth became available at a later date. Although it was not expected that any statistically significant results would be obtained from an examination of these catalysts because of the limited amount of material and the varying test conditions, it was nevertheless decided to carry out such an examination since it was considered this would usefully provide an insight into the mechanisms of deactivation of the catalysts and would allow suitable experimental techniques of micro-examination to be developed.

2.2.1. Chemical Analysis of the Catalysts

Chemical analyses of these catalysts and a nominally similar fresh catalyst are shown in Figure 2.1, where it can be seen that 50% of the active species is lost within the first 8 000 km (5 000 miles) of service, and thereafter, the rate of loss is much reduced, only an additional 10% being lost after 32 000 km (20 000 miles). The lead content of the catalyst increased monotonically with the service

Figure 2.1. : (a) Fractional loss of wash-coat and active species
(b) Accumulation of lead deposits on the catalyst as a function of test mileage

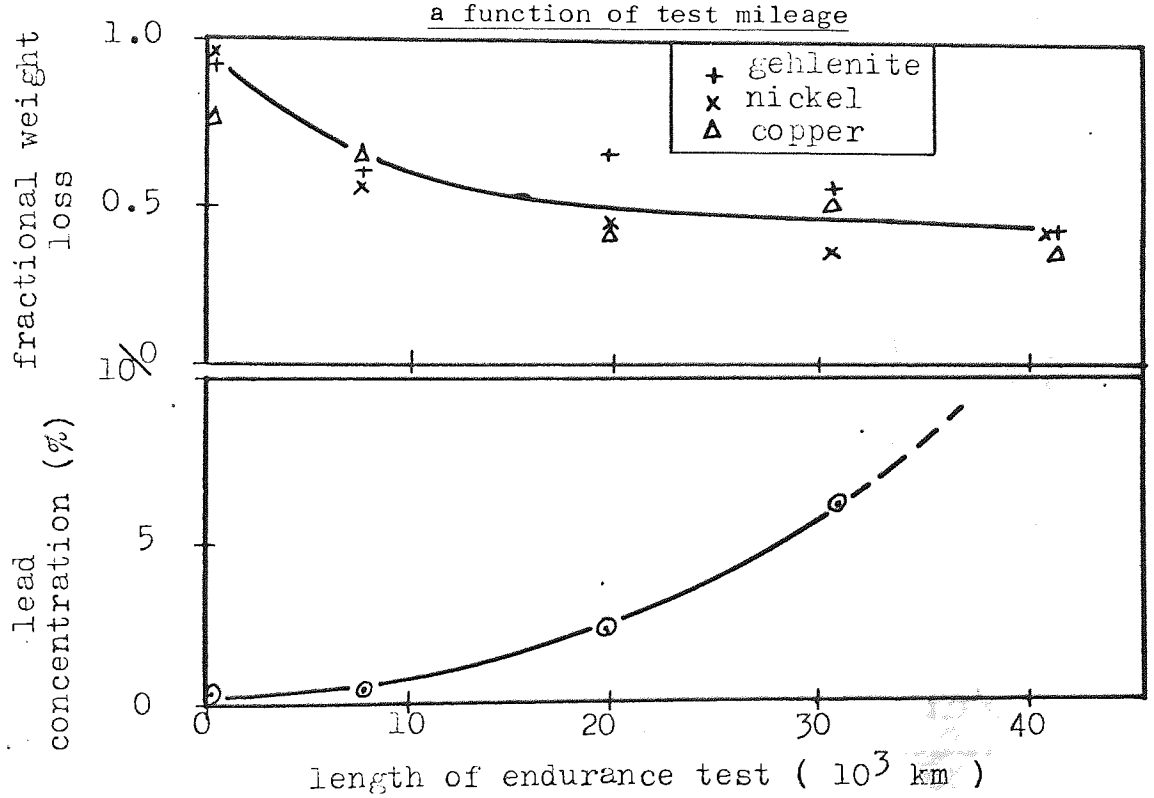

life and the rate of deposition of lead appeared to increase with life . This was probably because the observed deposition rate was a net effect, i.e. any lead depositied in the early stages of the endurance run would have probably been lost with the coating. The rate of lead deposition would therefore be expected to increase as the rate of loss of coating decreased. Samples of a catalyst taken from a Marina (TJO 550K) after 43 840 km (27 400 miles) were analysed

in a similar manner and the results plotted in Figure 2.2 to show the effect of distance from the inlet face on the loss of wash-coat and active species, and accumulation of lead deposits. This particular catalyst, RX2, was an example of a catalyst on a corrugated matrix, ex Minnesota Mining and Manufacturing Company Ltd, a photograph of which is shown in Figure 2.11, whereas the previous samples were on an

Figure 2.2. : The fractional loss of the wash-coat and active species as a function of distance from the inlet face in Catalyst RX2

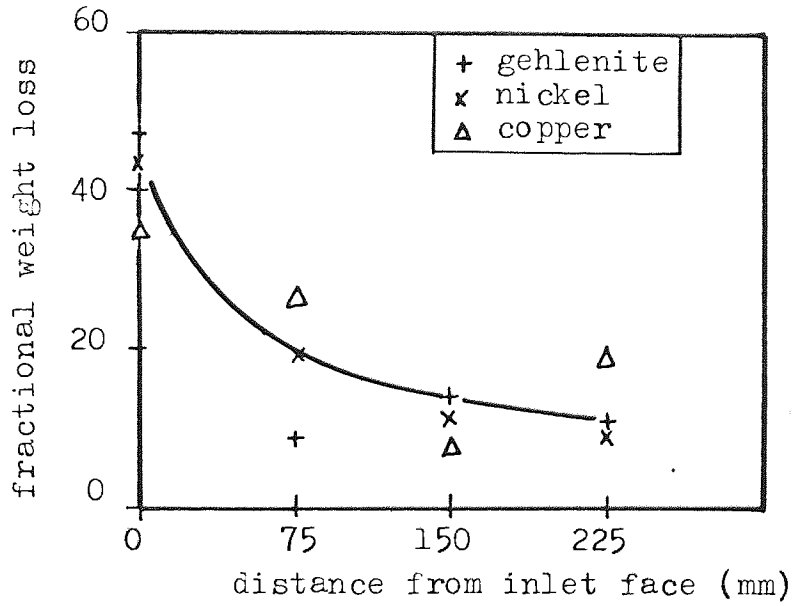

Figure 2.3. : The accumulation of lead deposits as a function of the distance from the inlet face in catalyst RX2

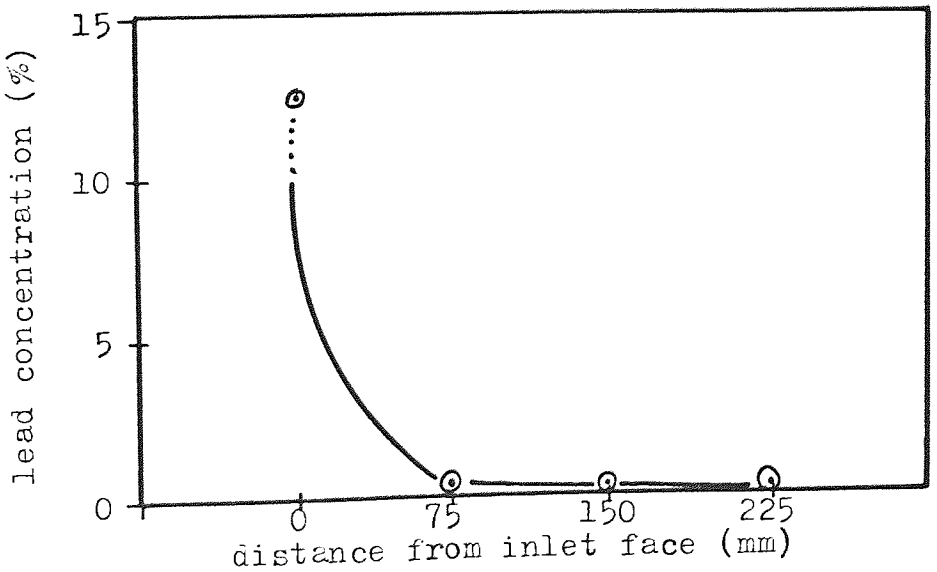

extruded matrix with 225 square cells per square inch. The catalyst consisted of three 101.6cm (4in) diameter by 7.62cm (3in) long matrix blocks and the analysis samples covered the whole length of the catalyst. It can be seen from Figure 2.3 that the lead deposits were heaviest at the inlet face and little or no lead penetrated the first block of the catalyst. From Figure 2.2 it can be seen that the fractional loss of wash-coat and active material was most severe at the inlet face.

2.2.2. Physical Examination

Optical examination of an unused catalyst showed that the coating accumulated at the cell wall corners, probably due to surface tension effects during preparation. The thickness of the coating varied from 25 to 200μm (0.025 to 0.2mm), as shown in Figure 2.4. Large cracks could be seen in the coating at the corners of the cells where it was thickest. These were thought to occur during the drying of the slurry. By adjusting the focus it was seen that many of the pores in the cordierite contained gehlenite. This is shown more clearly in Figure 2.5. In the electron-probe microanalyser (EPMA) it was seen that the nickel and copper were evenly distributed throughout the gehlenite on a macro scale penetrating into the pores of the cordierite with the gehlenite as shown in Figures 2.6 and 2.7. At higher magnification it was possible to see that after testing, the nickel and copper were not distributed completely uniformly but it was barely possible to resolve the largest nickel-copper rich "areas". In these "areas" the ratio of nickel to copper varied from 2.8 to 4.8 after 7680km (4 800 miles) and from 0.9 to 1.1 after 20 480km (12 800 miles). Because of the difficulty in resolving the metal crystallites it would be dangerous to attach too much importance to

this finding but ICI have found that the nickel and copper tended to segregate in service under the cyclic, oxidising and reducing conditions inherent in the dual-bed catalyst approach. Although the metallic elements are completely soluble in each other, the oxides are relatively insoluble ; CuO has a maximum solubility in NiO of approximately 5% and NiO has a maximum solubility in CuO of approximately 35%. The molar free energy of reduction for these oxides differs considerably, the value for CuO is -24 kcals.mol^{-1} and for NiO is -2.9kcals.mol^{-1}. It was assumed that this provided the driving force for the segregation.

Figure 2.4. : Scanning electron micrograph. Polished cross-section of a fresh monolith catalyst, Q0775

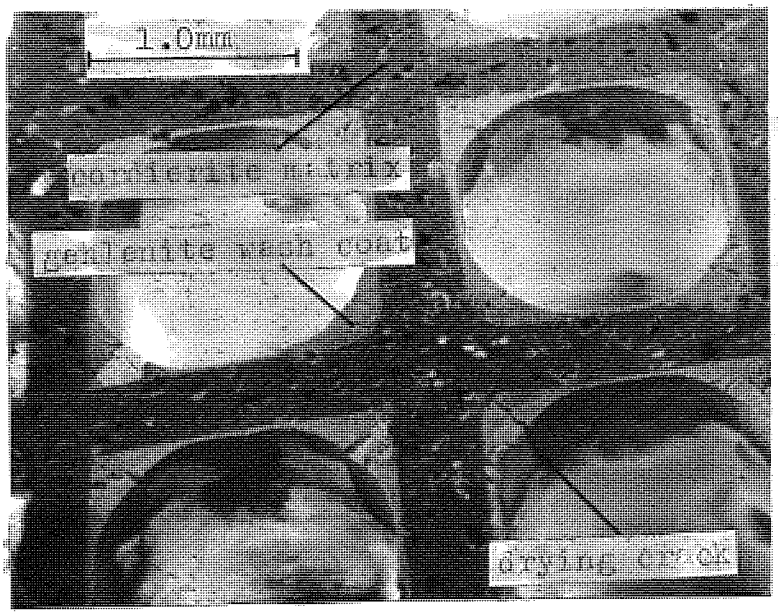

It was found that the concentration of both nickel and copper in the matrix increased during service. After 20 480 km (12 800 miles) the concentration of nickel had increased from 0.5% to approximately 3% although the variation was quite marked, ranging from 1.5% to 4.6%

Figure 2.5. : Composite optical micrograph of a polished cross-section of a fresh monolithic catalyst, Q0775

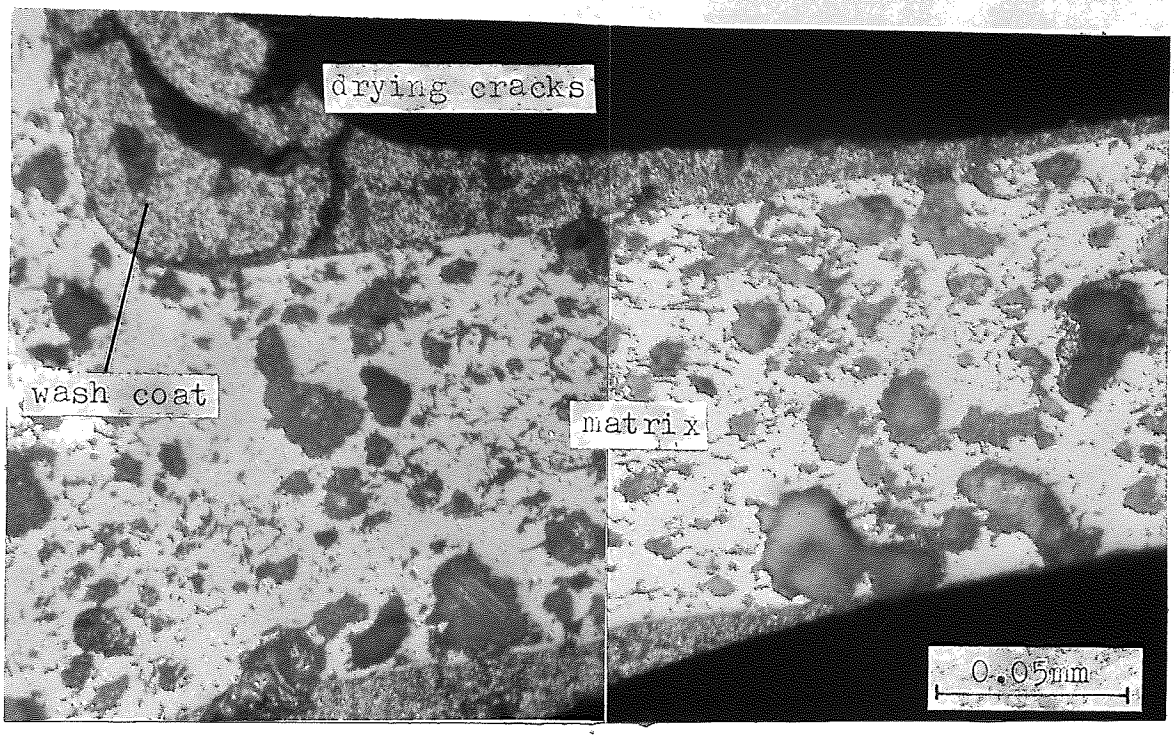

which was probably due to variations in density of the cordierite. The concentration of the copper increased from 0.06% to 0.4% over the same distance. Analyses of a fresh and an aged catalyst are given in Table 2.1.

Examination of the catalysts in the scanning electron microscope showed that the loss of coating usually occurred by cracking of the coating to form discrete islands which broke away from the support as shown in Figures 2.8 to 2.10. Figure 2.10 shows the initial stages in this sequence, the fresh catalyst contained many large drying cracks, but the bulk of the coating was apparently uncracked. After a short time in service, the wash-coat has cracked badly to form discrete islands in Figure 2.9, and some of the thicker material at the cell wall corners has already been lost. Further testing which

Figure 2.6. : Scanning X-ray micrographs of a fresh monolithic catalyst, Q0775, in a Cambridge Microscan V electron probe micro-analyser. The gehlenite wash-coat is clearly defined by the Ni, Cu and Ca-Kα images. The presence of gehlenite and the active species in matrix pores is also shown.

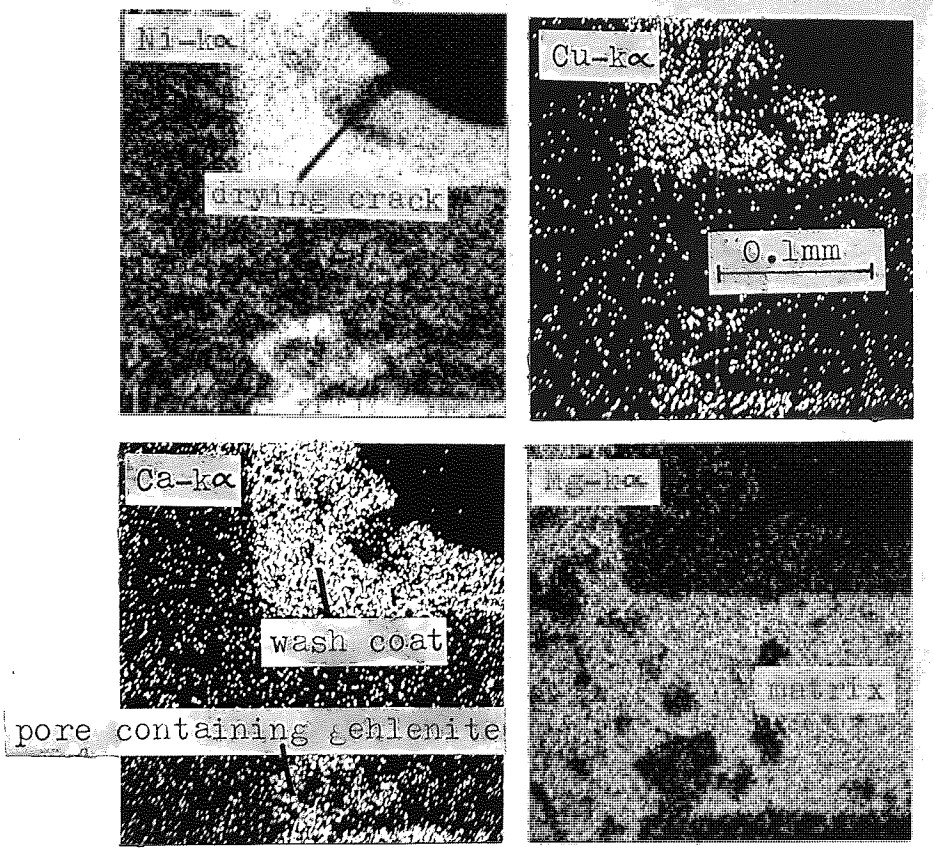

subjects the catalyst to severe vibration in a rapidly moving gas stream results in further loss of the wash-coat with the associated active species as shown in Figure 2.10. In this micrograph, the remains of the wash-coat are seen to be mainly along the centre of the cell walls where the wash-coat was thinnest. Eventually some of the channels were virtually cleared of coating over several millimetres as seen in Figure 2.11. It was observed, however, that frequently such channels were flanked by channels in which the coating was still relatively intact. It can be seen in Figure 2.11 (b) that some of the coating (and active species) usually remained and was seen as debris on

Figure 2.7. : Scanning X-ray micrographs of a catalyst, QO775, after 7680 km (4 000 miles) in service, in a Cambridge Microscan V electron-probe microanalyser. The bulk of the coating which contained the active species has been lost

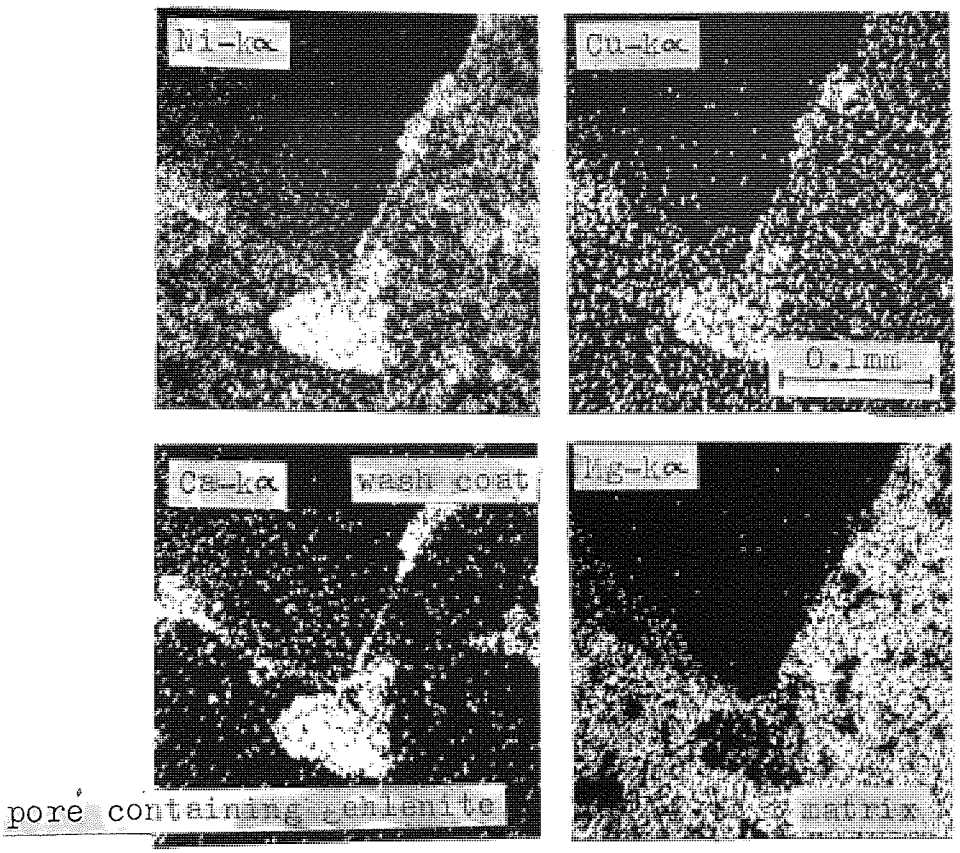

the surface of the primary support even where the channels appeared to be cleared. This was to be expected since the mechanical keying between the coating and the support was good, as shown in Figure 2.12, since the gehlenite containing slurry easily entered the surface pores during the coating operation.

The matrix walls at the inlet face of the catalyst were covered in

Table 2.1. : X-ray micro-analysis of selected areas from a fresh monolithic catalyst, Q0775, and one taken from a vehicle after 7680 km (4800 miles), Q0709.

Catalyst	Area of analysis	Ni(%)	Cu(%)	Ca(%)	Mg(%)	Ni/Cu
Q0775, fresh catalyst	support	0.47	0.057	0.11	10.2	8.2
		0.61	0.063	0.14	11.4	9.7
		0.53	0.069	0.21	6.3	7.7
	wash-coat	33.8	4.8	9.6	0.26	7.0
		32.1	4.0	10.4	2.5	8.0
		30.2	4.1	10.4	2.1	7.4
Q0709, 7680 km (4800 miles)	support	3.2	0.34	0.32	14.3	9.4
		1.7	0.28	0.07	16.0	6.1
		1.4	0.25	0.18	6.0	5.6
	wash-coat, overall	9.8	1.5	6.3	1.9	6.5
		33.2	6.1	8.7	0.85	5.4
		15.7	4.2	7.2	0.43	3.7
		11.8	1.4	11.0	5.4	8.4
Q0709, 7680 km (4800 miles)	Ni-rich "area" in wash-coat	40.0	14.3	2.82	0.45	2.8
		42.9	12.9	2.80	0.033	3.3
		20.8	5.2	3.38	0.26	4.0
		29.8	7.8	3.28	0.35	3.8
		15.7	3.3	4.41	0.13	4.8
		54.4	13.6	3.3	0.13	4.0
	wash-coat	10.7	1.5	12.1	0.86	7.1
		10.5	1.5	10.0	1.4	7.0
		9.4	1.2	11.4	1.1	7.8

a deposit as shown in Figure 2.13 which was found to consist essentially of a mixture of lead oxides and lead phosphates.

The active metal crystallites were observed and a typical structure is shown in Figure 2.14 where the small, spherical metal crystallites

Figure 2.8. : Scanning electron micrograph of a fresh monolithic catalyst, QO775. Note how the coating has collapsed into surface pores in the cordierite

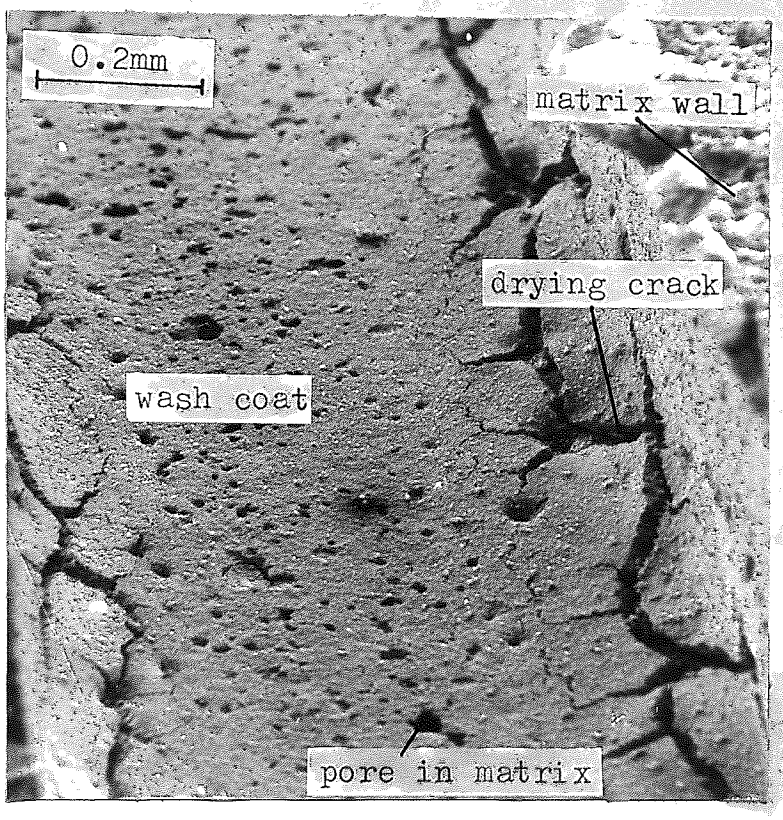

can clearly be seen. The crystallite size after testing is given in Table 2.2, which shows that much of the growth occurred very rapidly after the oxide was reduced to the metal. Because of the nature of the technique, only very small areas were examined and may not be representative of the whole catalyst, but the micrographs reproduced are typical of the structure observed. This is particularly relevant when assessing particle size from the micrographs.

Figure 2.9. : Scanning electron micrograph of catalyst R66 after approximately 160 km (100 miles)

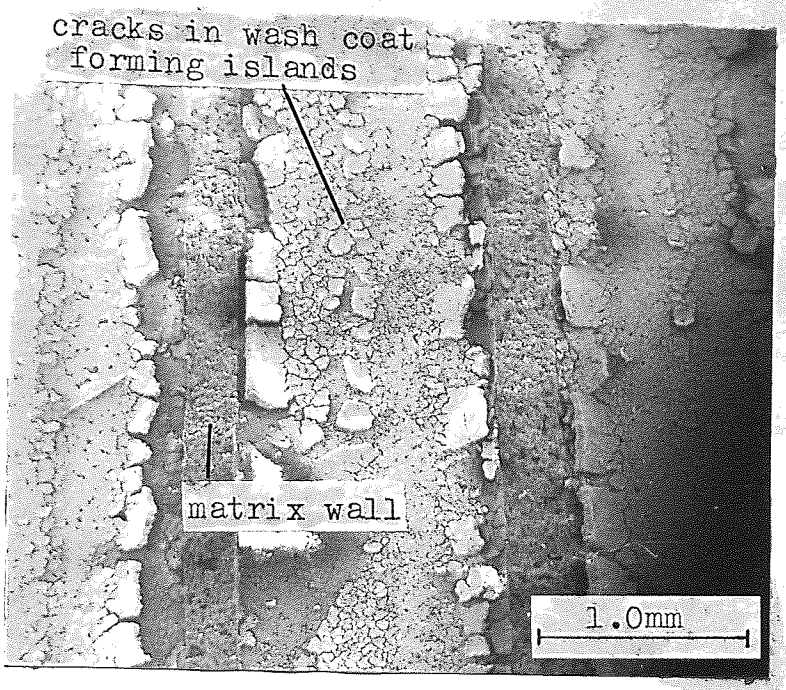

Figure 2.10. : Scanning electron micrograph of catalyst Q0709 after 7680km (4800 miles) in service

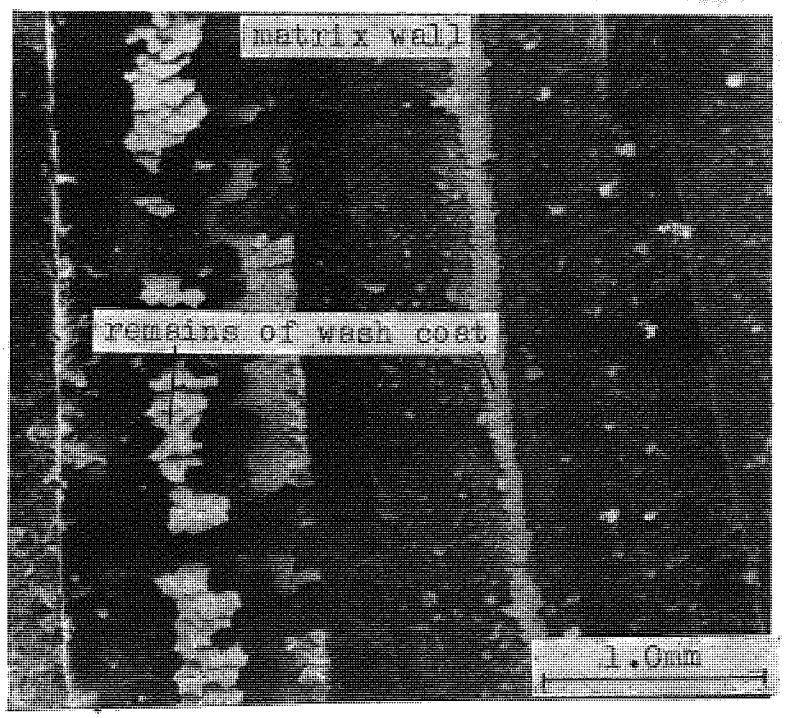

Figure 2.11. : (a) Scanning electron micrograph of catalyst R66 after 20 480 km (12 800 miles)
(b) A higher magnification micrograph showing the highly sintered matrix material with debris from the coating on the surface

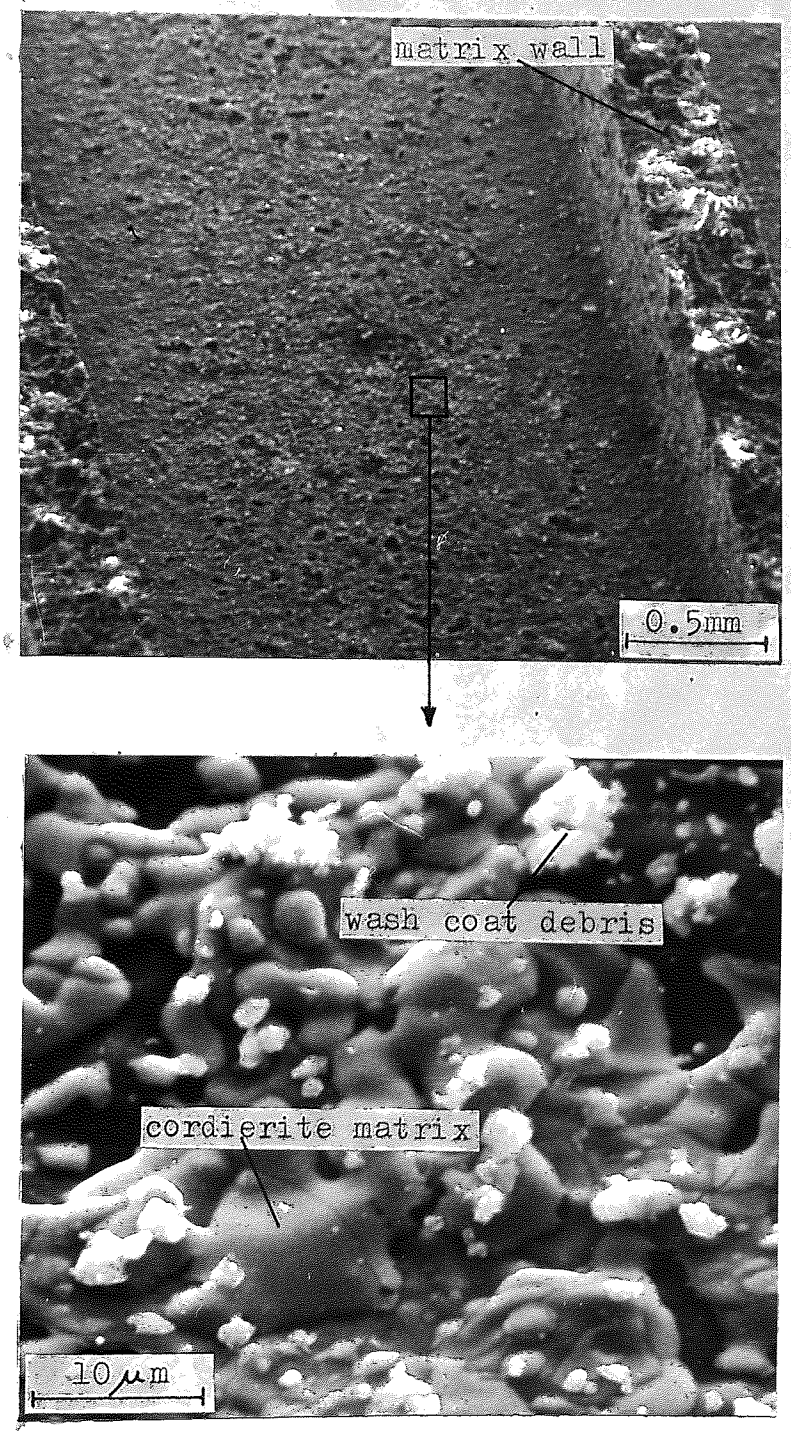

Figure 2.12. : Scanning electron micrograph of a polished cross-section of a fresh monolithic catalyst (Q0775)

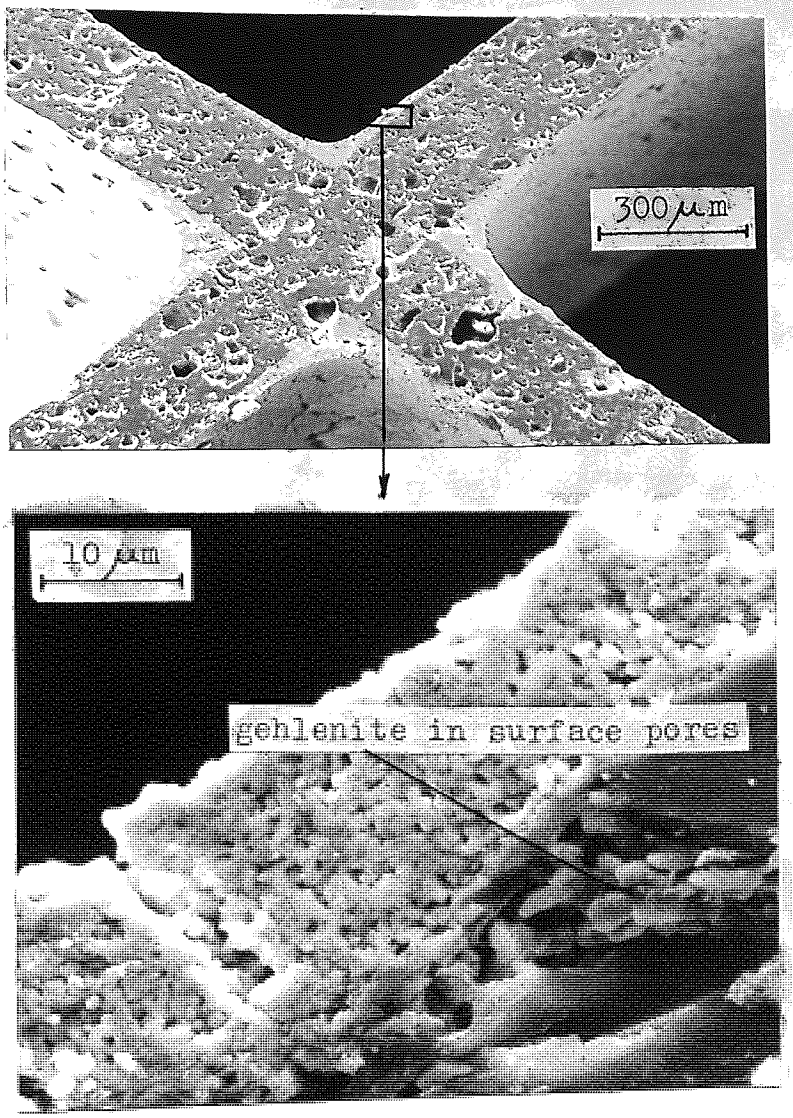

2.3. Catalytic Activity of the Endurance Tested Catalysts

Temperature-activity scans for some of the catalysts are given in Figure 2.15, where it can be seen that the activity was dependent on service conditions rather than service life. The 7680 km (4800 miles) catalyst sample (Q0709) was from 40-50mm away from the inlet face, and that a sample taken from the inlet face would be less active by an unknown factor. It can be seen that the light-off

Figure 2.13. : Scanning electron micrograph of the inlet face of catalyst RX2 after 48 000km (30 000 miles) in service with heavy deposits containing Pb and P.

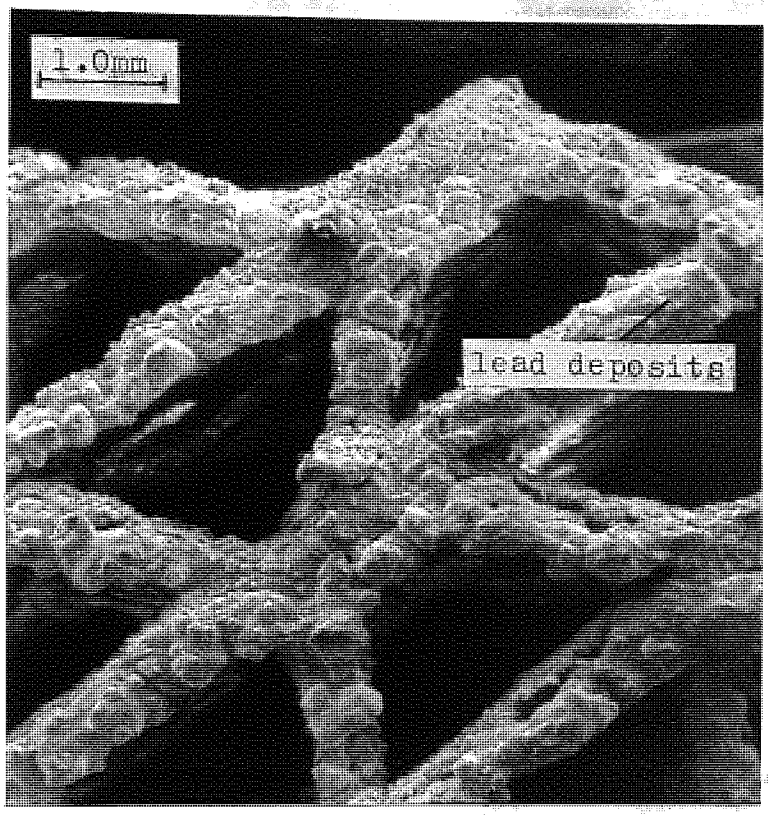

temperature was increased by an amount dependent on the test conditions but conversion at 700°C is still almost complete.

One considers that rate of crystallite aggregation appeared to be negligible by 8000 km (5000 miles) and that the rate of loss of active species was also very slow after this distance, then any further deactivation of the catalyst must have been due to poisoning. This would be dependent not only on the concentration of poisons in the exhaust gas stream, but also on their distribution on the catalyst and chemical composition which are in turn, dependent on temperature, gas flow rate over the catalyst, and exhaust gas

Figure 2.14. : Scanning electron micrograph of an extraction replica from catalyst Q0709 after 7680km(4800 miles) in service

composition. On this assumption a successful catalyst formulation should be such that a high surface area of active species was presented to the exhaust gases after 8000 km (5000 miles) or 170 hours , assuming an average speed of 48km.hr^{-1} (30 mph), by which time the structure would be relatively stable.

2.4. Scope of the Investigation

At the commencement of the project most automobile manufacturers were already looking to the three-way catalysts rather than the dual catalyst system since it would take up less space, and the engine

Figure 2.15. : The catalytic activity for reduction of NO of some endurance-tested catalysts

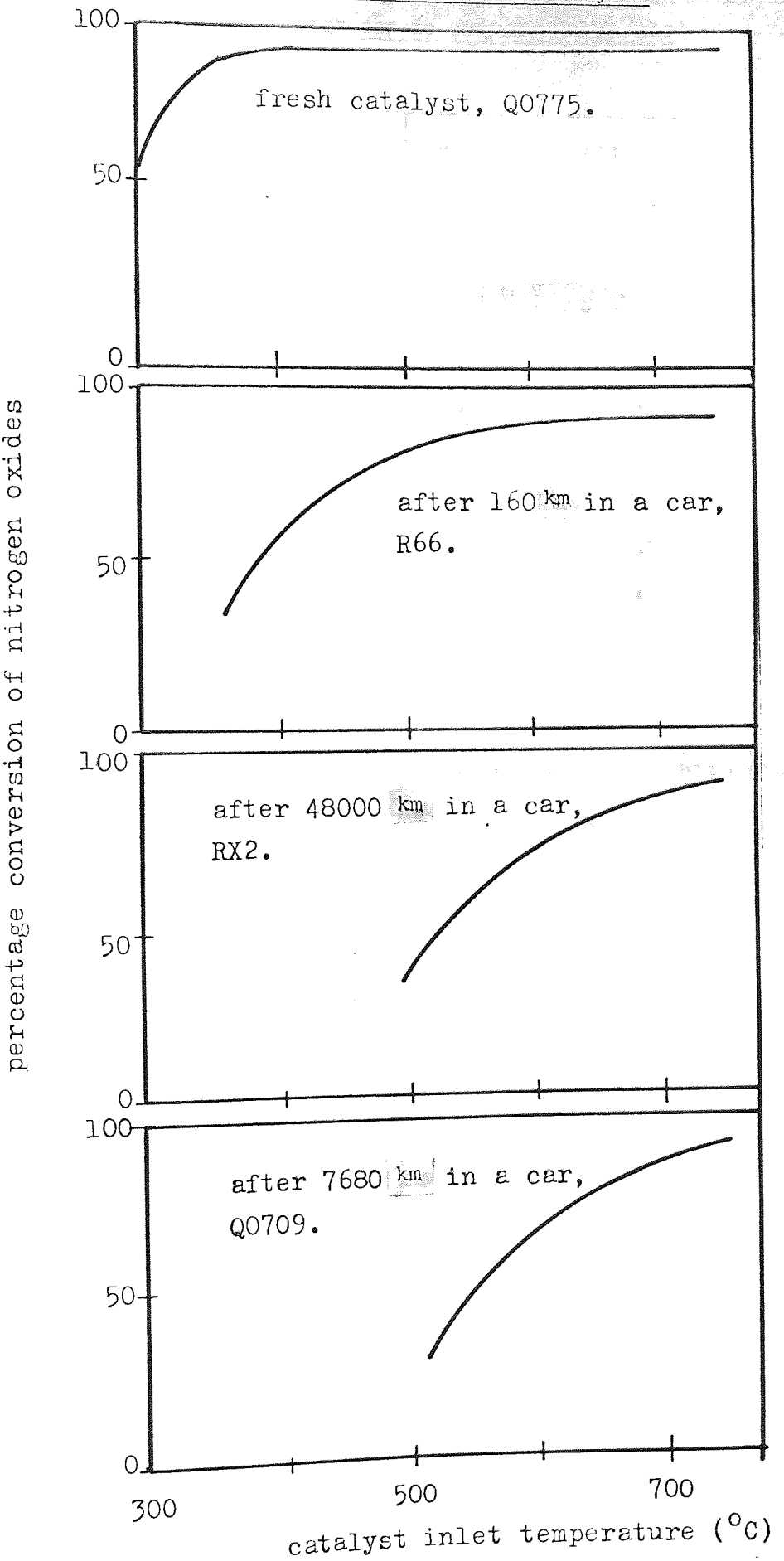

Table 2.2. : Metal crystallite size of the catalysts after removal from cars as a function of mileage (*inlet temperature high due to use of excess air)

Catalyst	Test mileage km (miles)	Metal Crystallite size (μm)
Q0775	0	0.05
R66	160 (100)	0.3
Q0709	7680 (4800)	0.50
RX1	20480 (12800)	0.36

could be run with a leaner air-fuel ratio. There were a number of problems to be solved, however, and by this time, ICI, for a number of reasons did not wish to pursue the development of their base-metal reduction catalysts and B L Cars, not wishing to commit themselves completely to the unproven three-way catalyst, arranged this jointly sponsored project. The present catalyst as described above was the result of a considerable amount of experimental work by ICI, both in the laboratory and on engine test-beds, and the present investigation must be viewed in the light of this effort. The supervisory committee decided that since the time available was restricted, the investigation should concentrate in the first instance on the deactivation of granules (to eliminate the wash-coat effects) in a sterile atmosphere. It was agreed that the areas of study should include the effects of thermal ageing in a synthetic exhaust at and above service temperatures, on metal crystallite aggregation and its relation to activity. The effects of total metal content of the catalyst and the effect of the nickel-copper ratio on the stability of

the structure were to be investigated. It was also agreed to test and examine a series of matrix catalysts to investigate the causes of the loss of wash-coat, and to maintain a link with the complex real conditions in which the catalysts must work.

3. EXPERIMENTAL

3.1. Experimental Catalysts

Gehlenite granules, designated Q1005 made from 3mm diameter rod chopped to pass through a B.S.S. 5-7 sieve were obtained from ICI Ltd. A sample of Q1005 granules were impregnated by ICI with 17.2% nickel oxide and 2.3% of copper oxide and designated Q1006. All other granular catalyst samples were prepared from Q1005 by impregnating with copper and nickel nitrates (Analar Reagents, British Drug Houses Ltd.) to give total metal oxide loadings of from 2.5% to 50%. Nickel-copper ratios ranged from 5% to 75% copper. The catalysts designated G1 to G14 were chemically analysed as a check on metal contents, the nominal formulations of the catalysts are shown in Table 3.1.

Table 3.1. : Nominal formulation of the granular catalysts

Catalyst Batch no.	Total metal content (%)	Ni/Cu
G1	20	Nickel only
G5A	20	19
G6	20	9
G8	20	1
G9	20	0.3
G13A	50	3
G14	20	3
G16	10	3
G16A	5	3
G17	2.5	3

The strengths of the solutions used were normally such as to give

the desired concentration with one immersion. However, the 50% metal oxide catalyst sample required several impregnations. After 5 minutes soaking in the aqueous solution the granules were removed and rolled between absorbent paper to remove the surplus solution, dried at 80°C and then calcined at 500°C to a constant weight (usually about 4 hours).

A series of monolithic catalysts, designated M1-M6 were prepared by ICI to the composition shown in Table 3.2 for testing in an engine dynamometer. A photograph showing the physical form of a selection of catalysts is shown in Figure 3.1.

Table 3.2. : Formulation of the monolithic catalysts prepared by ICI for engine dynamometer testing

Catalyst Sample no.	Total metal loading (%)	Weight fraction of coating materials (%)	Ni/Cu
M1	0	7.5	-
M2	15.1	7.0	9
M3	14.3	8.0	5
M4	12.5	4.7	4
M5	4.8	7.2	3
M6	17.1	5.7	4

3.2. The Ageing Rig

3.2.1. Catalytic Reactors

The ageing rigs are shown in Figure 3.2. They consisted of two wire-wound furnaces controlled by West Thyristor control units which contained the catalytic reactors. The associated gas analysers were

Figure 3.1. : Typical catalyst samples analysed in the present investigation

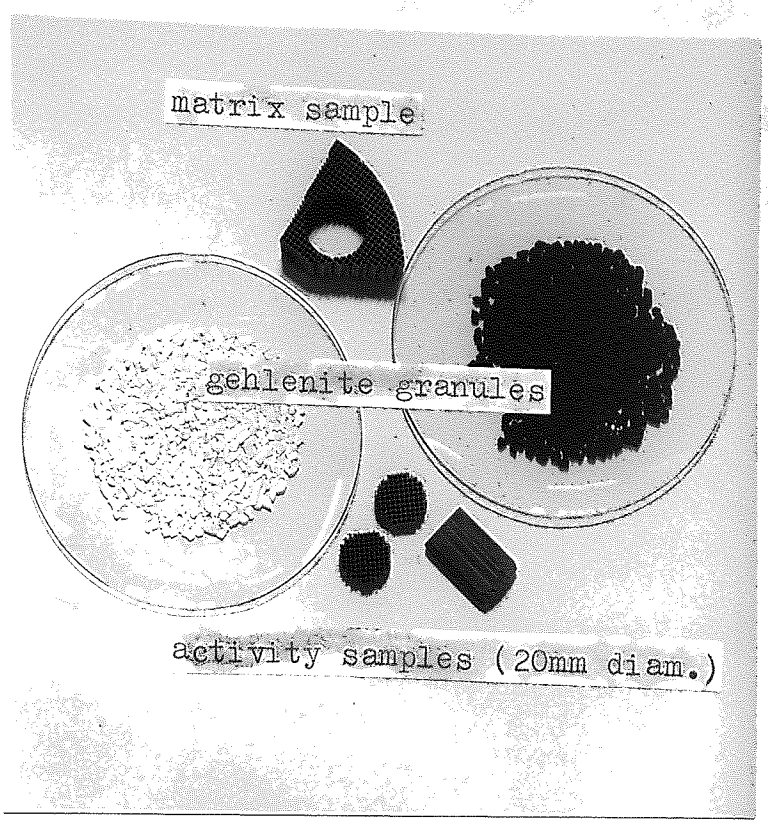

connected to the reactors via a console unit which also contained filters, condensers and pumps. The catalytic reactor used for this work is shown schematically in Figure 3.3, At present, two are in use. They consist essentially of two Concentric 310 type stainless steel tubes as shown in Figure 3.4, the inner tube actually being the sample holder is 20mm internal diameter. Provision was made for sampling the gas stream before and after passing over the catalyst. The sample is set back from the hot zone of the furnace, and the outer tube contains a 31mm diameter, 150mm long codierite matrix which acts as a pre-heater to heat the gas to the required temperature before contacting the sample. This ensures the axial and radial temperature gradients in the sample are kept to a minimum ; the

Figure 3.2. : Photograph of the ageing rig showing the two reaction furnaces, the main console unit and the gas analysers

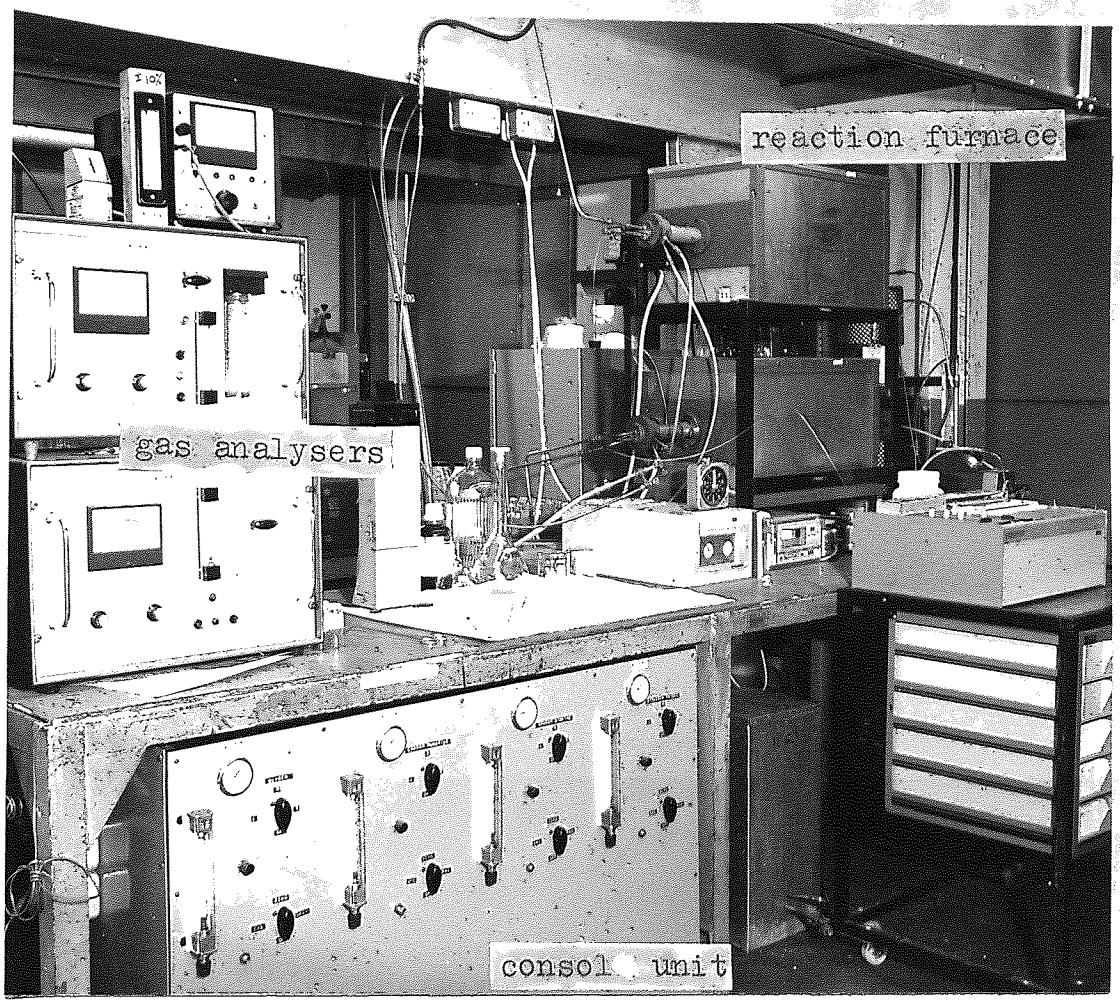

temperature distribution in a matrix-type sample produces a $10^{o}C$ difference from the centre to the edge and $15^{o}C$ difference from the leading edge to the back.

The synthetic exhaust gas was based on nitrogen from a liquid nitrogen tank ; the other components, except for water, were added in a blender which brings about counter-current mixing and in which there is a system of baffles to ensure thorough mixing of the gases.

Figure 3.3. : Schematic view of reaction furnace

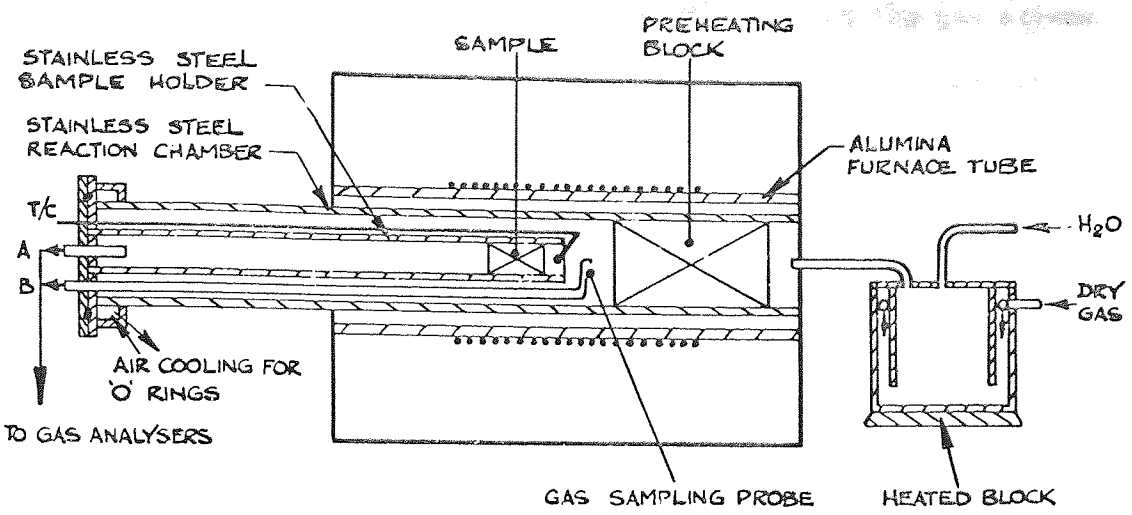

Figure 3.4. : The sample holder assembly ready for insertion into the stainless steel reaction chamber. The alumina furnace tube with the furnace windings and the reaction chamber have been removed from the furnace for maintenance

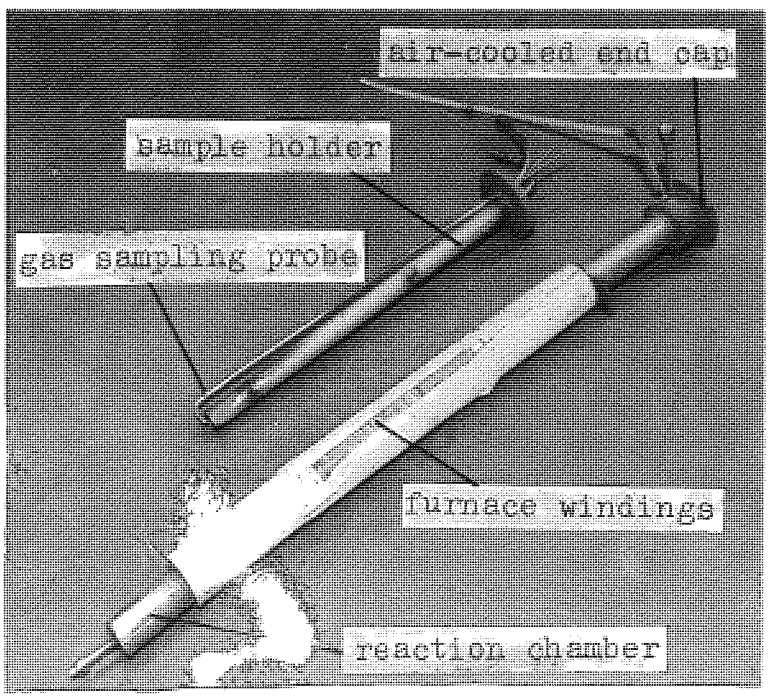

Water vapour was added to the gas stream separately just before the gas enters the furnace. A peristaltic pump supplied water at a constant known rate, to a heated, enclosed pot, and the gas stream passed into the pot through a perforated tube to ensure thorough mixing. Unless otherwise stated, all activity measurements and thermal ageing were carried out in a synthetic exhaust gas, the composition of which was :

0.25% O_2 ; 10% CO_2 ; 10% H_2O ; 2.5%CO ; 1500ppm ; balance N_2

The gas stream was then passed through the pre-heating zone and over the catalyst sample. One thermocouple was placed immediately in front of, and another behind the sample to monitor the gas temperature.

3.2.2. Gas Analysis

The gas was sampled before and after the catalyst at every data point. The gas sample was drawn through a condenser to remove the bulk of the water, and then passed through a second condenser and a fine glass fibre filter (Whatman, GF/A). It was then pumped to the gas analysers at a controlled flow rate. The gas flow system is shown in Figure 3.5. Carbon monoxide and carbon dioxide were measured using infra-red analysers (The Analytical Development Company Ltd.), nitric oxide by a chemiluminescent analyser (Luminex, BOC Ltd.) and the oxygen by a method dependent on the paramagnetic susceptibility of oxygen (Taylor Servomex). Ammonia was determined by a wet-chemical analysis. A measured amount of gas was passed for a set time through a known volume of demineralised water in the first condenser. The concentration of ammonia in the water was then determined colourimetrically using Nessler's reagent (BDH-Lovibond Comparator method).

Figure 3.5. : A schematic view of the gas-flow path into the reaction furnace and the analytical equipment

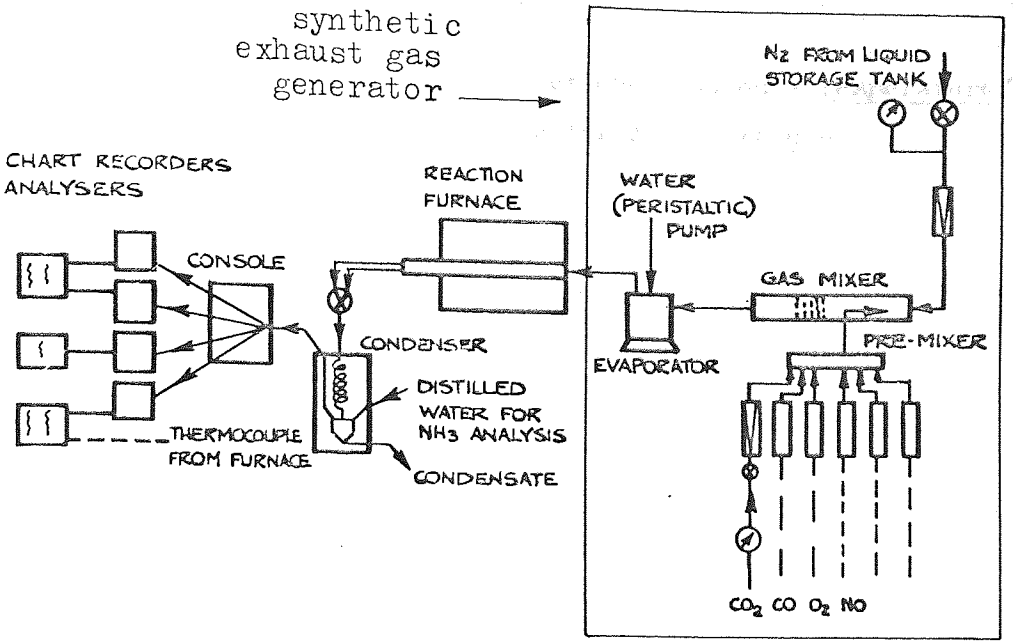

3.3. Activity Testing Procedure

A given volume of the granules (9.3cc, equivalent to 7.5gms Q1006) or a constant length of matrix samples, was placed in the specimen holder and secured with 3mm long sections of 20mm diameter cordierite matrix which fitted the specimen holder exactly. In order to determine the effect of time and temperature on particle growth, the samples were then aged in the synthetic exhaust atmosphere at temperatures ranging from 650°C to 1000°C for up to 250 hours. Periodically, the temperature was reduced to 500°C for measurement of the catalytic activity of the samples at a space velocity of $10^5 hr^{-1}$. This particular temperature was chosen because of the activity/temperature response curve. At 500°C conversions were sensitive to catalyst condition, and were in the range 40-70%. More usually, the activity was measured over the temperature range 300°C to 700°C, and the results from this procedure will be referred

to as a temperature/activity scan. All activity testing was carried out using the standard synthetic exhaust gas unless otherwise stated.

Figure 3.6. : The hysteresis effect observed on a temperature/activity scan for Q1006 granules

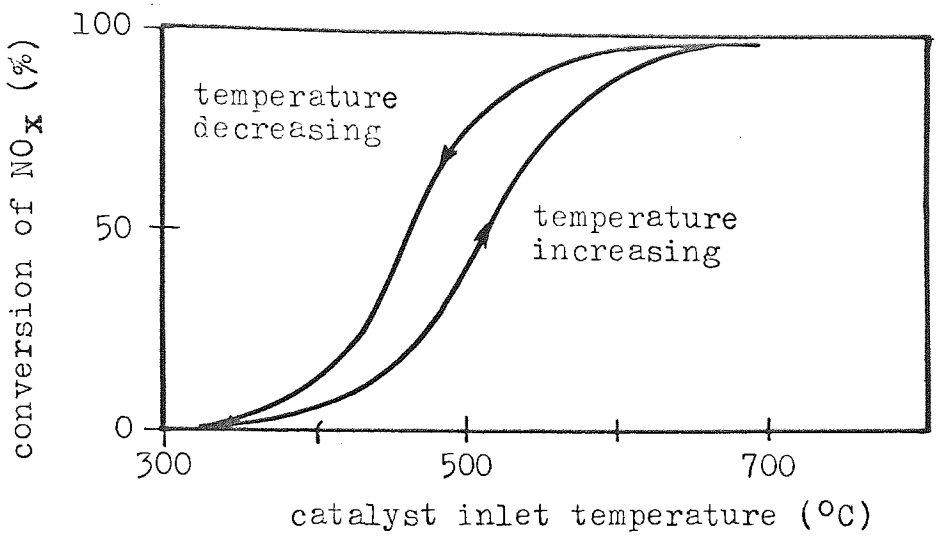

Continuous recording of the NO content of the outlet gases and the catalyst temperature showed that at low temperatures (essentially $< 500^{o}C$) there was a time lag before the NO content attained equilibrium at the set temperature. This gave rise to a hysteresis effect as shown in Figure 3.6, and was probably due to the partial oxidation of the catalyst surface and subsequent reduction on returning to temperatures greater than $500^{o}C$. In order to obtain consistent results, a procedure was adopted whereby all catlysts were held at $700^{o}C$ for 30 minutes before being brought to the test temperature. The only exception to this rule was made for those catalysts aged below $700^{o}C$, which in this case, were held at the ageing temperature overnight, prior to testing.

Conversion data for the catalysts was correlated by use of the empirical power-law rate equation :

$$r = k_2 p^a \qquad \ldots\ldots\ldots 3.1.$$

and the mass balance equation for integral, plug-flow reactors :

$$\frac{V}{F} = \int_0^x \frac{dx}{r} \qquad \ldots\ldots\ldots 3.2.$$

The integrated forms of equation 3.2, after substitution of equation 3.1 are :

$$\text{for } a \neq 1, \quad k_2 = H \cdot \frac{X_o^{(1-a)}}{1-a} \; 1-(1-x)^{1-a} \qquad \ldots\ldots\ldots 3.3.$$

$$\text{and for } a = 1, \quad k_2 = H \ln(1/1-x) \qquad \ldots\ldots\ldots 3.4.$$

By using a blank change of unimpregnated pellets, the catalytic response of the furnace was determined and it was found that at 750°C, some 5% of the nitric oxide was converted with no measurable formation of ammonia. This decreased as the temperature was lowered so that at 650°C only 2% conversion was observed. Again, no ammonia was detected.

3.4. Physical Examination

Three techniques for following the aggregation of the active metal crystallites in the matrix catalysts were considered. The first was scraping the wash-coat from the matrix and dispersing the powder on a formvar film for examination by transmission electron microscopy (TEM). The second was removal of the wash-coat by a plastic film technique and examination of the extraction replica by TEM or scanning electron microscopy (SEM). Finally, direct examination of the surface of a small section of the coated matrix by SEM.

Difficulties in the interpretation of the structures were experienced using the first technique and the ceramic particles were too large for selected area electron diffraction. In the light of work carried out using the SEM it was considered that the small metal crystallites were too closely associated with the ceramic support particles to be viewed properly by transmission techniques since the ceramic particles were much larger and opaque to the electrons at the accelerating voltage of 20KV used. The other two techniques were similar, but one involved examination of a fresh surface whereas the latter involved examination of the surface presented to the exhaust gases. No differences between the structures were observed in the scanning electron microscope, and since examination of the whole matrix gave additional information about the coating, and did not involve lengthy specimen preparation, it was decided to use this technique.

Similar considerations were applied to examination of the granules but in this instance, the whole crushed granules were dispersed on the formvar film for examination by TEM, and the internal surface was examined simply by breaking the granule. It was decided in this case that the cross-section of the granules gave more consistent results because of the presence of dust on the outer surface of the granules caused by attrition during handling and testing. Again, no significant difference in size or morphology of the structures was detected. Metal particle sizes were found by measuring up to 50 particles in each of several areas, to give a total number of particles counted of between 300 - 500. The results were sorted into about 12 size classes and expressed as a cumulative number distribution, the mean particle size was defined as the value below which 50% of the particles occurred.

All surface areas were determined by Imperial Chemical Industries Ltd. at their Agricultural Division Research and Development Laboratory, Billingham, using a Micromeritics model 2200 surface area analyser, and Krypton adsorbate.

3.5. Thermal Ageing

Thermal ageing of the catalysts was carried out in one of two ways. The first, pure thermal ageing, was carried out in situ in the ageing rigs, using the standard synthetic exhaust so that the samples were not subject to vibration or catalyst poisons. The effect of thermal ageing depended both on the time and temperature, but was not the product of the two. Over the time scale considered there was a limit to the change in metal crystallite size, dependent on the temperature, and hence on the degree of deactivation of the catalyst.

The second ageing procedure was carried out in engine dynamometer rigs, and so samples were subjected to thermal effects, vibration and poisons.

The catalysts M1-6 were sectioned axially so that a segment from each of the 6 samples could be cemented together to form a standard-sized catalyst, 4 ins. by 3ins. long, as shown in Figure 3.7. This was then mounted in an 18/8 stainless steel box supported by woven "Knitmesh", a stainless steel wire mesh which was a standard procedure used at the British Leyland Air Pollution Control Laboratory. This arrangement is shown in Figure 3.8. Testing was carried out using a 1.8L Marina engine automatically controlled to cycle between fast running and slow running conditions to give recorded catalyst temperatures of

between 800°C and 600°C. The fuel contained 0.013g.L^{-1} (.05g.gal^{-1}) of Pb so that the engine would produce about 10g of lead over 5 000 miles. The total cycle time was 70 secs. which gave approximately 8 500 cycles during a simulated 5000 mile test. Exhaust gas composition and engine speed are also shown in Table 3.3.

Figure 3.7. : The segments of catalysts M1-6 prior to the cementing together to form a standard-sized catalyst block

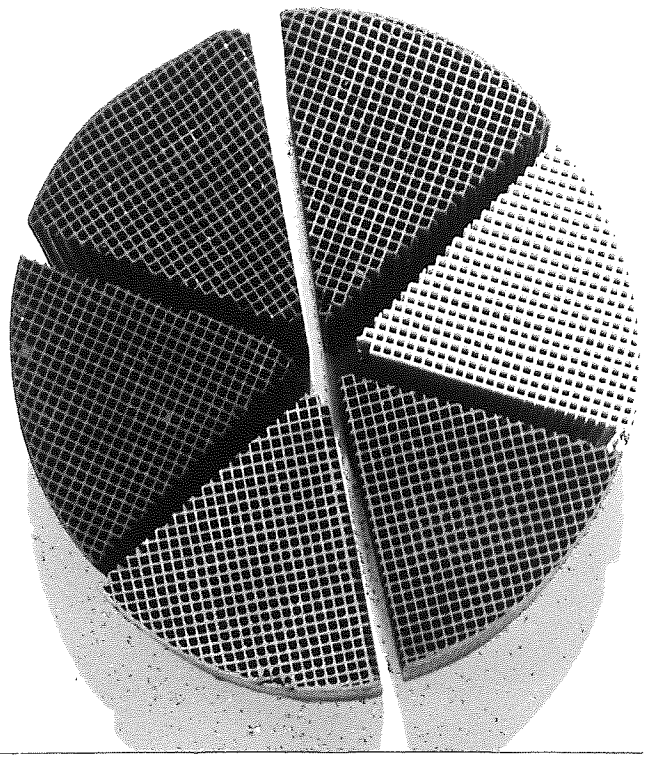

Table 3.3. : Experimental parameters for the engine dynamometer tests

dynamometer tests

		Slow running	high-speed running
Catalyst inlet temperature		576°C	811°C
engine speed		1200rpm	3400 rpm
Exhaust gas analysis	O_2	1.5%	0.65%
	CO	0.64%	0.31%
	HC	340ppm	120ppm
	NO_x	110ppm	3050ppm

Figure 3.8. : A catalyst exhaust box which has been cut open after testing to remove the catalyst

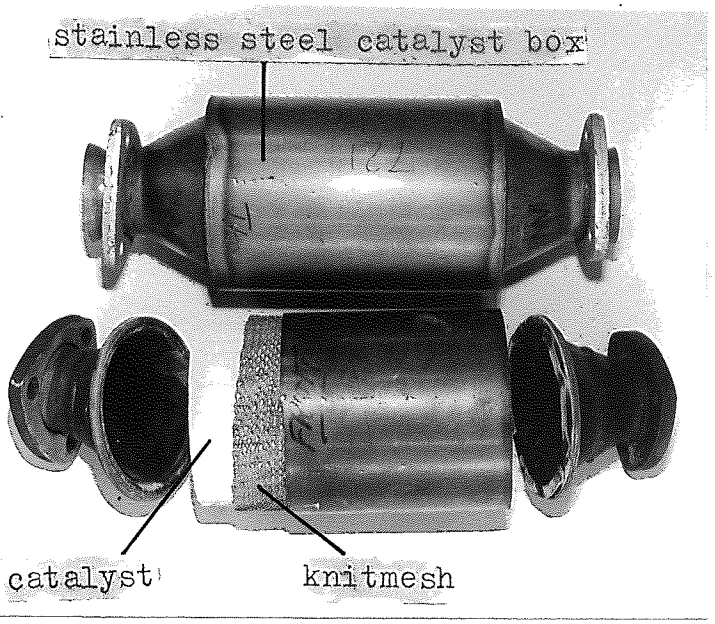

Catalysts M7-M13 were also tested in this way but samples M21-M23 were presented to the exhaust gas in a different manner. 20mm diameter samples were trepanned from the catalysts and these were inserted into a carrier. This was an uncoated catalyst block drilled to accept twelve 20mm x 15mm long samples. Four of these were stacked to form a composite block and tested in the above manner. A photograph of samples tested in this arrangement is shown in Figure 7.9.

4. THE THERMAL AGEING OF GRANULAR CATALYSTS

4.1. The Deactivation of Q1006 Granules by Thermal Ageing

Thermal ageing at temperatures between 650-1000°C displaced the temperature activity curve for Q1006 to higher temperatures, as shown for 1000°C in Figure 4.1. The "light-off" temperature (the temperature at which 50% conversion occurs) is an important practical parameter in convertor design. However, for the purpose of comparing catalytic activities of different catalysts, the reaction rate constant, k_2, derived from equations 3.3 and 3.4, is more correctly used. Under a wide range of conditions, the reduction of nitric oxide over nickel-copper catalysts has been shown to be approximately of first order, therefore k_2 was calculated from equation 3.4, and the change in the value of this parameter used to assess the effect of thermal ageing on Q1006 granules. In Figure 4.2, the reaction rate constants have been normalised with respect to their initial values and plotted

Figure 4.1. : The activity of Q1006 granules after ageing in the synthetic exhaust gas at 1000°C as a function of temperature. (1) 0hr; (2) o.15hr; (3) 0.5hr; (4)24hr.

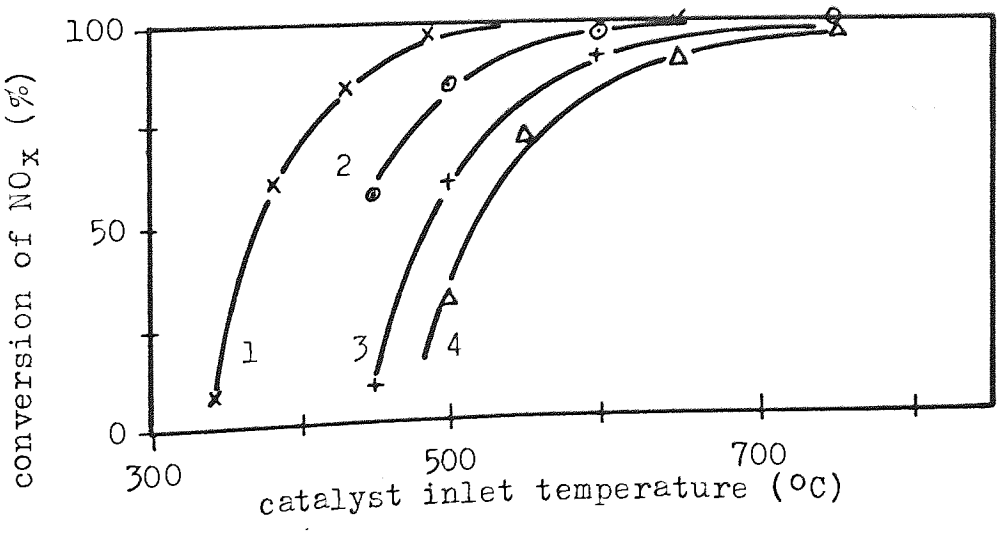

against ageing time. It should be noticed that in Figure 4.2(b) the scale on the time axis is smaller by a factor of ten than in Figure 4.2(a). There was apparently a limiting value to the decrease in activity of the catalyst for practical purposes, indirectly proportional to the ageing temperature.

Figure 4.2. : The deactivation of Q1006 granules after thermal ageing in the synthetic exhaust gas as a function of ageing time: (a) ageing temperature of 800°C and below ; (b) ageing above 800°C

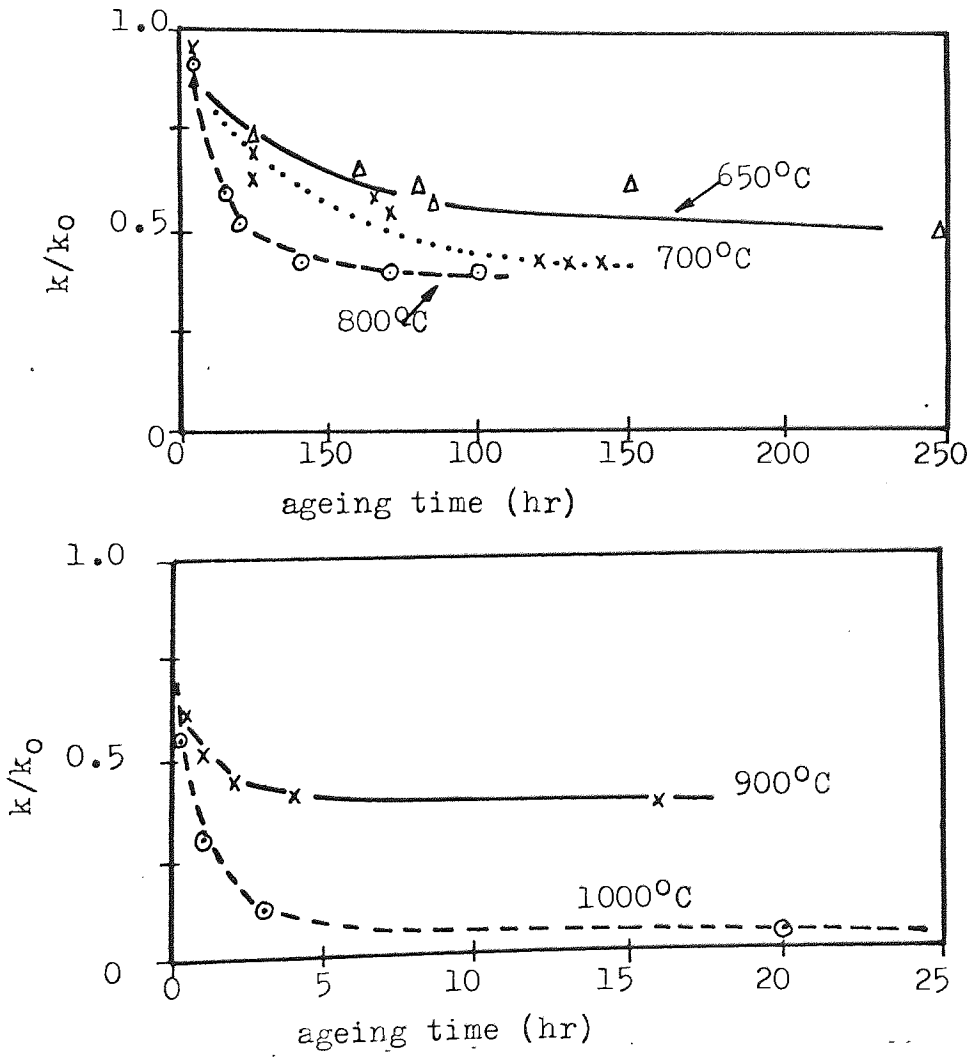

This means that a few minutes at 1000°C is equivalent to 24 hours at 800°C or 250 hours at 650°C, i.e. the catalyst has lost approximately

50% of its original activity at a reaction tepmerature of 500°C. Of course, Figure 4.1. shows that even after 24 hours at 1000°C in a sterile atmosphere, the catalyst is still capable of close to 100% conversion of nitric oxide at reaction temperatures above 700°C. Intuitively, however, the aged catalyst would have fewer available active sites because of the decrease in surface area, and it would have a lower resistance to poisoning.

4.2. The Structure of Q1006 Granules

4.2.1. Optical Microscopy

The freshly impregnated granules were a reddish brown colour due to the presence of nickel and copper oxides. After ageing or testing in a reducing atmosphere, the metal oxides were reduced and the colour of the granules changed to black or dark grey. Streaks of a lighter, straw colour near the front of the catalyst bed indicated that some nickel oxide was still present. This is a feature of these catalysts. Near the front of the bed, the presence of oxygen in the exhaust gas maintains the catalyst in an ineffective oxidised condition. The oxygen reacts with the carbon monoxide, and once used up, the nickel oxide may then be reduced to the active metal as described in Figure 4.3. In a fresh catalyst the active species was not resolved in the optical microscopy. It was just possible to resolve the larger particles in the aged catalysts, using an oil-immersion objective to give magnification of X960. The active metal species had a high reflectivity compared to the oxides, so that it was easily recognisable. The maximum size varied considerably with occasional

Figure 4.3. : The situation at the inlet face of a catalyst in overall reducing conditions in the presence of oxygen. Reduction of the oxide is necessary for the catalyst to be active (51)

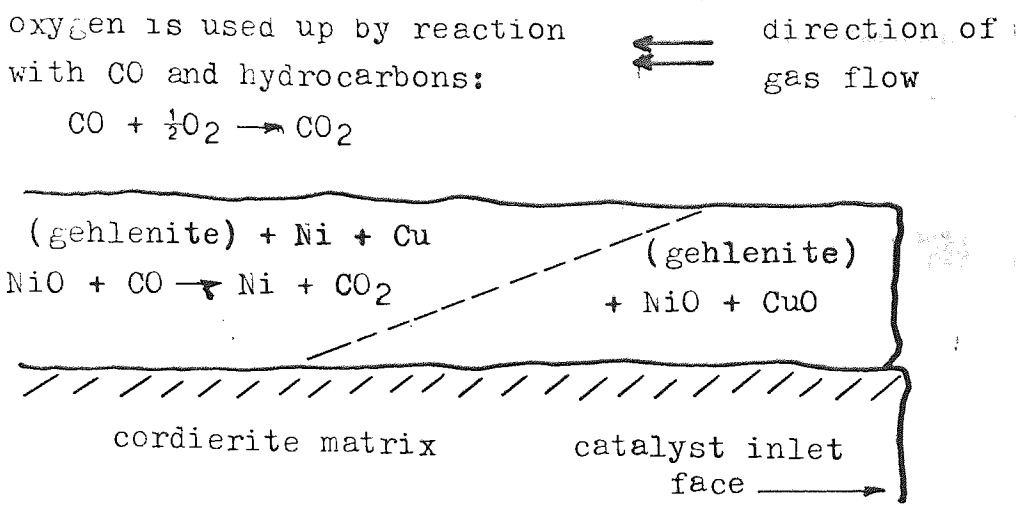

particles as large as 10μm metal compared with the ceramic. It was observed that the metal was not homogeneously distributed in all the granules, but formed a shell in many samples of approximately 1mm thick around a central core which contained no metal. Many of the Q1005 granules contained cracks from the manufacturing process which acted as channels for the solutions of nitrates during the impregnation stage. In these granules the active species were found to have penetrated throughout the whole of the granule.

4.2.2. X-Ray Diffraction Analysis

X-ray diffraction analysis of a powder from several whole, crushed granules, aged for 100 hours at 800^{o}C showed that the nickel oxide had been substantially reduced to the metal, no elemental copper was positively identified because of the small amount present, and the interference of overlapping lines from the gehlenite. The copper would be expected to have alloyed with the nickel since impregnation from the double nitrate solution brings the metals into intimate

contact. Several lines indicating possible traces of iron spinel and anorthite ($CaO.Al_2O_3.2SiO_2$) were present in the original gehlenite and remained after ageing. One unidentified, very weak line did appear during ageing at d = 2.15 Å. This was not due to compounds formed from the reaction of the active species with the support material to form nickel or copper aluminates.

4.2.3. Scanning Electron Microscopy

All the aged samples were examined in cross-section, and on some of the granules, comparisons were made with the external surface, but generally no definite trends in metal crystallite size with distance from the surface were observed. It was also found that no differences were observed between the microstructure of the fully reduced catalysts and those which exhibited the colour streaking referred to above. The porous nature of the granules is shown in Figure 4.4, but it will be shown later (Chapter 5) that the nitrate solutions do not easily penetrate further than 1.0 mm into the granules. The size of the metal oxide crystallite in a fresh sample of Q1006 is shown in Figure 4.5.

The scanning electron micrographs in Figure 4.6 from specimens aged at temperatures from 650°C to 900°C show that, in general, the morphology of the metal crystallites was similar throughout all the catalysts, although there were instances when cuboidal rather than spherical crystallites were observed, as in Figure 4.6(d). Where these cuboidal or angular crystallites were formed, they were always closely associated with the spherical crystallites, and no significant difference in the proportion of nickel and copper were found by x-ray energy dispersive analysis so that it was not possible to attribute any significance to the shape. It was possible that the angular crystallites had not been reduced during ageing. Surface

Figure 4.4. : Scanning electron micrograph of a fracture face of a fresh Q1006 granule

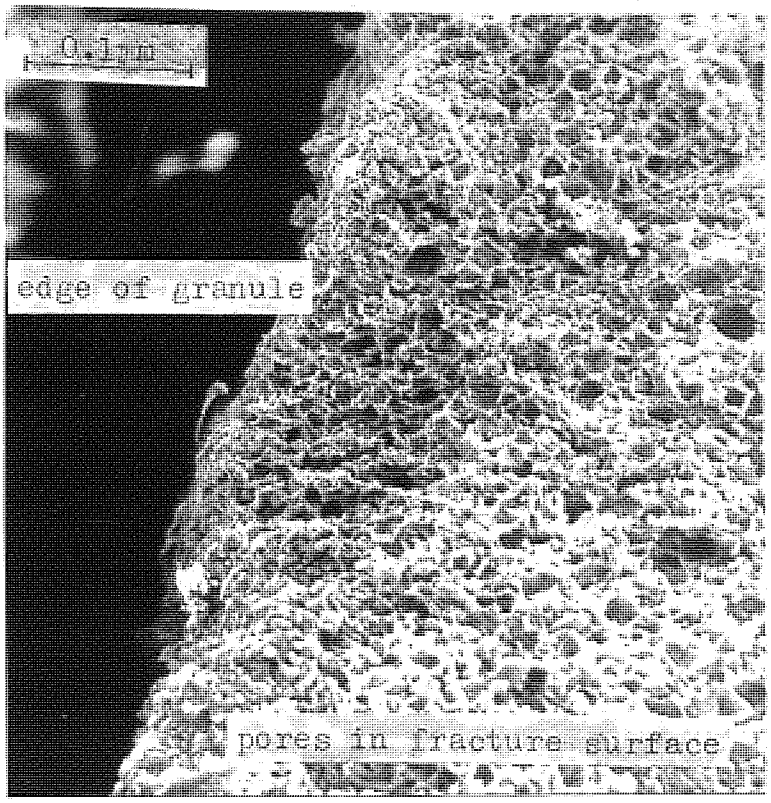

Figure 4.5. : Scanning electron micrograph of a fracture face of a fresh Q1006 granule. The metal oxide crystallites are supported by, and outline the gehlenite granules

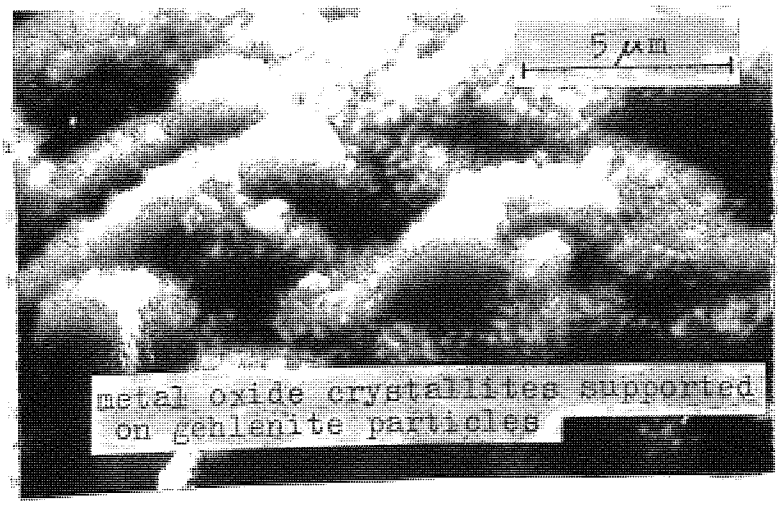

energy considerations suggest that metal crystallites at the ageing temperatures would have sintered to give the lowest surface to volume ratio, i.e. in the form of a sphere.

It can be seen from Figure 4.6 that the size of the metal crystallites was proportional to the ageing temperature, and a discussion of the effect of thermal ageing on the mean particle size is given below in Section 4.2.4. Catalyst poisons were deliberately eliminated from the synthetic exhaust gas ; therefore it was assumed that the deactivation reported above was due entirely to the loss of surface area of the active species, due to aggregation of the metal crystallites. X-ray fluorescence analysis did, in fact, show sulphur and phosphorus to be present in the fresh Q1006 granules to the extent of between 0.02 and 0.05%, together with very small trace amounts of potassium and chlorine. Despite the presence of these poisons a correlation was shown to exist between the catalytic deactivation and the increase in particle size as discussed below in Section 4.2.4.

X-ray energy spectra for the large metal crystallites, shown in Figure 4.7, and the surrounding substrate were obtained from the scanning electron microscope with a Kevex attachment. These are shown in Figures 4.8 and 4.9. It can be seen that the large spheres were rich in nickel and copper with some calcium, aluminium and silicon, since the analyses were carried out using an accelerating voltage of 20KV which would cause x-rays to be emitted from a depth of about 1 μm. The spectra from the metal particles were often seen to contain peaks due to the constituents of the gehlenite. X-ray diffraction analysis did not show any chemical reaction between the nickel and copper and the gehlenite so that the spherical particles may be confidently assumed to be a nickel-copper alloy.

Figure 4.6. : Scanning electron micrograph of a fracture face of Q1006 after thermal ageing in the synthetic exhaust gas. The small ($< 1\mu m$) metal crystallites are supported on the larger gehlenite particles

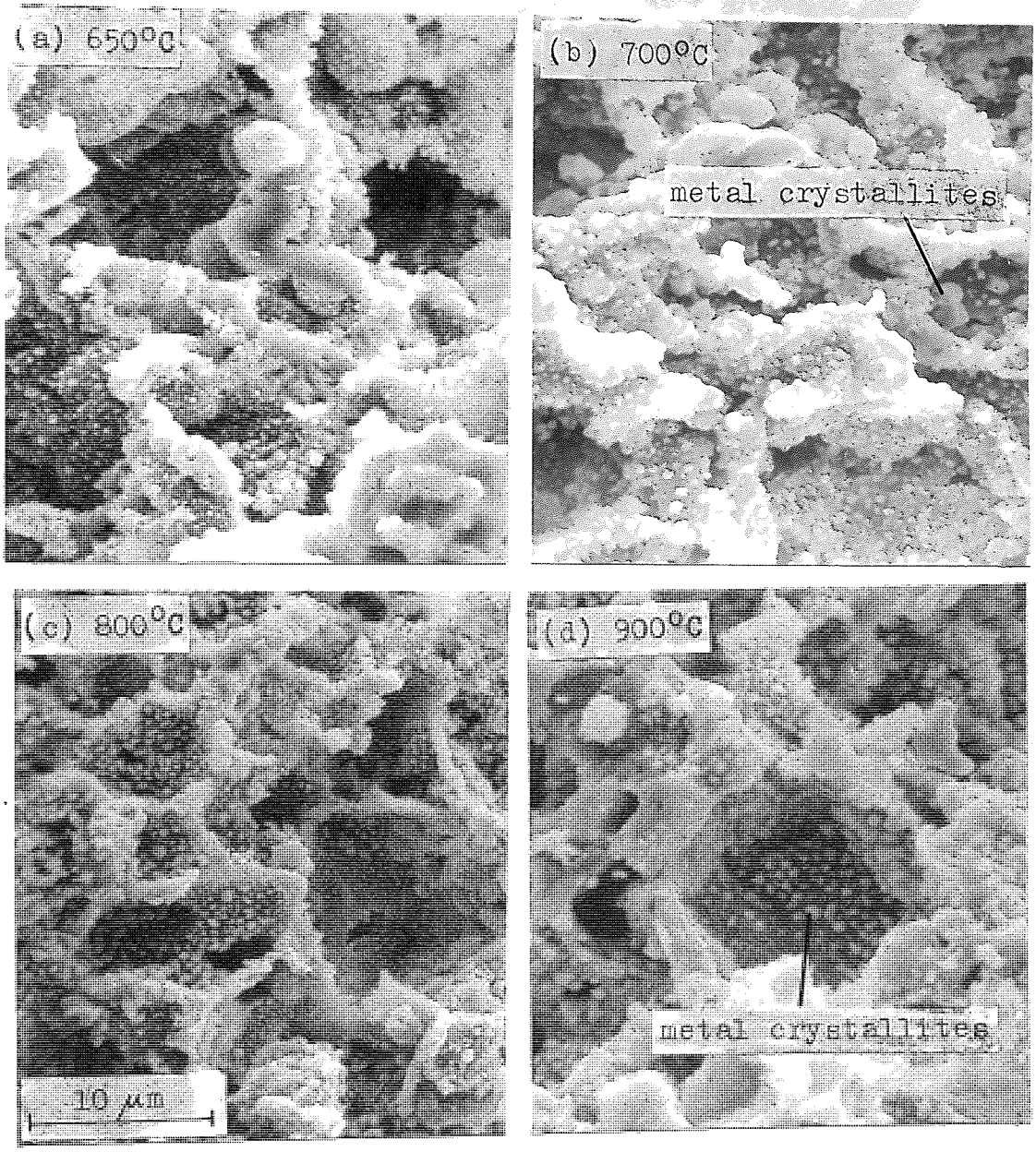

4.3. The Distribution of the Active Metal

4.3.1. Metal Crystallite Size

As shown above, the metal crystallites increased in size by a process of aggregation, often referred to loosely in the literature as

Figure 4.7. : Scanning electron micrograph of a fracture face of catalyst Q1006 after thermal ageing at 1000°C in the synthetic exhaust gas

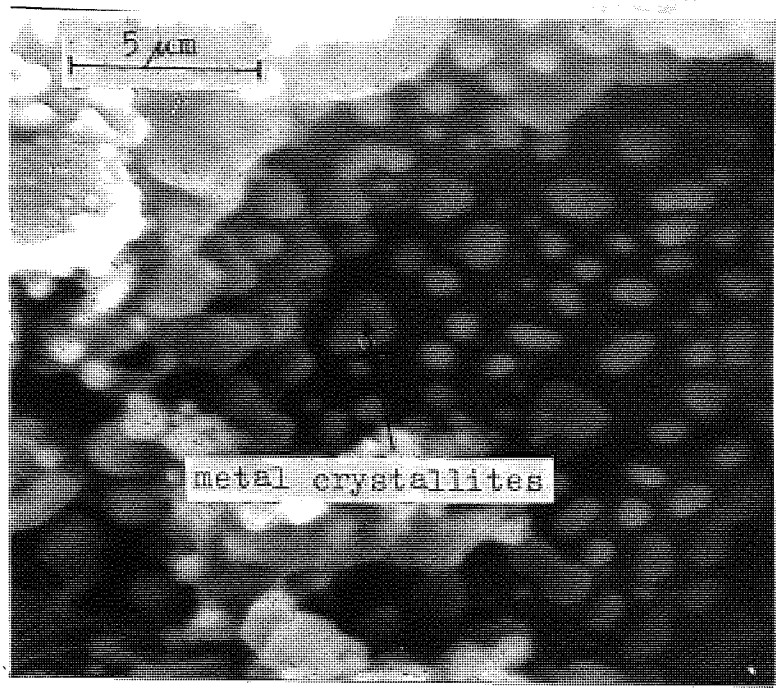

Figure 4.8. : Characteristic x-ray energy spectrum from the metal crystallites in Figure 4.7, obtained from a Kevex energy dispersive analyser in conjunction with the SEM

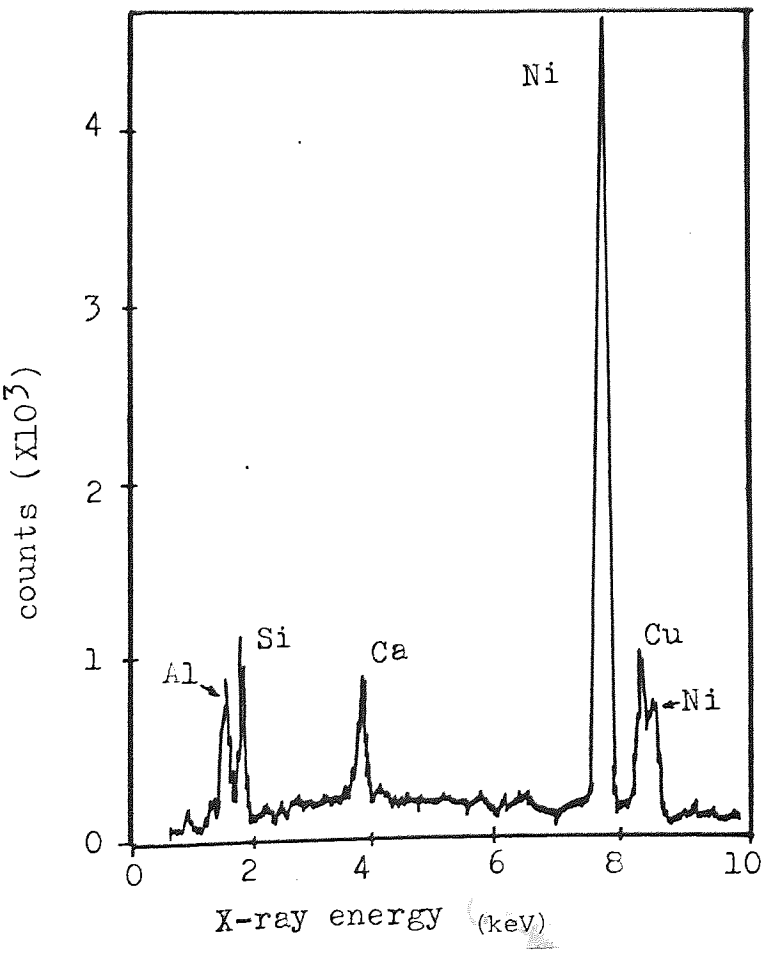

Figure 4.9. : Characteristic x-ray energy spectrum from the area surrounding the large crystallites shown in Figure 4.7, obtained from a Kevex energy dispersive analyser in conjunction with the SEM

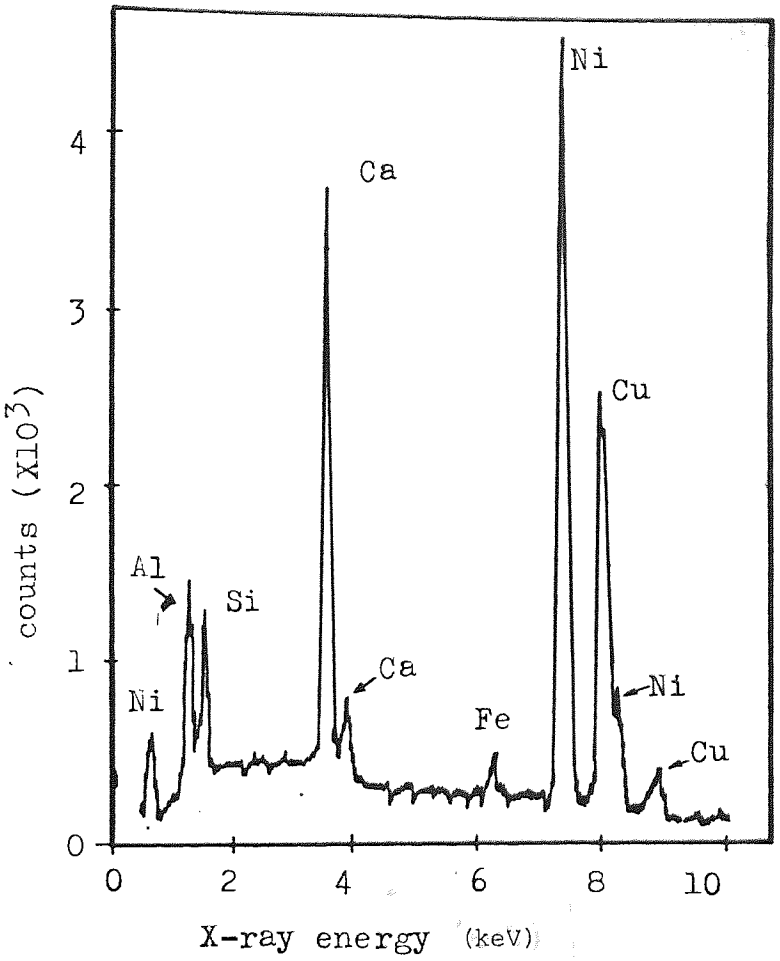

Figure 4.10. : Metal crystallite size distribution after thermal ageing in the synthetic exhaust gas

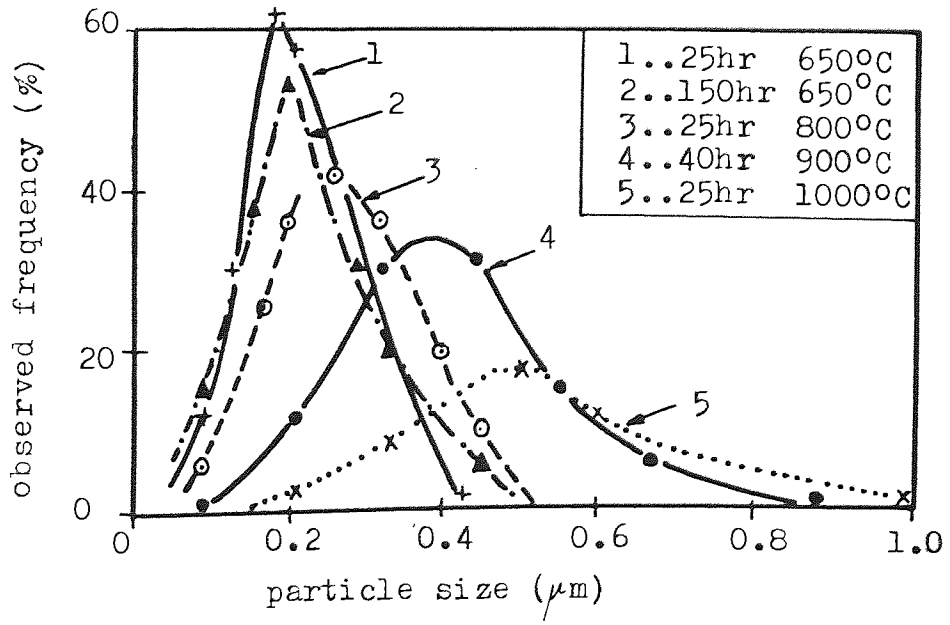

sintering. The crystallite size distributions were determined and in general, all had the same skew distribution as shown in Figure 4.10. It can be seen that the distributions were skew with a tail towards the larger particle sizes. After ageing, the width of the distribution had increased while the minimum size remained less than 0.05 μm. The rate of aggregation was proportional to the ageing temperature and this dependence on temperature was pronounced, 30 mins at 1000^{o}C having the same effect as 10 hours at 800^{o}C or 250 hours at 650^{o}C, which reflected the pattern observed for the decrease in activity described above. The mean particle sizes evaluated from the particle size distributions are given in Table 4.1, plotted according to equation 1.2 in Figure 4.11. The slopes of the calculated regression lines shown in Table 4.2 are consistent, indicating a power-law order of 5.2 to 5.5, so that it was not possible to ascribe a definite mechanism to the aggregation of the metal crystallites according to the analysis described in Section 1.7.4. The rate constants for crystallite aggregation at the four temperatures were calculated from the respective slopes and plotted according to the Arrhenius relationship in Figure 4.12. A value of 37.2 kcals.mol^{-1} was calculated for the apparent activation energy from equation 1.22.

4.3.2. Surface Area Changes Due to Thermal Ageing

The specific surface area determined by the Brunauer, Emmet and Teller (BET) method shown in Table 4.3 was inversely proportional to the activity. This suggested that the deactivation was due to loss of surface area by crystallite aggregation. The surface area of the support granules was unchanged by ageing, remaining at approximately 0.6m^{2}g^{-1}, so that the loss of surface area observed was due to the increase in particle size. In fact, sintering and subsequent collapse

Table 4.1. : Average metal crystallite size as a function of thermal ageing in the synthetic exhaust gas. The original crystallite size, Do, was 0.06 μm.

Ageing temp. (^{o}C)	Ageing time t (hr)	Mean particle size D (μm) after time t at ageing temp.	D/Do
1000	0.5	0.24	4.0
	1	0.28	4.7
	10	0.45	7.5
	16	0.49	8.1
	25	0.52	8.7
	50	0.57	9.4
900	0.5	0.20	3.3
	1	0.18	3.0
	2	0.20	3.3
	16	0.26	4.3
	40	0.37	6.2
	72	0.40	6.7
800	0.5	0.11	1.8
	4	0.16	2.7
	25	0.25	4.2
	50	0.22	3.7
	72	0.25	4.2
	100	0.33	5.5
650	2	0.09	1.5
	25	0.18	3
	50	0.16	2.7
	150	0.21	3.5
	250	0.24	4.0

Table 4.2. : Results of a linear regression analysis of log(D/Do) on log t for data given in Table 4.1 and plotted in Figure 4.11.

Ageing temperature	1000^{o}C	900^{o}C	800^{o}C	650^{o}C
Slope = 1/n	0.19	0.18	0.18	0.19
Intercept = $(\log k_1)/n$	0.67	0.47	0.32	0.14
Correlation coeff.	.995	.95	.96	.97

Figure 4.11. : Metal crystallite size as a function of time after thermal ageing in the synthetic exhaust gas, plotted according to equation 1.2.

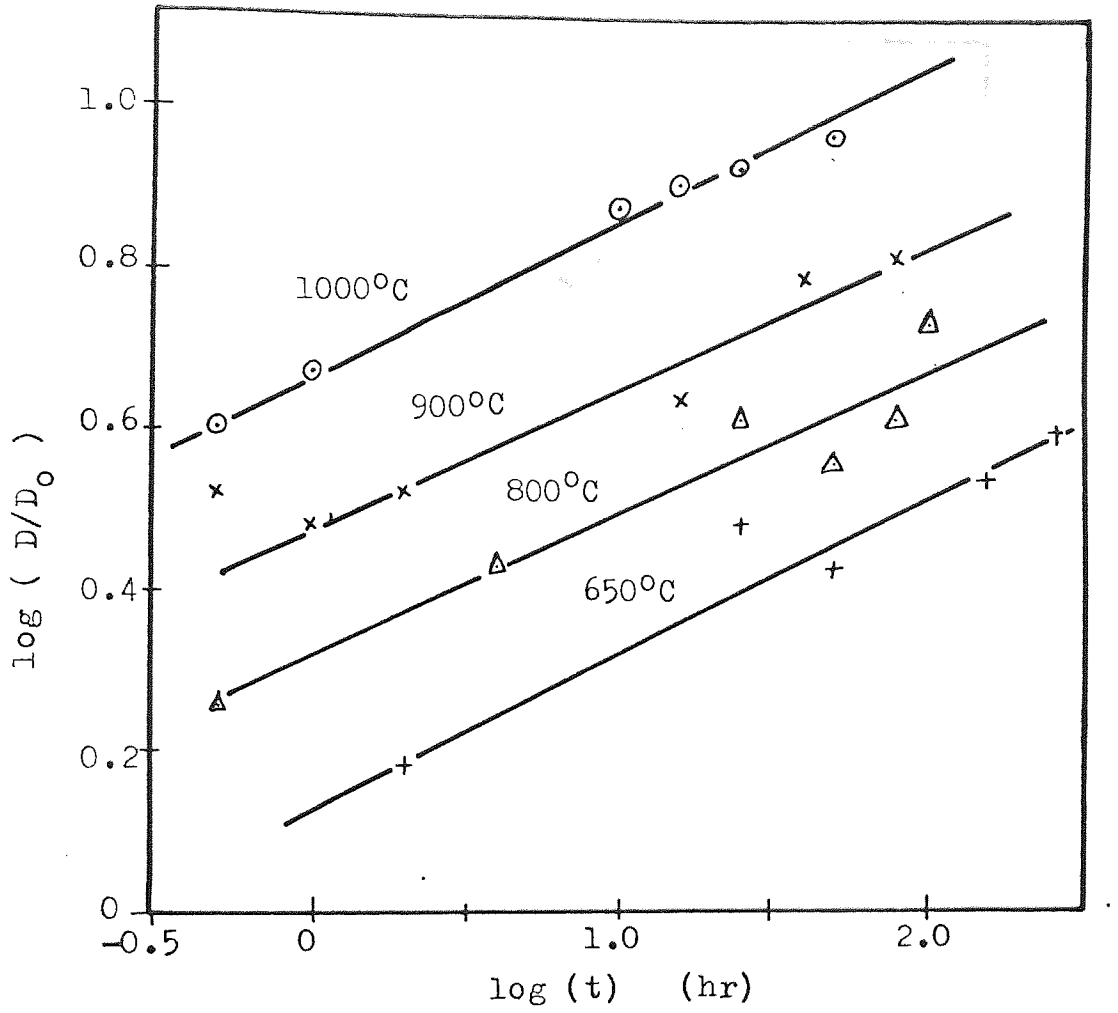

of the gehlenite support structure would not be expected since, in the preparation of the granules, the extruded material was sintered at 1130°C. The total apparent surface area (TASA) of the metal crystallites was calculated from the particle size distribution by the method of Davis et al[129] which assumes the particles are perfect spheres. This calculation confirmed that the metal crystallites contributed the majority of the total surface area. The calculated value of the TASA is greater than the observed BET surface area because with the former, the whole surface area of the sphere is

Figure 4.12. : The rate constant for metal crystallite aggregation plotted according to the Arrhenius relationship in equation 1.22.

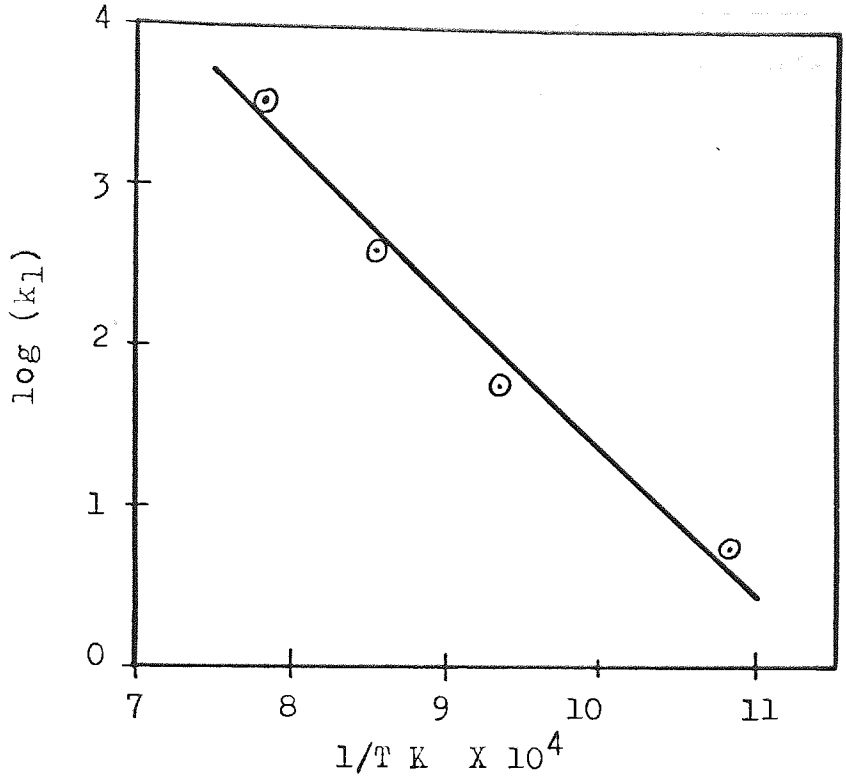

considered, and also because of errors in measuring the very small particle size tail of the distribution. This contributes a relatively large part of the surface area. The surface area determination by the BET method uses several grammes of the catalyst so that the largest source of error is probably the particle size determination which, by necessity, is very selective of the material. Because of this it was felt that the surface area would provide a more consistent measure of the dispersion of active metal on the substrate. Therefore the surface area was used for the remainder of the investigation to characterise the active metal dispersion.

Table 4.3. : The specific surface area of Q1006 granules after thermal ageing in the synthetic exhaust gas. The surface area of a fresh sample of Q1006 was $3.9 m^2 g^{-1}$

Ageing temp. (°C)	Ageing time (hr)	Specific surface area determined by BET method ($m^2.g^{-1}$)	Specific surface area calculated(TASA) ($m^2.g^{-1}$)
650	150	2.4	-
	250	2.1	-
800	0.5	3.6	5.0
	4		5.1
	25	2.6	3.3
	50	2.3	3.0
	100	2.1	2.6
900	0.5	1.3	-
	2	1.2	-
	16	0.8	-
	40	0.7	-
	72	0.9	-

4.4. Correlation of Deactivation with Crystallite Aggregation

Loss of activity by poisoning and by physical loss of the wash-coat/ active species have been eliminated by ageing granules in a sterile atmosphere in these experiments. Therefore, the three possible mechanisms for the deactivation of these thermally aged samples are loss of metal surface area by reaction with the substrate, sintering and subsequent collapse of the substrate, and finally aggregation of of the metal crystallites.

Reaction of the nickel and copper oxides with the gehlenite :

no reaction had been detected between nickel oxide and gehlenite at temperatures up to $1200^{o}C$ (126)(127) in oxidising atmospheres and in this present investigation, no reaction between the active species

and the support was detected by x-ray diffraction after 100 hours at 800°C in the standard synthetic exhaust atmosphere.

Sintering and subsequent collapse of the support structure :
the support granules had been sintered at 1130°C during preparation and would therefore not be expected to experience further sintering at the temperatures of the ageing tests, also the surface area remained constant for control samples at approximately $0.6 m^2 . g^{-1}$.

Aggregation of the metal crystallites :
activity normalised with respect to the initial activity of samples with a constant volume fraction of active species has been plotted in Figure 4.13 versus surface area (proportional to I/D^2). It can be seen that the normalised activity was inversely proportional to the square of the mean particle size of the metal crystallites.

Figure 4.13. : The deactivation of Q1006 granules after thermal ageing in the synthetic exhaust gas as a function of surface area (proportional to I/D^2)

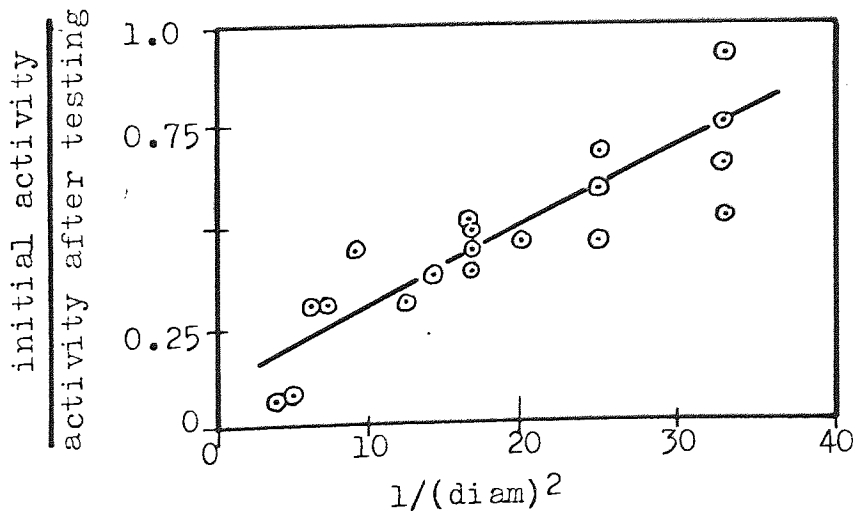

It was therefore concluded that the deactivation of the Q1006 catalysts by thermal ageing was due to the aggregation of the metal crystallites. Only two of the variables affecting the rate of aggregation discussed in Section 1.7, the metal loading per unit surface area and the surface energy of the active metal species are easily controlled. The operating temperature is constrained by the rate of reaction to achieve the required conversions of nitric oxide, and the exhaust gas composition is determined by the need for reducing conditions over the catalyst.

4.5. Some Observations on the Mechanism of Aggregation

Crystallites in the size range 0.1 to 1.0 μm would be unlikely to be mobile in the sense of the constant Brownian motion envisaged in the crystallite migration theory. However, it is possible that crystallites in an unstable position with respect to gravity could actually move across the support surface as suggested in Figure 4.14.

Figure 4.14. : The effect of surface texture on the stability of metal crystallites

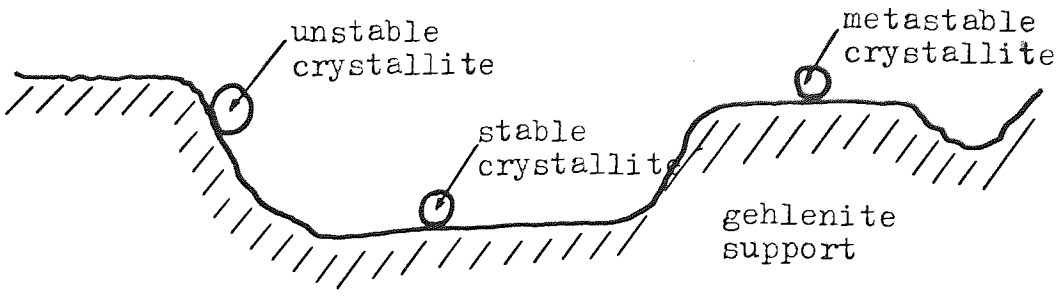

This is perfectly feasible since the substrate is not wetted by the nickel-copper alloy. The interfacial surface energy between the metal and the gehlenite may be calculated simply from the geometry of the particle since the shape will be determined by the interplay of the surface tensions between the metal and atmosphere (γ_{LV}), the substrate and the atmosphere (γ_{SV}) and between the metal and the substrate (γ_{SL}) as shown in Figure 4.15.

Figure 4.15. : Geometrical construction to calculate the interfacial surface energy

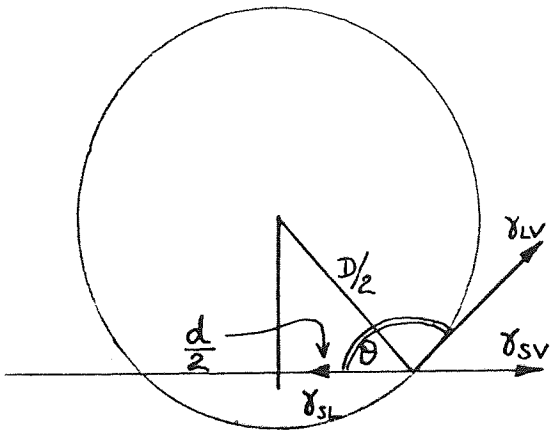

As part of a parallel investigation into the chemical compatibility of gehlenite and the metal oxides[130] a number of samples of gehlenite were impregnated with copper oxide and aged at temperatures of up to 1300°C in a reducing atmosphere. Copper, whose melting point is 1080°C, was extremely mobile at these temperatures and the resultant, very large, spherical crystallites (up to 4.0mm) were easily handled with fine tweezers. The diameters of the crystallites, D, and of the base, d, were measured under a microscope using an eyepiece graticule and the results are shown in Figure 4.16, the interfacial surface energy between the copper and the gehlenites was then calculated from :

$$\cos\theta = (\gamma_{sv} - \gamma_{sl})/\gamma_{LV} \quad \ldots\ldots\ldots 4.1.$$

now, $\cos^{-1}(d/D) + 90^{o} = 132 \pm 8^{o}$

$\gamma_{sv} = 90.5\ N.m^{-2}$ (Alumina at $1800^{o}C$)

$\gamma_{lv} = 127\ N.m^{-2}$ (Copper at $1130^{o}C$)

$\gamma_{sl} = 203\ N.m^{-2}$

Figure 4.16. : The relationship between crystallite diameter and the chord length (Figure 4.15)

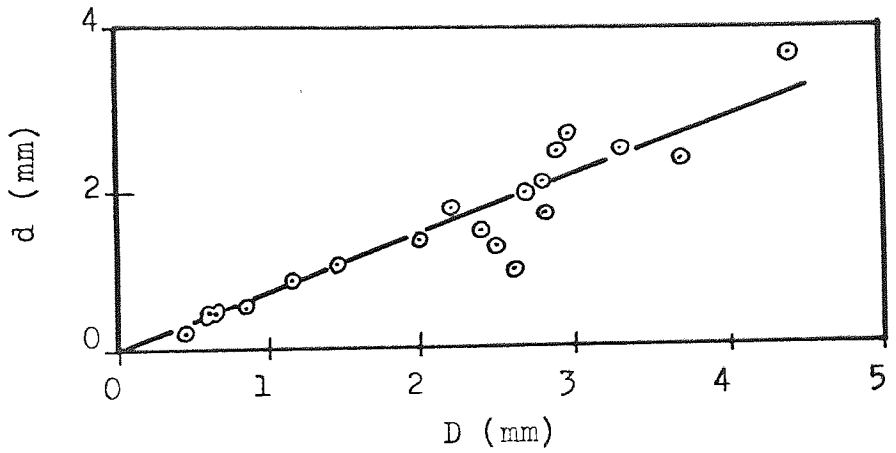

This relatively large scatter was thought to be due to difficulties in measuring d accurately since many of the samples were cooled rapidly to room temperature in air, and the crystallites suffered surface oxidation. This value compares with that of 192 $N.m^{-2}$ found by Pilliar and Nutting[128] who measured the interfacial surface energies of several metals on gamma-alumina from the shape of sintered crystals. By the same technique. They also found nickel to have a value of 214 $N.m^{-2}$.

A situation where this movement of crystals may have occurred is shown in Figure 4.17, although an alternative possible explanation is that adjacent crystallites have grown asymmetrically towards each other and have finally impinged to form the neck.

Figure 4.17. : Scanning electron micrograph of a cross-section of Q1006 after 100hrs at 800°C in the synthetic exhaust gas

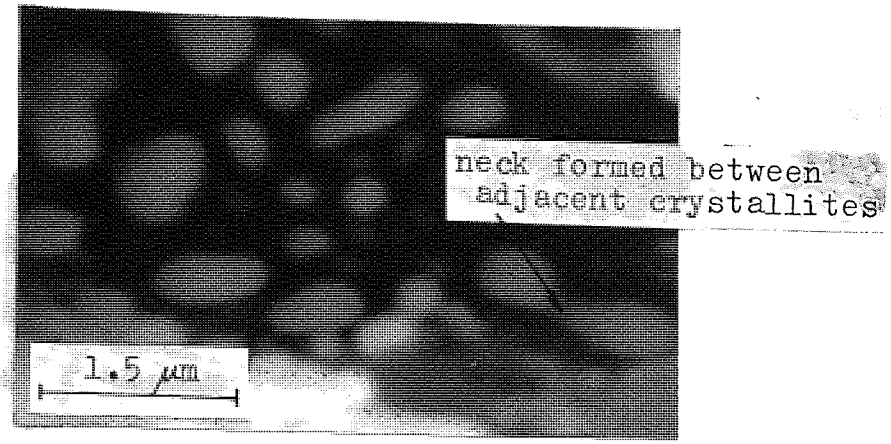

5. COMPOSITION OF THE CATALYST

5.1. The Structure of the Granular Catalysts

The catalyst support granules (Q1005) contained many large pores, as can be seen in Figure 5.1. Despite this, as has already been noted in Chapter 4, the metal nitrate solutions did not penetrate to the centre of all the samples. This, however, was not necessarily a problem since only an outer shell, perhaps a few microns in depth, is effectively acting as a catalyst because of mass transfer limitations in this application. High magnification scanning elctron micrographs from catalyst G13A (50% metal loading) are shown in figures 5.2 and 5.3. These show (Figure 5.3) an area from the centre of a granule

Figure 5.1. : Scanning electron micrograph of a fracture face of a catalyst with a metal loading of 50%. Supported on Q1005 granules (G13A)

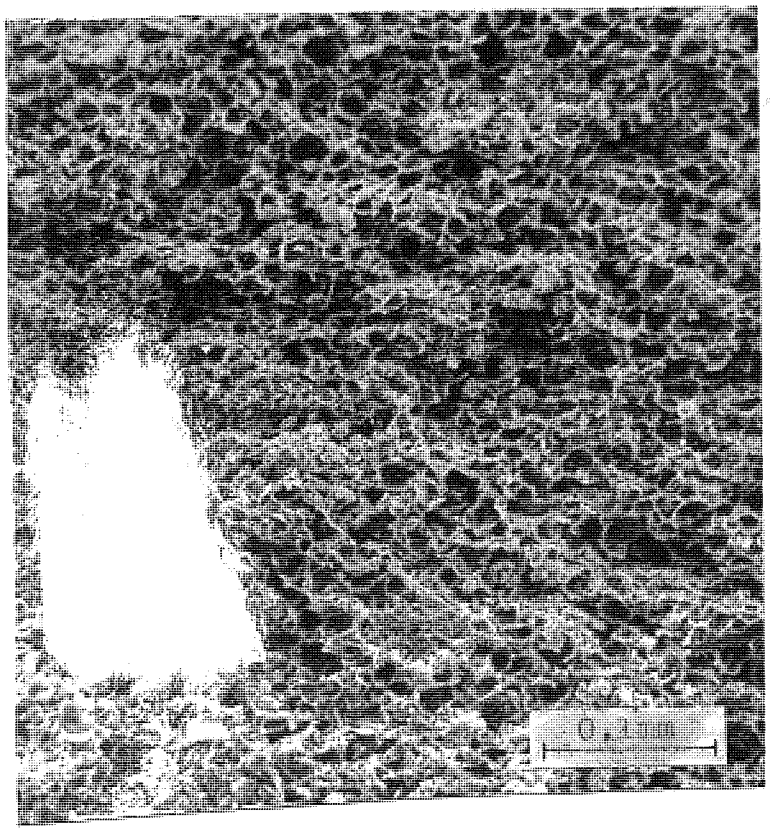

Figure 5.2. : Scanning electron micrograph of a fracture face of catalyst G13A after thermal ageing for 24 hours at 800°C in the synthetic exhaust gas

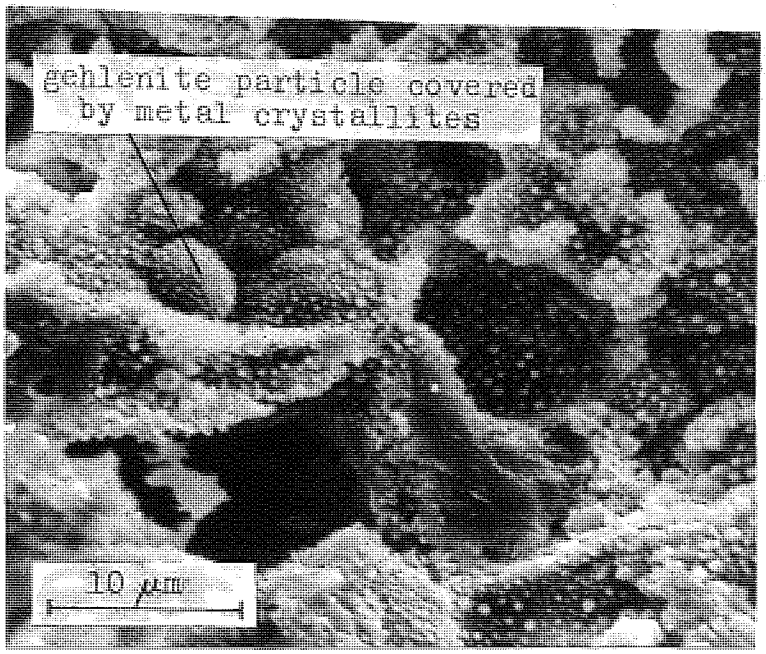

Figure 5.3. : Scanning electron micrograph of a fracture face of the centre of a G13A catalyst granule after 24 hours at 800°C in the synthetic exhaust gas

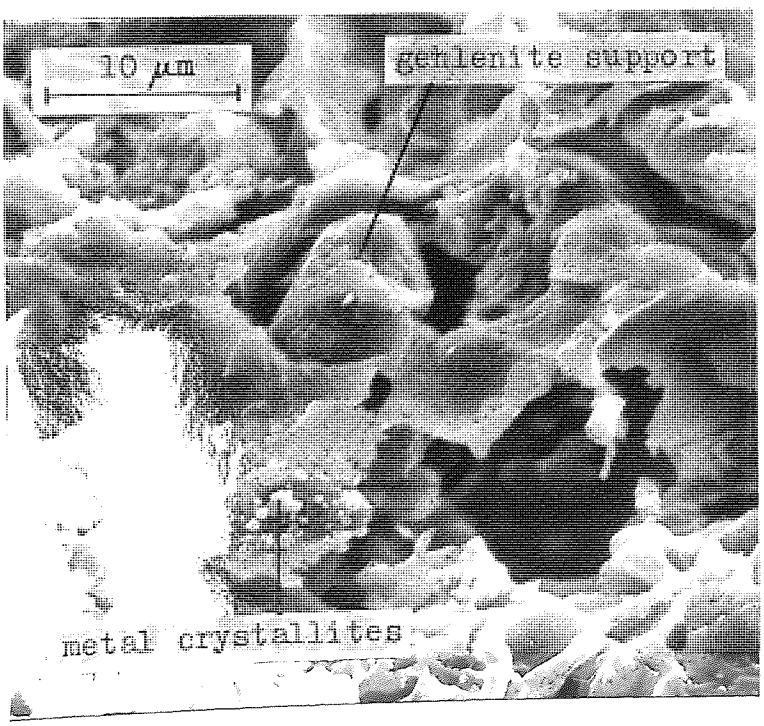

where little active metal is present and a more typical structure (Figure 5.2). In the latter, the metal crystallites can be seen in the pores and supported on the smaller gehlenite particles. This type of structure was not affected by the composition of the granules. The metal crystallite size was proportional to the metal loading, but the copper to nickel ratio had little effect, as can be seen in Figures 5.4 and 5.5. These show typical structures of a copper-free catalyst (G1) and one with a nickel to copper ratio of 0.3 (i.e. 75% copper in the active species).

Figure 5.4. : Scanning electron micrograph of a fracture face of catalyst G1 after thermal ageing for 24 hrs at 800°C in the synthetic exhaust gas

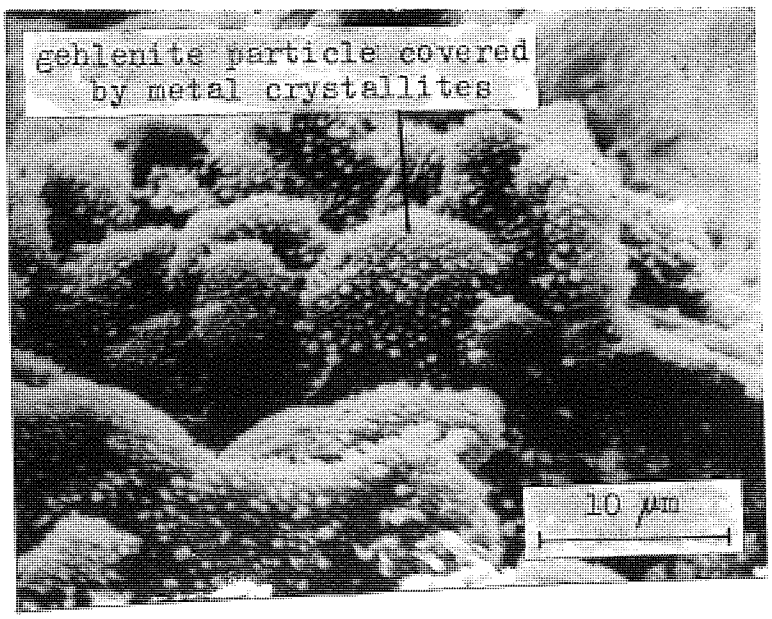

5.2. The Metal Loading of the Catalysts

It was shown in Chapter 4 that deactivation of Q1006 granules by thermal ageing was proportional to the degree of aggregation of the

Figure 5.5. : Scanning electron micrograph of a fracture face of catalyst G9 after thermal ageing for 24 hrs at 800°C in the synthetic exhaust gas

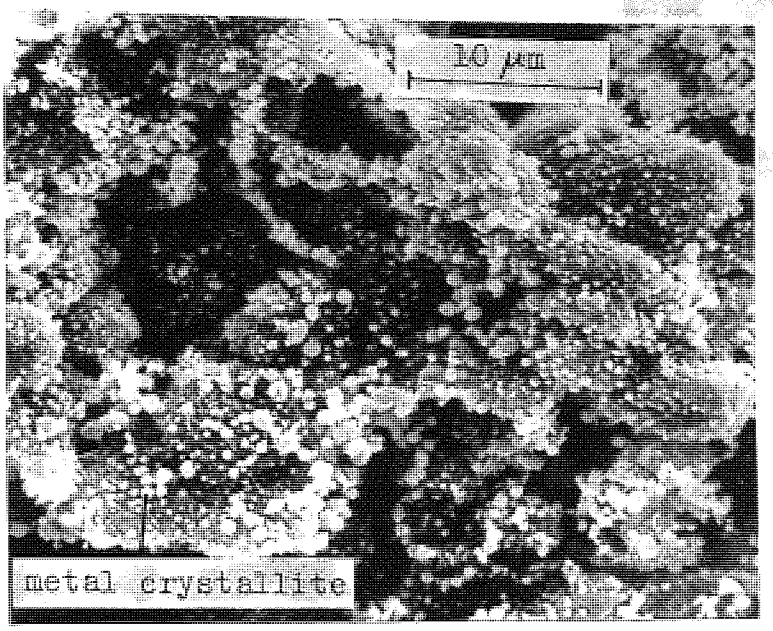

active metal crystallites. There are two methods available to vary the parameter "metal loading per unit surface area". The metal loading is equivalent to the metal concentration for granular catalysts. The methods are : reduction of the weight fraction of the metal in the catalyst, or increase of the surface area of the support. The surface area of the support depends, to a large extent, on the materials used. For example, very high surface areas of the order of $100 m^2.g^{-1}$ or more can be achieved with gamma-alumina or silica. Dalla Betta[98] has shown that it is possible for an 8 w/o copper-nickel alloy on a silica support, with a surface area of $300 m^2.g^{-1}$ to have very high metal dispersions (metal surface area per unit metal volume), with metal crystallite diameters measured in nanometers. However, the disadvantage with these high surface area supports is that at the temperatures encountered with these automobile exhaust catalysts, copper and nickel oxides react readily to form inactive aluminates

or silicates. The support must therefore be manufactured from unreactive stable materials. In this present application, surface areas of less than $1.0 m^2.g^{-1}$ for the secondary support are common. Therefore, decreasing the metal concentration was considered to be the most practical way to reduce the metal loading per unit surface area of the support.

As expected, a decrease in metal loading increased the total surface area as measured by gas absorption although the increase was not pro rata. A decrease of the weight fraction of metal by an order of magnitude from 0.5 to 0.025, increased the surface area from 4 to only $10 m^2.g^{-1}$, as can be seen in Table 5.1. In the previous chapter it was shown that catalytic activity was proportional to the surface area of the active species at a constant metal loading. However, it can be seen from Figures 5.6 to 5.8 that the variation in metal loading had a more significant effect than the variation in surface area under these conditions.

Table 5.1. : Specific surface areas as a function of metal loading after thermal ageing at 800°C in the synthetic exhaust gas

Catalyst	Metal oxide content (%)	Surface areas $m^2.g^{-1}$ of catalyst	
		as calcined	aged for 24hrs at 800°C
G13A	50	4.3	1.0
14	25	3.9	1.7
16	10	*	3.6
16A	5	*	1.2
17	2.5	10.2	5.5

* Not determined

Figure 5.6. : Temperature activity scans for G13A (●), 14 (+), 16 (△), 16A (⊙) and 17 (X) in the fresh condition in the standard synthetic exhaust gas.

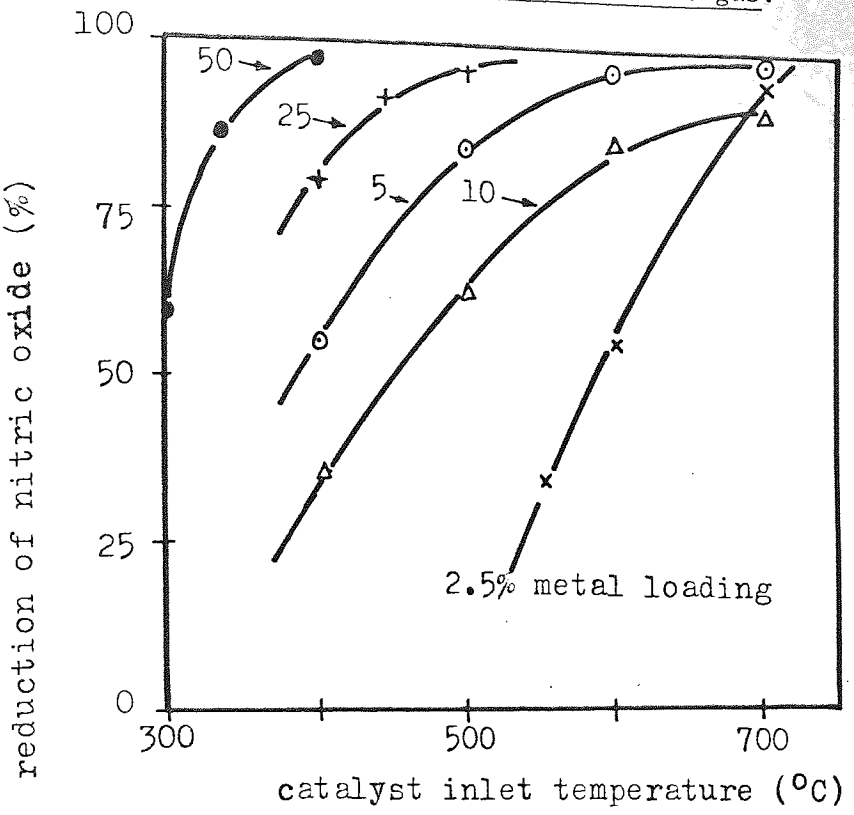

Figure 5.7. : Temperature-activity scans for G13A (●), 14 (+), 16 (△), 16A (⊙) and 17(X) after thermal ageing for 24 hrs at 800°C in the standard synthetic exhaust

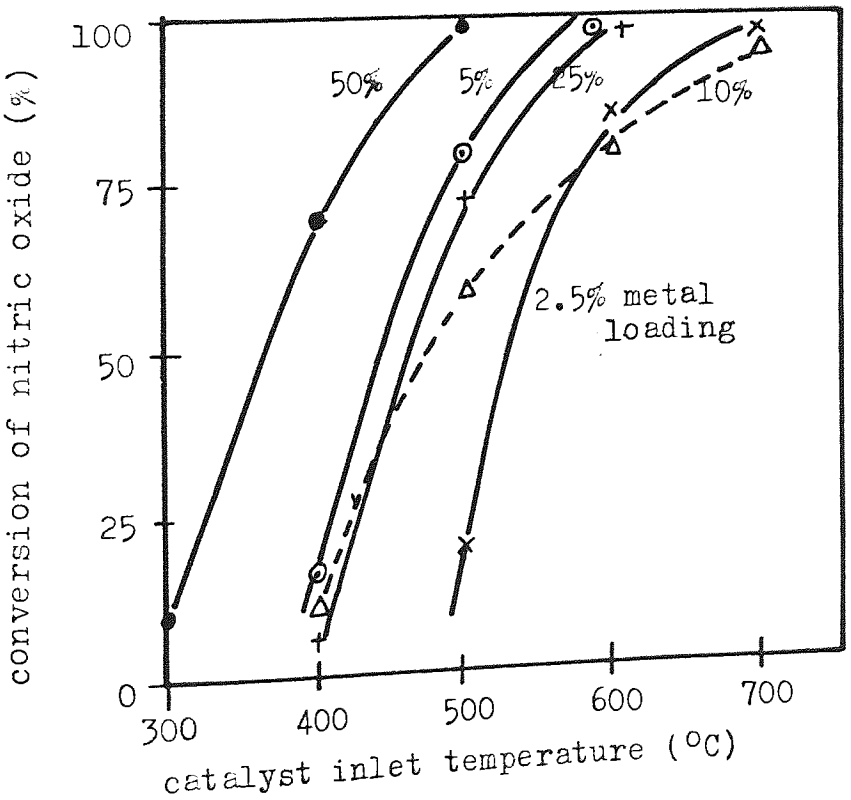

Figure 5.8. : Temperature-activity scan for G13A (●), 16 (Δ) and 17 (X) after thermal ageing for 24 hrs at 1000°C in the standard synthetic exhaust

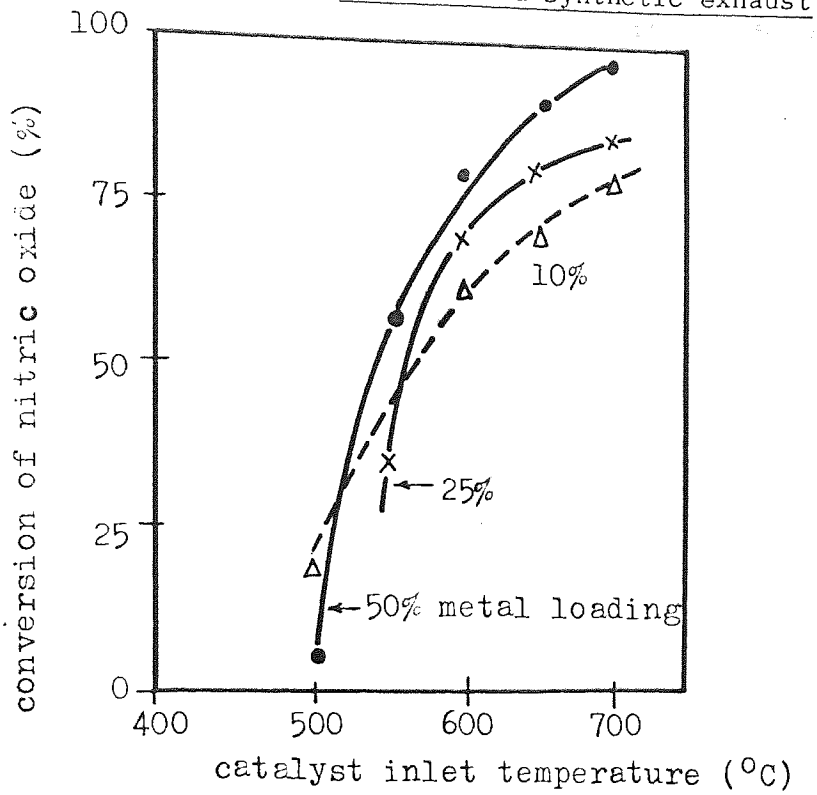

This may be explained by one or a combination of the following :

1. Some part of the catalytic activity was due to the concentration of the migrating species on the support surface, which is proportional to the metal concentration in the catalyst and hence the metal loading.
2. Oxygen acts as a temporary poison for this reaction, by combination with the active sites on the metal crystallites; it was possible that the metal crystallites were surrounded by an oxygen-rich layer, so that the nitric oxide and reducing agents must diffuse across this barrier before reaction can occur.
3. Very few of the metal crystallites on the lower metal loading catalysts may be in the reduced form so that although they have a higher total surface area than the high metal loading catalysts, the number of available active sites is limited.

The first is a possible, though not a complete, answer since nickel-copper in the bulk form as monel is an active catalyst for the reduction of nitric oxide under these conditions. The mechanism of crystallite aggregation proposed by Flynn and Wanke[99] proposed that at high temperatures an equilibrium was set up between the metal species migrating across the support, and that in the crystallites. It is possible that the migrating particles are efficient for the catalytic reduction of nitric oxide.

It is likely that the migrating particles are molecules rather than atoms since it has been shown that platinum crystallites grow more rapidly in a gaseous atmosphere than in a vacuum[100]. Since these migrating particles would be very mobile, it is not necessary that they should be large enough to accommodate more than a single gas molecule since they will undergo many collisions, during which the reaction between the nitric oxide and the reducing agents could take place.

The assumption of an oxide layer through which the reactants diffuse is arguable since the available oxygen on the low metal loading catalysts would have to cover a greater area so that the barrier to the reactants would be reduced. It has also been shown that the oxygen was used up at the inlet side of the catalyst bed with little or no oxygen being detected after the catalyst. Towards the exit side of the bed there would be insufficient oxygen for complete coverage of the metal surfaces. However, the surface area was increased by only $2\frac{1}{2}$ times whilst the weight fraction was reduced by 20 times, so that there is considerably more bulk of metal in the higher metal loading catalysts. Thus the oxygen was depleted nearer the inlet face, leaving a larger volume of the bed unoxidised. The surface area effect was

swamped by the volume effect, and does not show up in the observed results.

Selwood et al.[131] investigated the reduction of nickel oxide which is notoriously difficult over a wide range of conditions and found that under cyclic conditions the formation of nickel metal from the oxide required the formation of fresh nuclei, even though metal and metal oxide phases were in contact with each other. The formation of these nuclei was greatly enhanced by additions of copper or platinum group metals to the nickel, so that the addition of copper facilitated the reduction of nickel oxide[131][132].

In the present investigation it was found that the low metal loading catalysts had a relatively high dispersion of the active species. The mean particle sizes calculated from the surface areas are shown in Table 5.2. For the reduction of the metal oxide particles to occur, a large number of nuclei are required because of the very small particle size. It is probable and indeed, has been shown by x-ray diffraction analysis, that not all the crystallites were reduced even in the high metal loading catalysts, but that some metal oxide persisted even after ageing at 800^{o}C in the synthetic exhaust gas, for up to 100 hours. Therefore, it was assumed that in the high metal loading catalysts, the amount of reduced active species was greater than in the low metal loading catalysts. Unfortunately, no apparatus for the measurement of metal surface areas was available during the investigation to prove or disprove this assumption. However, temperature-activity scans for the catalysts indicate that this was indeed the case. The results for the aged samples shown in Figures

Table 5.2. : Metal crystallite size calculated from the surface area as a function of metal loading

Catalyst	mean particle size (μm)	
	as calcined	aged 24hr/800°C
G13A	0.12	0.38
G14	0.06	0.12
G16	*	0.02
G16A	*	0.03
G17	0.002	0.003

* Not determined

5.7 and 5.8 indicated that, as expected, the high metal loading catalysts had lost activity, particularly at the lower temperatures, $\lesssim 600^{o}C$, whereas the aged samples of G17 ($2\frac{1}{2}$% metal loading) had, in fact, improved slightly after ageing at 800°C, and although subsequently losing activity upon ageing at 1000°C, this sample was still more active than the fresh sample.

5.2.1. The Correlation of Activity with Surface Area

The surface areas measured for the five catalysts in this series showed a discrepancy for the catalyst G16A, as shown in Figure 5.9. Results for this catalyst were very low compared with G17 and G16, the metal loadings of which bracket G16A. The reason for this was not immediately apparent, but the activity results from Figure 5.6 and 5.7 suggested that this difference in surface was a real effect and not an error in measurement. It was assumed that some unknown difference in the preparation technique was the cause of the discrepancy, as chemical analysis showed that the metal contents were within $\pm$ 3% of the nominal values, so that the most immediately obvious cause was ruled out. If the surface area was low due to the metal loading, then

Figure 5.9. : Specific surface area as a function of the metal loading after thermal ageing for 24 hrs at 800°C in the synthetic exhaust gas

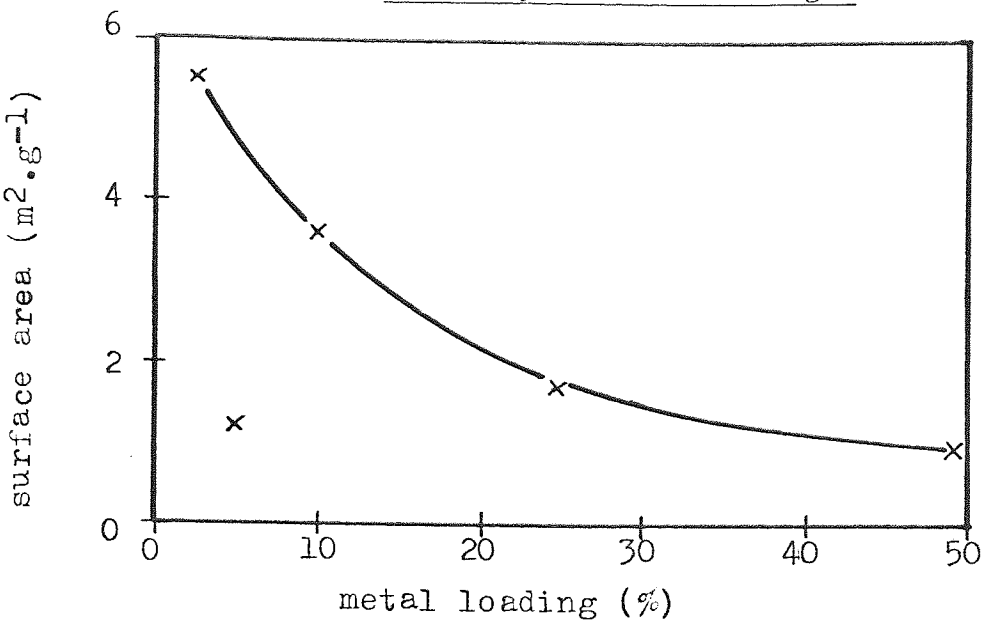

the activity would be expected to have been similar to G13A and G14, whereas in fact, it fell between G14 and G16. A second possibility was that the active species was concentrated towards the outer edges of the granules in the four catalysts G13A, 14, 16 and 17 but not to the same extent in G16A. It was not readily understood why this difference in concentration gradients should have occurred but could possibly have been due to differences in the rate of heating when the catalysts were dried after impregnation with the nitrate solutions. A slow rate of heating may have allowed time for the solution in the pores of the granules to have diffused further into the centre of the granule, the driving force for which could be assumed to be capillary action.

If the results from catalyst G16A are neglected then the activity was proportional to the metal loading above 10% metal as shown in

Figure 5.10 : Reaction rate coefficient (R_2) as a function of metal loading, in the fresh condition

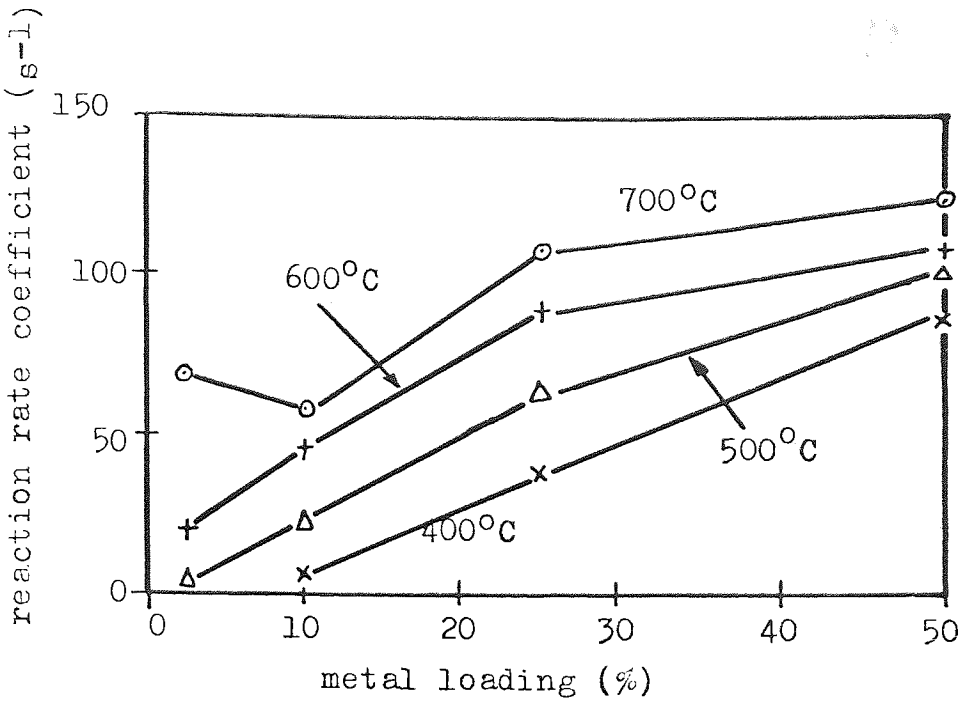

Figures 5.10 to 5.12. Below 10% metal loading, the surface area increased rapidly and it was though that this explained what appeared to be a minimum value of activity at the 10^{w}/o level, i.e. the activity is dependent on both the surface area and weight fraction of active species

Figure 5.11. : Reaction rate coefficient (R_2) as a function of metal loading. Samples thermally aged for 24 hrs at 800°C in the standard synthetic exhaust gas.

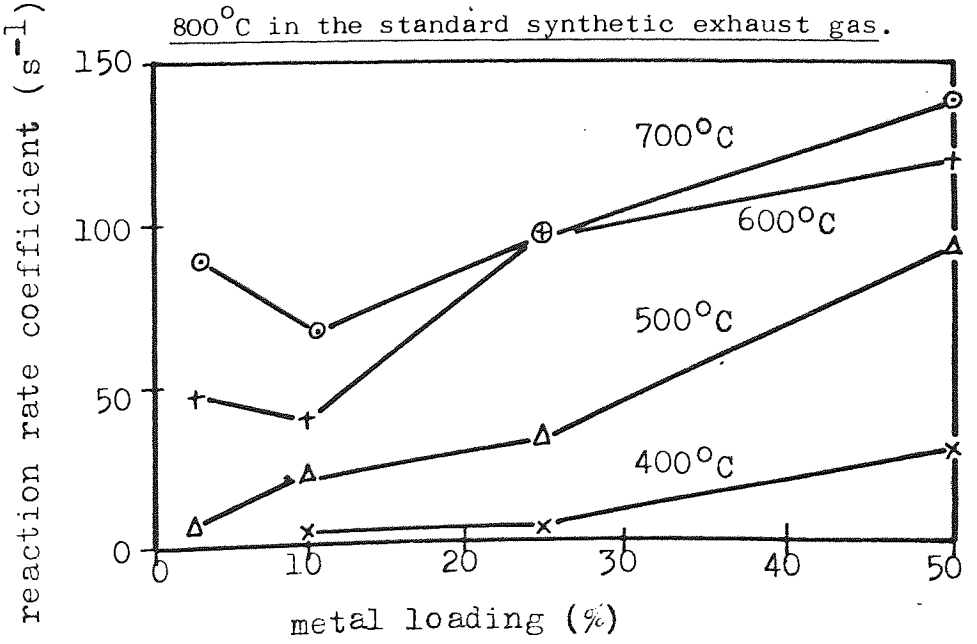

Figure 5.12. : Reaction rate constant (k_2) as a finction of metal loading. Samples thermally aged for 24 hrs at 1000°C in the standard synthetic exhaust gas

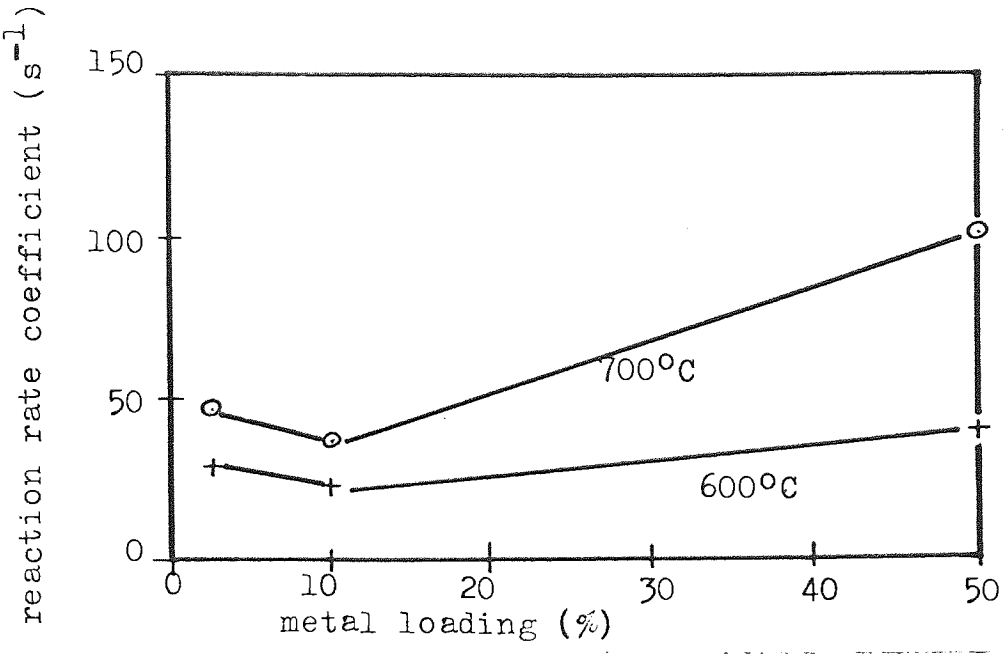

5.2.2. Deactivation by Thermal Ageing

The metal loading of the catalyst did not appear to have a significant effect on the deactivation by thermal ageing, as shown in Figures 5.13 and 5.14. It has already been suggested that the improved activities observed for G17 on ageing were a result of incomplete reduction of the fresh sample. The same conclusion was also reached from results obtained after ageing the catalysts for up to 120hrs at 800°C as shown in Figures 5.15 and 5.16. In the previous chapter it was shown that the deactivation by thermal ageing at 800°C had reached an apparent measurable limit at 50 hrs and further deactivation was negligible. The metal loading of the catalyst did not affect this observation for the range of samples considered, the rate of deactivation based on the initial activity was similar for both G13A and G17. Nevertheless, G13A had a significantly higher activity than G17, particularly at all temperatures below 700°C.

Figure 5.13. : Deactivation after 24 hrs at 800°C in the standard synthetic exhaust gas as a function of metal loading

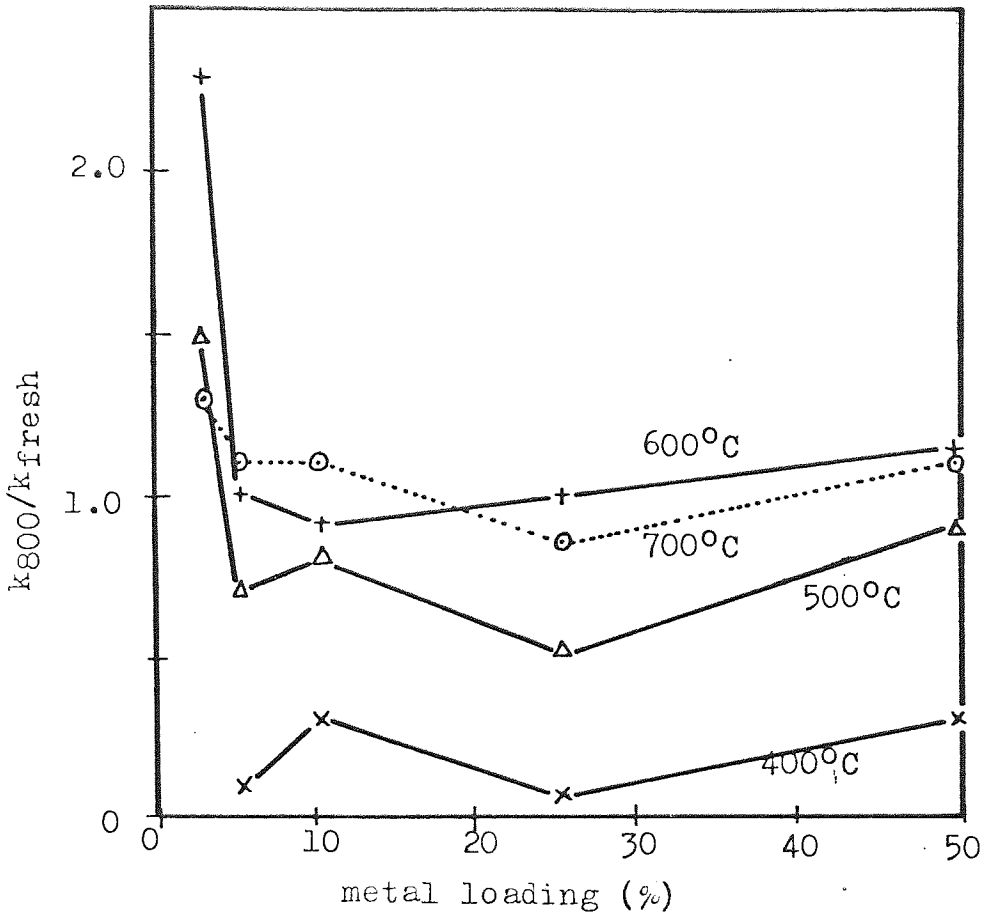

Figure 5.14. : Deactivation after 24 hrs at 1000°C in the standard synthetic exhaust gas as a function of metal loading

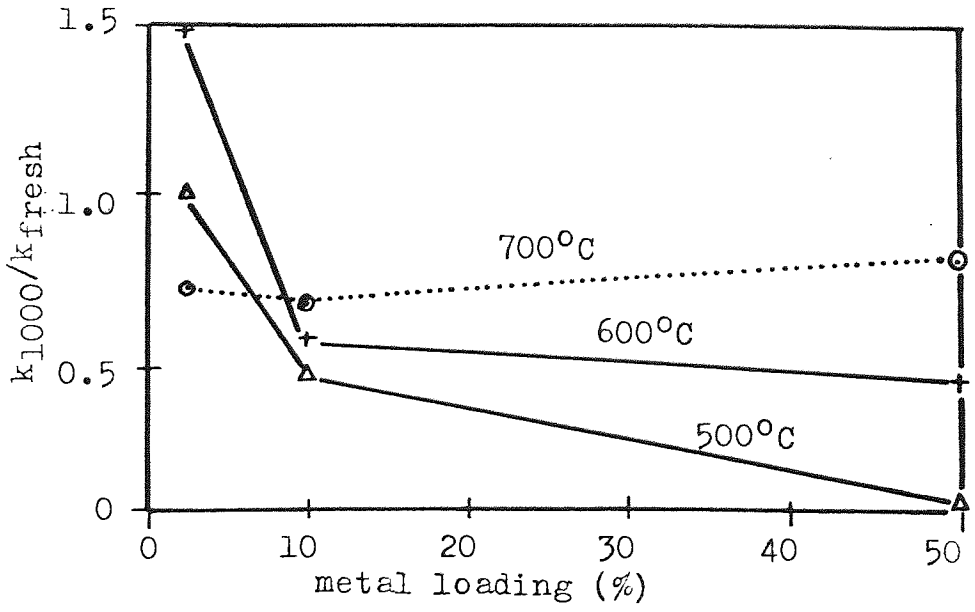

Figure 5.15. : Temperature-activity scans for G13A, thermally aged for up to 120 hrs at 800°C in the standard synthetic exhaust gas

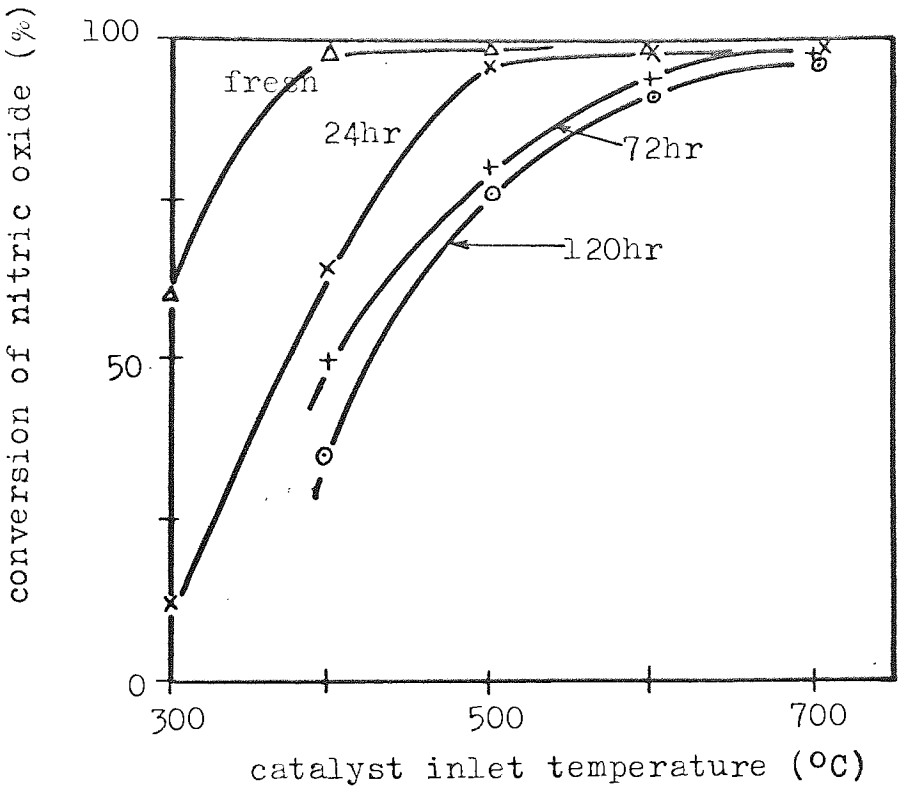

Figure 5.16. : Temperature-activity scans for G17, thermally aged for up to 120 hrs at 800°C in the standard synthetic exhaust gas

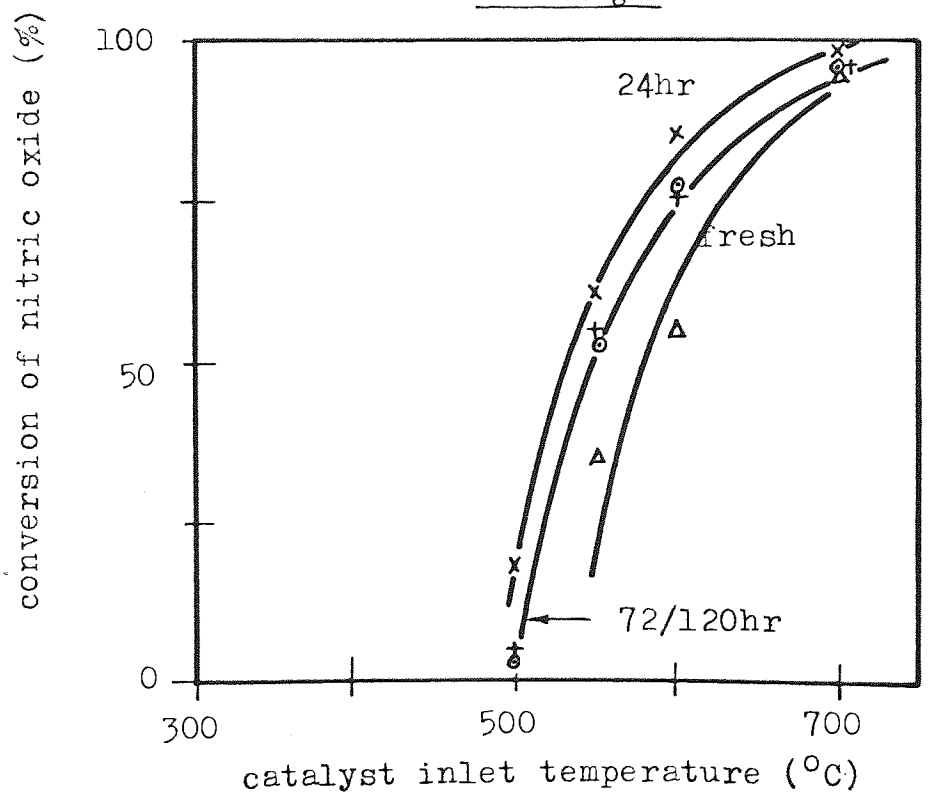

The rate of decrease of total surface area was greater in the high metal loading catalysts as is shown in Table 5.1, a decrease in surface area of 75% in G13A compared to a decrease of 50% in G17 when aged at 800°C. However, this decrease in surface area was not accompanied by a similar decrease in catalytic activity. It can be seen in Figure 5.13 that although there is a large decrease in surface area in G17, the activity has, in fact, increased. This was further indication that the catalyst in the fresh condition still contained a large proportion of unreduced metal oxide when tested. If provision had been made to fully reduce all the catalysts before testing, then the deactivation would have reached its apparent limiting value. Thus, there is no advantage in lowering the metal contents of the catalysts. In fact, ICI practice was to manufacture these catalysts with the highest practical metal loading on matrix catalysts, for example, where the secondary support does not need the strength of the granules and has a high porosity the proportion of active species to wash-coat was approximately 60%. It becomes uneconomical to try to increase this, since the volume fraction of metal species at this level is approaching the volume fraction of pores.

The results from Figures 5.6 to 5.8 are plotted according to the Arrhenius relationship in Figures 5.17 to 5.19. Particularly for the aged samples, there is a definite "knee" which is characteristic of a reaction controlled by diffusional processes at the higher temperatures, i.e. above the "knee". The effect of diffusional resistance in catalysts has been reviewed by Wheeler[131] who showed that the observed reaction rate is proportional to the reaction rate constant as shown in equation 1.21 where the reaction was not diffusion controlled and derived an expression for the observed reaction rate

under diffusion controlled conditions :

$$R_{obs} = \frac{\pi(\bar{D}/2)}{2^{n/2}} \sqrt{\bar{D}k_2 D_c \cdot X_o^{(1+n)}} \qquad .....5.1.$$

and therefore :

$$\text{Observed Rate} \propto \sqrt{K_2} \qquad .....5.2.$$

so that

$$E_{obs} = \tfrac{1}{2} \times E_{true} \qquad .....5.3.$$

Calculation of activation energies for the reduction of nitric oxide, from the curves in Figures 5.17 to 5.19, showed that the activation energies from above the "knee" were approximately half of those from below the knee, so that the reaction rate is limited by mass transfer limitations. It can be seen in Table 5.3 that, in general, there is an increase in activation energy with decrease in metal loading and with increase in the severity of the ageing. The

Figure 5.17. : Arrhenius plots of the reaction coefficients from Figure 5.1. (Fresh condition)

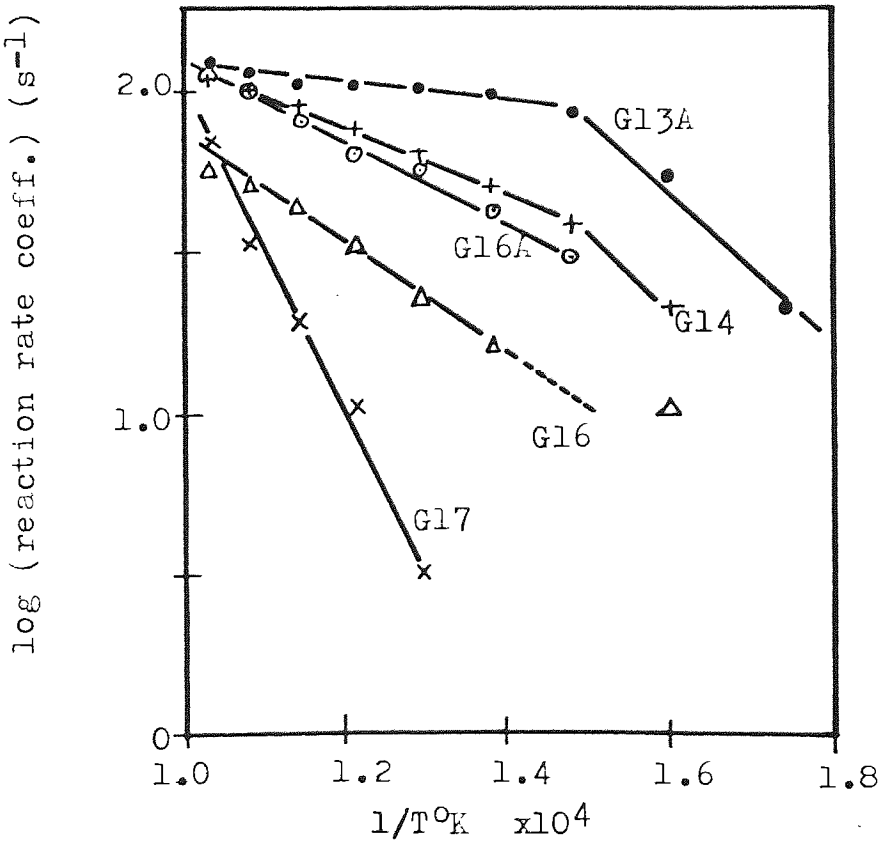

Figure 5.18. : Arrhenius plots of the reaction rate coefficients from Figure 5.2. Samples thermally aged 24 hrs at 800°C in the standard synthetic exhaust gas

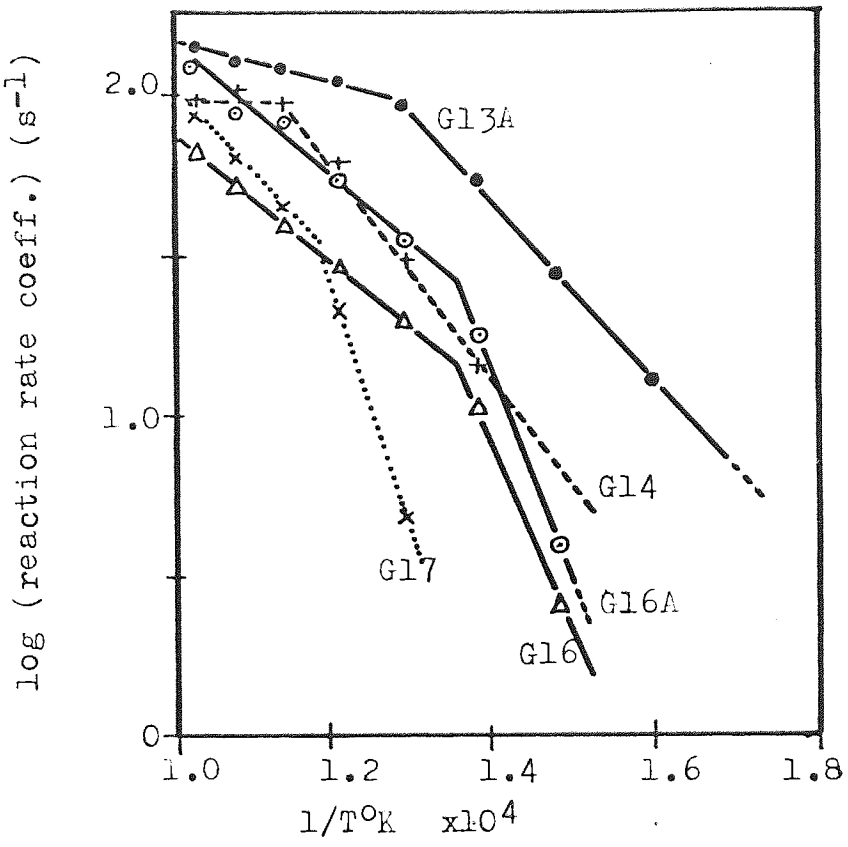

values found here for the activation energy compare with 8 kcals.mol^{-1} found by Bauerle et al.[83] for the reduction of nitric oxide by carbon monoxide over nickel-copper supported catalysts.

In summary, it can be said that the activity of these catalysts was proportional to the metal loading and that the rate of deactivation by crystallite aggregation was not dependent on the metal loading above 5%, and therefore there is no advantage to be gained in reducing the metal loading for these catalysts.

Figure 5.19. : Arrhenius plots of the reaction rate coefficients from Figure 5.1. Samples thermally aged 24 hrs at 1000°C in the standard synthetic exhaust gas

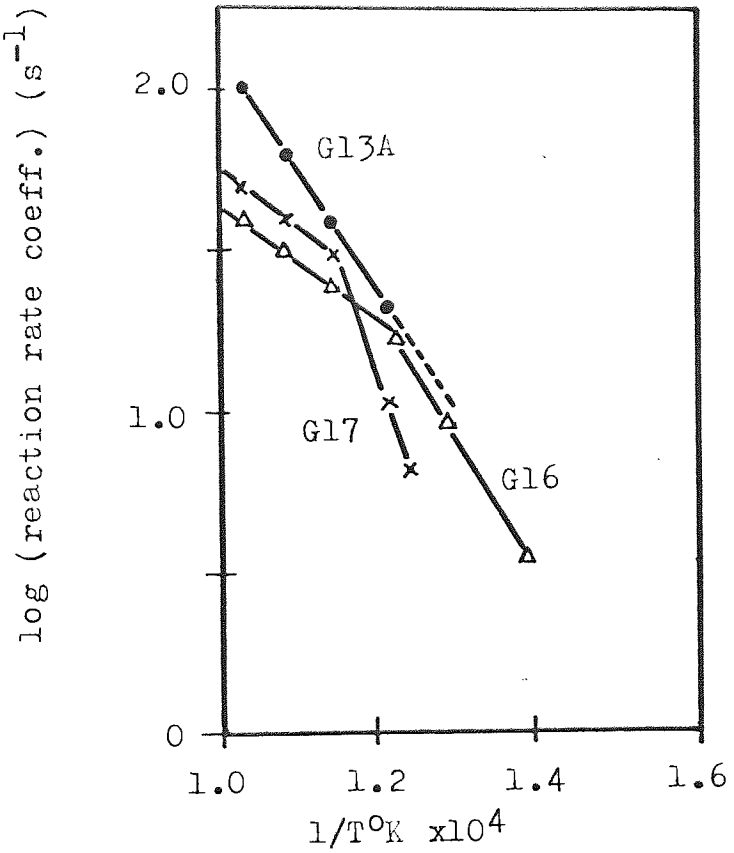

Table 5.3. : The activation energy for nitric oxide reduction as a function of metal loading and thermal ageing in the standard synthetic exhaust gas

Catalyst	Measured activation energies (kcals.mol^{-1})		
	No ageing	Aged 24 hrs at 800°C	Aged 24 hrs at 1000°C
G13A	4.5	4.5	7.6
G14	4.7	6.8	-
G16	3.6	12.4	7.5
G16A	2.6	13.0	-
G17	10.4	15.8	13.2

5.3. Composition of the Active Species

It was seen in Chapter 1 that the surface energy of a metal was one of the factors governing the rate of aggregation of the metal crystallites in supported metal catalysts. The addition of copper to nickel causes a small (10%) decrease in surface energy. It was thought possible that addition of copper to improve the activity of nickel catalysts would accelerate the ageing of nickel copper catalysts by crystallite aggregation. The optimum copper content of a catalyst for the reduction of nitric oxide in automobile exhaust was not clear from a search of the available literature , as shown in Chapter 1, therefore the effect of copper content on the catalytic activity of nickel-copper supported catalysts was investigated. Because of the possible changes in selectivity, with changes in copper content, the net removal of nitric oxide was used to compare the catalysts rather than the conversion of nitric oxide. This was because any ammonia produced over the reduction catalyst in a dual-bed system, would be re-oxidised to nitric oxide over the second oxidation catalyst. The net reduction in nitric oxide was calculated from :

$$X_{net} = \left[(NO)_{in} - (NO)_{out} - (NH_3)_{out}\right] / (NO)_{in} \quad .....5.4.$$

Temperature-activity scans for catalysts in the freshly reduced condition, and after ageing for 24 hrs at 800^{o}C in the standard synthetic exhaust, are shown in Figures 5.20 and 5.22 respectively. The copper content had a marked effect on the removal of nitric oxide from the synthetic automobile exhaust and the first-order reaction rate constants calculated from equation 3.4 are shown plotted against copper content in Figures 5.21 and 5.23. For the fresh catalysts,

Figure 5.20. : Temperature-activity scans as a function of copper content on the activity of the fresh catalysts in the standard synthetic exhaust gas

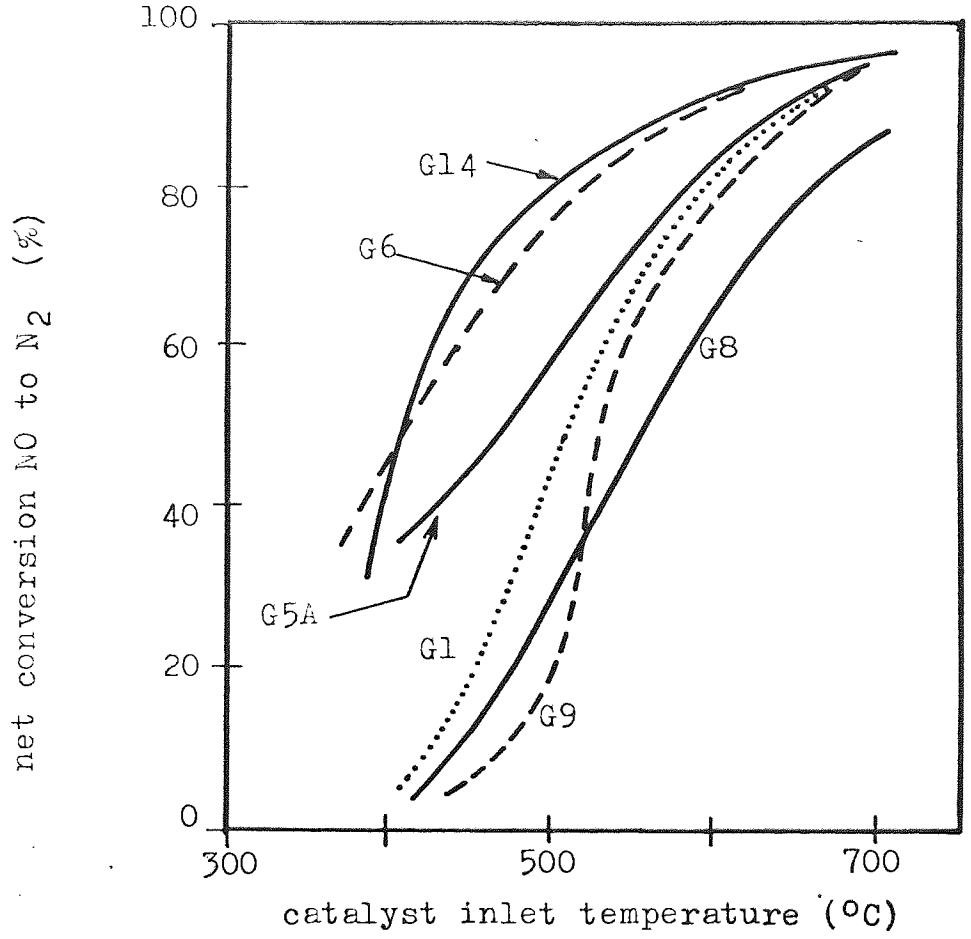

additions of copper up to 25% increased the activity, but further additions reversed this trend. The relationship between activity and copper content for the aged catalysts was similar but the maximum activity occurred at 10% of copper. The scatter of results at 700°C seen in Figures 5.21 and 5.23 was quite large, but reference back to Figures 5.20 and 5.22 show that the conversions of nitric oxide to nitrogen at this temperature are quite closely bunched, covering a range of only $\pm$ 3% conversion, which is close to the limits of accuracy for the activity measurements, and with the high conversions at 700°C, the errors are magnified in calculation of the rate constants.

Figure 5.21. : The reaction rate coefficient (k_2) as a function of copper content for the fresh catalysts

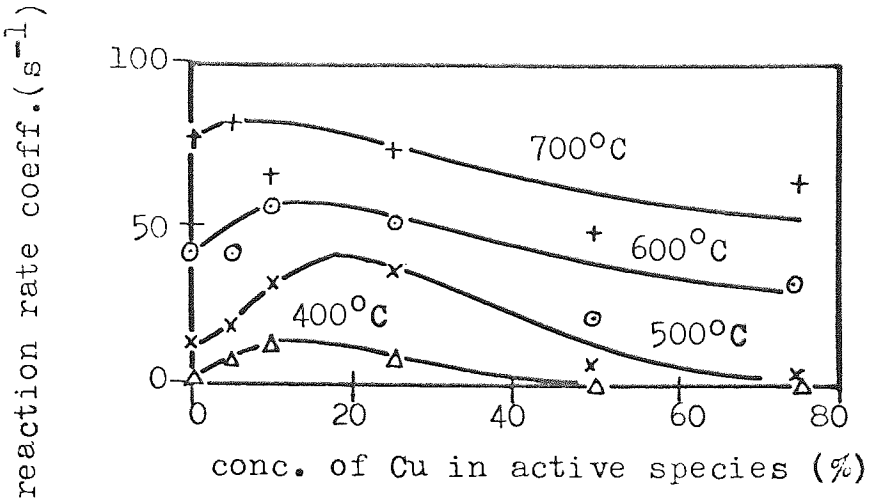

Figure 5.22. : Temperature-activity scans as a function of copper content on the activity after ageing for 24 hrs at at 800°C in the standard synthetic exhaust gas

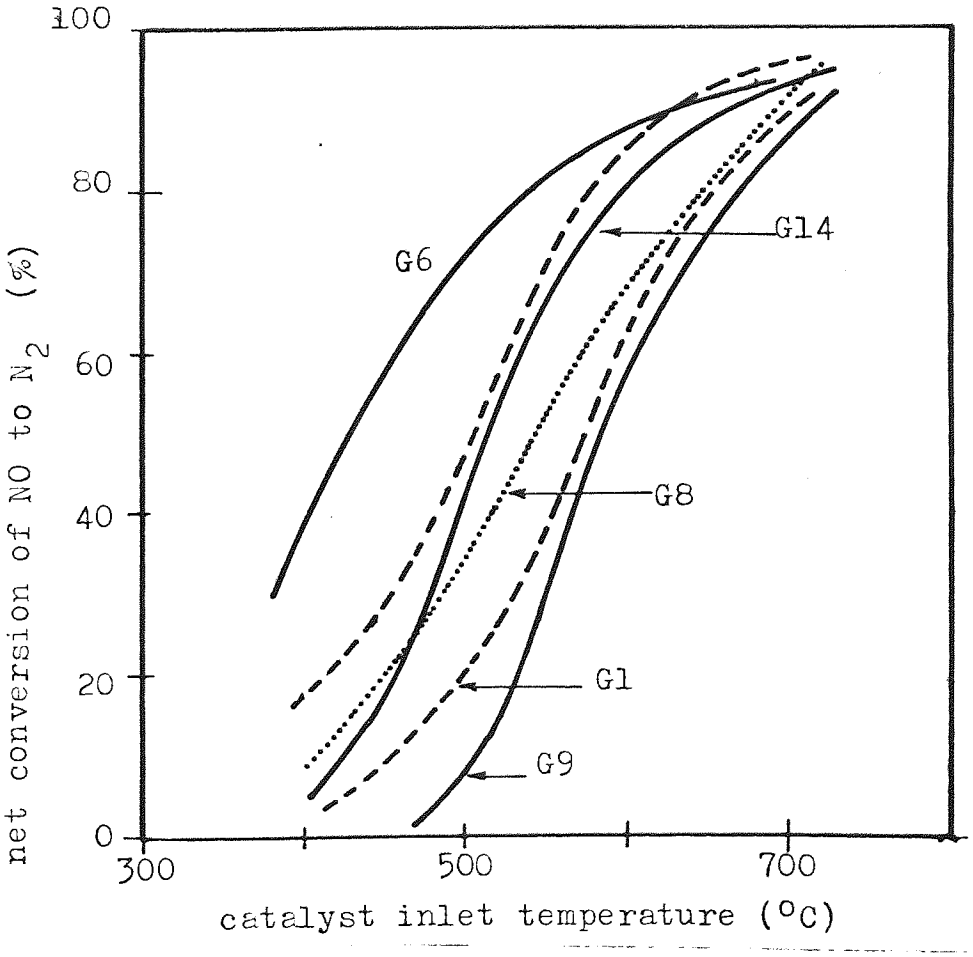

Figure 5.23. : The reaction rate coefficient (k_2) as a fraction of copper content after ageing for 24 hrs at 800°C in the standard synthetic exhaust gas

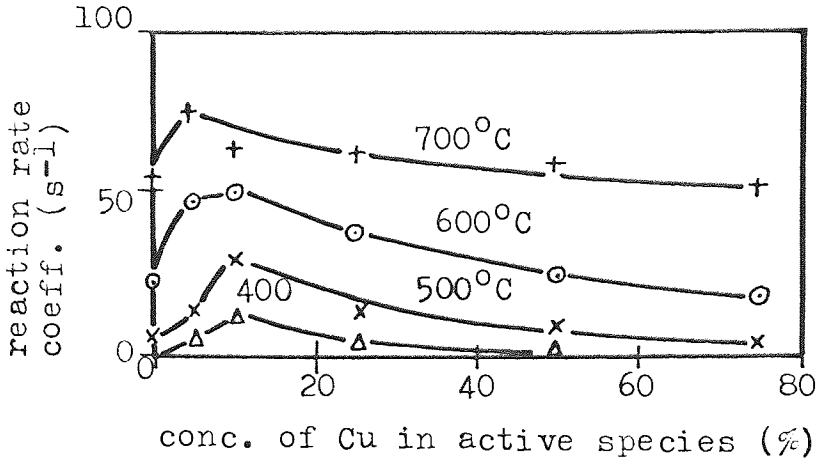

Figure 5.24. : Ammonia production as a function of copper content

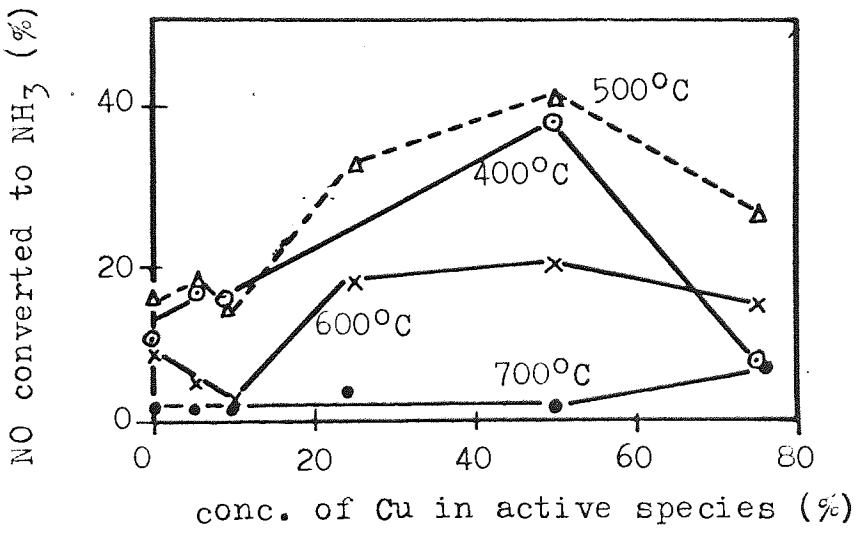

The effect of copper on the formation of ammonia over the aged catalysts is shown in Figure 5.24, where addition of copper up to 50% increased the production of ammonia. In fact, the selectivity for nitric oxide reduction to nitrogen as defined by :

$$\text{Selectivity} = X_{net}/X \qquad \text{.....5.5.}$$

and the observed maximum in ammonia production seen in Figure 5.24 was

due to the low conversions for G9 (75% copper - 25% nickel). The distribution and alloying of the active species on the catalysts was quite homogeneous in the aged catalysts as shown in Figure 5.26. The nickel-copper ratios in aged catalysts for about 50 crystallites were measured by non-dispersive X-ray analysis in conjunction with a scanning electron microscope. The results shown in Figure 5.25 are realistic, since the nickel and copper $K\alpha$ - peaks are very close, although the system was not suited to quantitative investigations.

Figure 5.25. : The distribution of copper from data obtained from a scanning electron microscope with a Kevex X-ray energy dispersive analyser

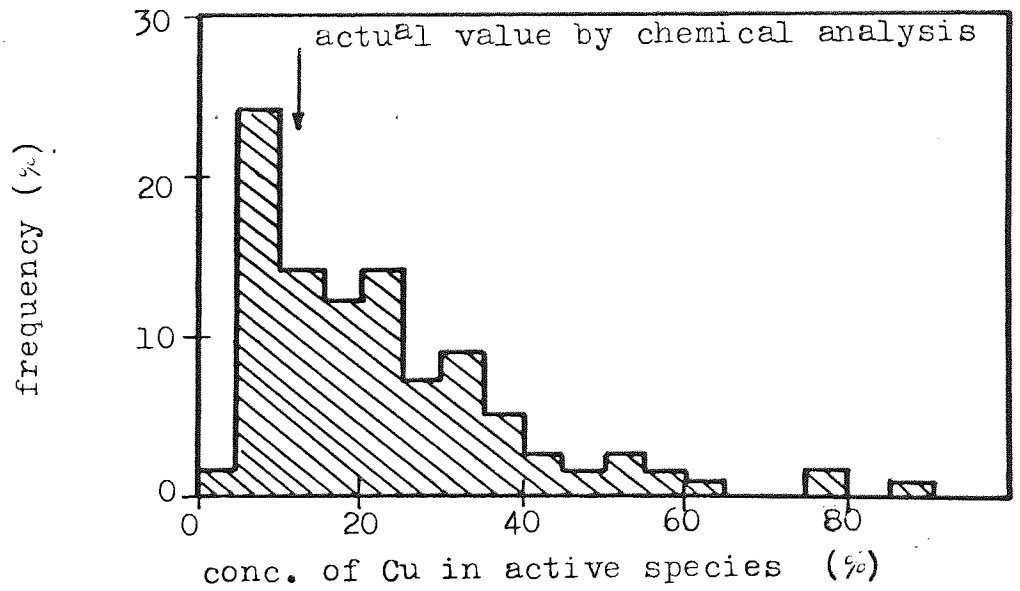

The majority of crystallites were within $\pm$ 5% of the nominal copper content of the catalyst of 11%. Some copper-rich crystallites were seen and occasionally, crystallites of almost 100% copper were observed.

Arrhenius plots of the data from Figures 5.20 and 5.22 showed the typical "knee" of reactions influenced by diffusional limitations. The calculated activation energies are shown in Table 5.4. There was a slight increase in the activation energy with ageing and the trend towards increased values with copper contents of greater than 10% reflected the relationship between activity and copper content seen in Figures 5.21 and 5.23.

Table 5.4. : The activation energy for reduction of nitric oxide as a function of copper content for samples freshly reduced and thermally aged for 24 hrs at 800°C in the standard synthetic exhaust gas

Catalyst	Copper content(%)	Activation energy, E_A ($kcals.mol^{-1}$)	
		fresh	aged
G1	-	9.2	7.5
G5A	5	4.5	6.7
G6	10	3.7	4.2
G14	25	6.8	8.7
G8	50	12.4	7.6
G9	75	14.1	21.0

The activity of the aged catalysts was normalised by dividing by the original activity. This value was then plotted against copper content in Figure 5.26 to compare the ageing of various catalysts. The results showed that up to 50% of copper improved the ageing resistance of the catalysts and was most probably due to homogenisation of the active species as a result of the aggregation process, although it was not possible to determine the degree of alloying prior to ageing because of the very small crystallite size. As the mean crystallite size increased, the probability that each

Figure 5.26. : Deactivation after ageing for 24 hrs at 800°C in the standard synthetic exhaust gas as a function of copper content

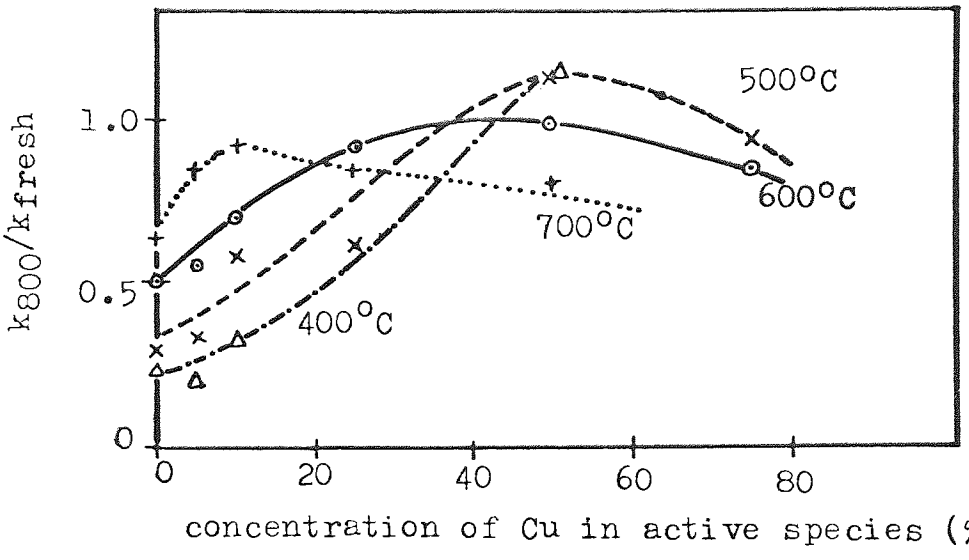

individual crystallite would have a value close to the nominal copper content of the catalyst increased, so that the intrinsic activity of the catalyst was increasing. Additions of copper above 10% had no further significant effect. The effect of copper additions on the rate of crystallite aggregation is shown in Table 5.5.

The decrease in surface area on ageing tended to increase with addition of copper, but the increase was not really significant. From these results it is possible to make a choice of the optimum level of copper in a supported nickel-copper catalyst for the removal of nitric oxide from automobile exhaust, based on both the catalytic activity and the resistance to thermal ageing. On both counts the optimum value was approximately 10% copper which agrees with the value that ICI has found to be best on the grounds of activity alone.

Table 5.5. : The reduction in specific surface area after ageing for 24 hrs at 800°C in the standard synthetic exhaust gas as a function of copper content

Catalyst	Copper content (%)	Total surface area ($m^2.g^{-1}$ catalyst)		Red^n in S.A. on ageing (%)
		fresh	aged	
G1	-	2.5	1.5	40
G5A	5	2.2	1.3	40
G6	10	3.3	1.8	45
G14	25	3.9	1.7	56
G8	50	4.4	2.2	50
G9	75	3.1	1.6	48

5.4. Implications of Thermal Ageing to Catalyst Formulation

Typically, a fresh catalyst system must remove more than 99% of the nitrogen oxides emitted, since some ageing is to be expected and a 90% removal of nitrogen oxides is the target figure for 1985 for the U.S. Legislation. The use of fractional conversions can be very misleading. For example, it has been shown that under conditions of pure thermal ageing, the parameter A/Ao, compared at 500°C, falls from 1.0 to less than 0.5, but Figure 4.1 shows that when compared at 650°C, the decline is from 1.0 to approximately 0.9 for the same catalyst. When compared at 750°C, the change in activity is barely measurable under these conditions since conversion is so nearly complete even after the severest ageing treatment. The use of an emissions test which measures mass emissions as embodied in the U.S. Federal Regulations[24] therefore gives a much fairer indication of the effectiveness of a catalyst when it is to be used under transient

conditions. But the object of this study was comparative rather than determination of absolute emission levels. Comparison of the conversions at low temperatures becomes relevant and emphasises the differences in catalytic efficiency.

It is not possible from the thermal ageing data to predict catalyst lives under service conditions, but it is interesting to compare the relative lives at different ageing temperatures. In Table 5.6, an arbitrary criterion, the time for the parameter A/Ao (at 500°C) to fall to 0.5, is used to compare catalyst lives. Of course, the projected lives are very short because, under practical conditions, the efficiency of the catalyst is measured at an average temperature of 750°C, and only a relatively small part of the overall emissions are related to periods when the catalyst is at such a low temperature as 500°C. The analysis does, however, point to the very marked reduction in lives experienced when the catalyst is at a high temperature for very short times. This means that the operating temperature of the catalyst should be the lowest compatible with the catalyst efficiency, and that temperature control must be an important consideration. The engineering of the system should ensure that high temperature transients are minimised or excluded. As described in Chapter 1, unburnt gases can give rise to exceptionally high catalyst temperatures, so that the engine should be kept well-maintained and properly tuned if the full life of the catalyst is to be realised. Neither metal loading (from 5-50%) or copper content was found to influence the rate of deactivation by thermal ageing of nickel-copper supported catalyst, but rather, as discussed above, the time, and particularly the temperature of the ageing treatments were of

Table 5.6. : Comparison of the lives of thermally aged catalysts under the arbitrary criterion A/Ao = 0.5 (at 500°C)

Ageing temp(°C)	Time for A/Ao=0.5 (hrs)	Predicted mileage at:	
		48Kmph (30mph)	80Kmph (50mph)
650	250	12000 Km (7500 miles	20000 Km (12500 miles)
700*	90	4320 (2700)	7200 (4500)
800	20	960 (600)	1600 (1000)
900	2	96 (60)	160 (100)
1000	1	48 (30)	80 (50)

* extrapolated

paramount importance. The limiting factor is probably the transport of material across the surface of the support as discussed in Chapter 1, and for a given surface area of support, the particle size rather than distribution is affected by the metal loading as shown in Tables 5.1 and 5.2, and therefore the interparticle distances over which the material must diffuse do not vary significantly.

6. AGEING OF MONOLITHIC CATALYSTS

6.1. Physical Examination of Catalysts M1-M6

Scanning electron microscopy of these samples revealed much additional information to that already obtained from the endurance tested catalysts described in Chapter 2. One interesting observation was that the system of cracks previously referred to as drying cracks was extended in many areas of the wash-coat by thermal ageing in a reducing atmosphere. A particularly bad example of this is shown in Figure 6.1. This suggested why the wash-coat in adjacent channels through a catalyst matrix should behave quite independently, such as in the situation shown in Figure 2.11. This cracking was considered

Figure 6.1. : Scanning electron micrograph of sample M4 after ageing for 24 hrs at 800°C in the standard synthetic exhaust gas

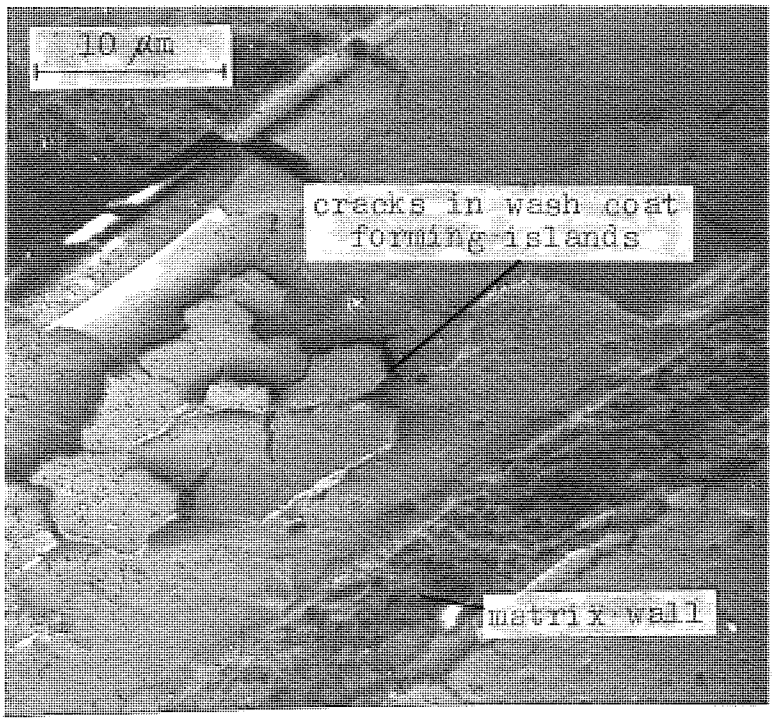

to initiate the process leading to loss of the wash-coat, so that where the coating was free of cracks after drying, it would remain in tact for the life of the catalyst . The extent to which these drying cracks occurred in the freshly deposited wash-coat varied considerably from the massive cracks observed at the corners of the channels to those shown in Figures 6.2 to 6.4. These smaller cracks may be partially healed during the subsequent sintering operation. The degree of cracking would not only depend upon the thickness of the coating, but also upon the rate of drying. An alternative method of coating the matrix which overcame these problems is discussed in Section 7.2.

The gehlenite particles themselves were clearly seen in catalyst M1, zero active metal content, the wash-coat itself was a loosely sintered structure with a relatively high porosity, containing many small drying cracks. The cracks formed before impregnation with the active metal, as shown in Figure 6.3, the structure of which may be compared to that shown in Figure 6.4. The latter is a micrograph of catalyst M5 (48% metal loading) in which the metal crystallites lie on and between the gehlenite particles. This catalyst has the lowest metal loading in this series of monolithic catalysts, with a metal concentration in the wash-coat of 40%. However, even at the higher levels of approximately 70% in catalysts M2, M3 and M6, the structures were very similar, the only difference being the size of the metal crystallites. Except for the loss of coating, ageing in the engine dynamometer rig did not result in any significantly different structures to those formed by thermal ageing. The metal crystallite sizes determined in five different ageing treatments are shown in Table 6.1. The very large crystallite sizes found in M4 were due to

Figure 6.2. : Scanning electron micrograph of a freshly coated sample (M1), sintered but containing no metal species. Area A is shown at a higher magnification in Figure 6.3.

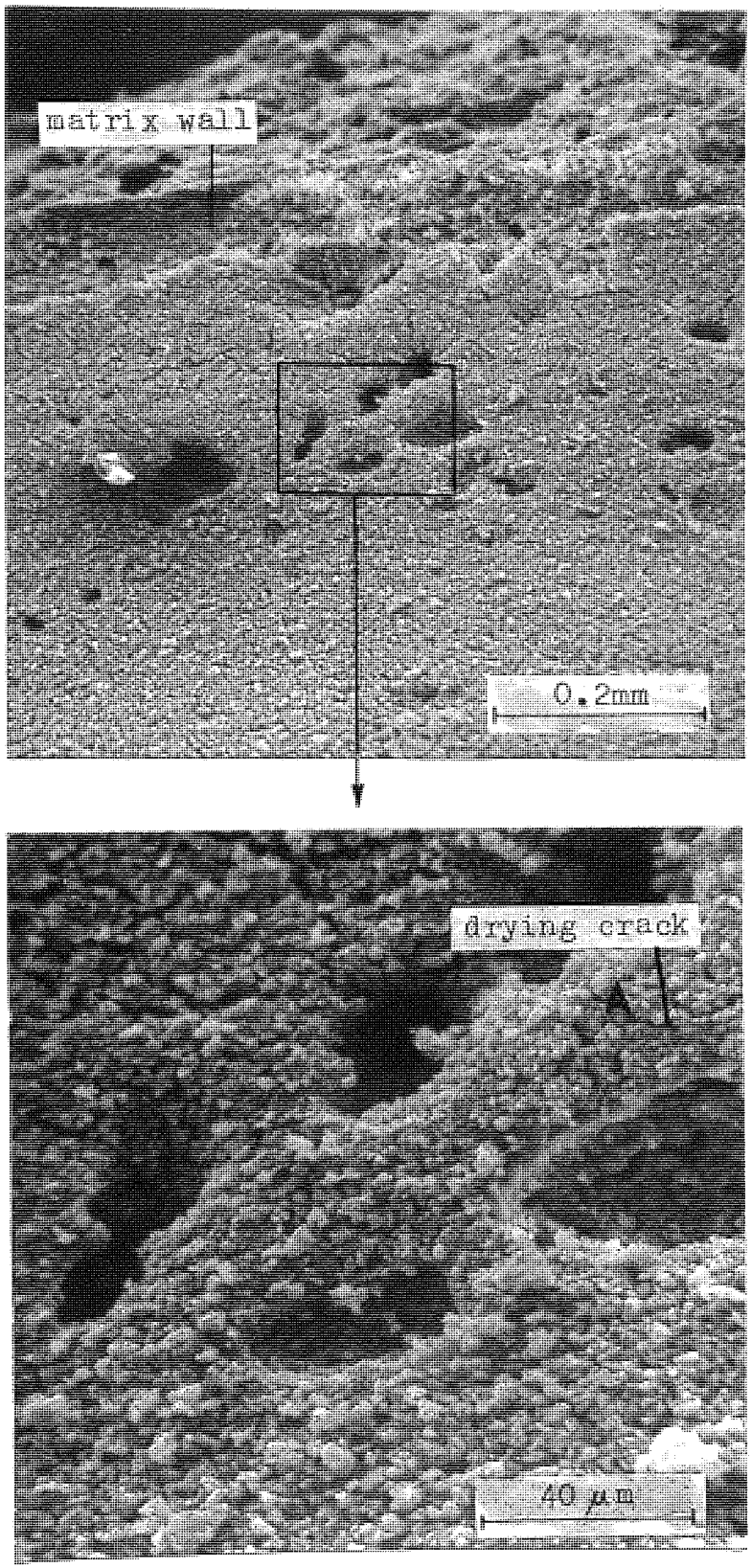

Figure 6.3. : Scanning electron micrograph of a freshly coated sample (M1), sintered, but containing no metal species

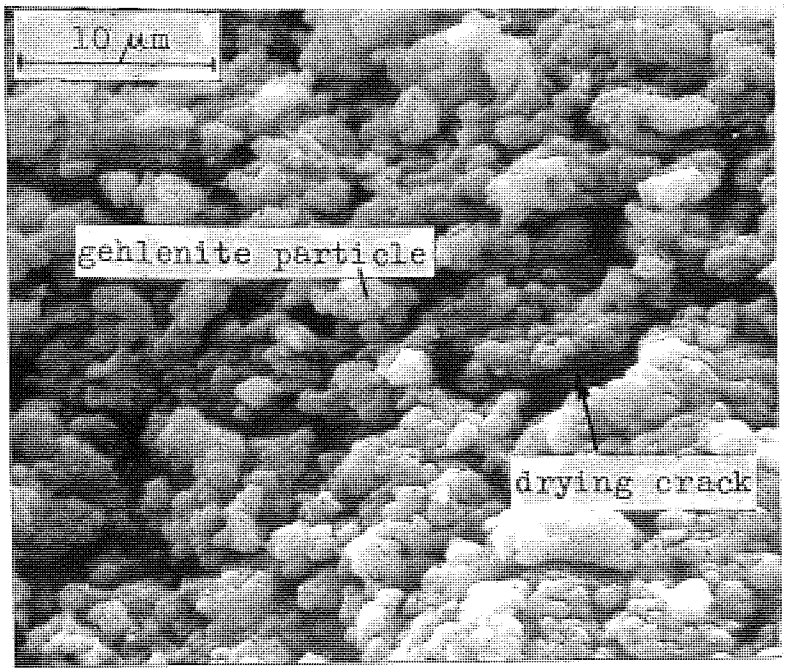

Figure 6.4. : Scanning electron micrograph of sample M5 after thermal ageing, 24 hrs at 800°C in the standard synthetic exhaust gas

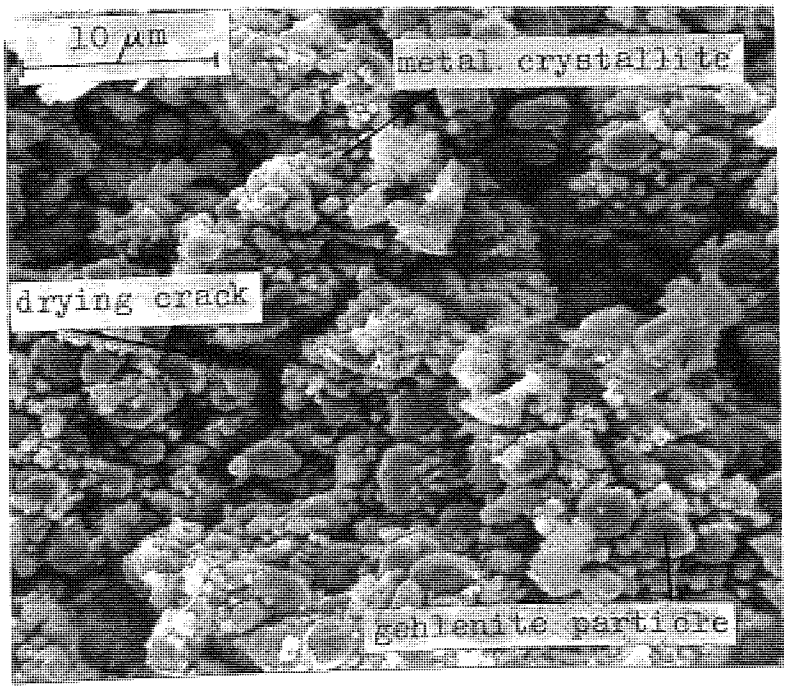

an inhomogeneous distribution of the active metal species. In many areas, a layer of metal oxides completely covered the wash-coat after impregnation, as shown in Figure 6.5. This led to some extremely varied, local structures as shown in Figures 6.6 and 6.7. As in the case of the endurance tested catalysts, virtually the complete coverage of wash-coat was lost in many areas, so that the matrix wall was left covered with debris, as shown in Figure 6.8.

Table 6.1. : The average metal crystallite size of catalysts M2-6 after various ageing treatments

Catalyst	Average metal crystallite size (μm)				
	Fresh	Synthetic exhaust gas / engine dynamometer			
		24hrs at 800°C	24hrs at 900°C	4000 km (2500miles)	8000 km (5000miles)
M2	.20	.35	-	-	.40
M3	.10	.30	-	-	.40
M4	.20	.90	2.50	1.00	1.15
M5	.05	.15	.40	.30	.20
M6	.15	.35	.70	.85	.85

6.2. Chemical Analysis

Chemical analysis of the engine tested catalysts for lead showed a very large scatter of results as shown by Table 6.2. However, the lead content correlated well at 650°C with the deactivation for the conversion of nitric oxide for each dynamometer ageing treatment as shown in Figure 6.9. At the very low conversions at 500°C there was no such dependence on the level of of lead. It is normal for catalysts to maintain "light-off" characteristics with low levels of poisoning, but to lose activity at higher temperatures. The difference between

Figure 6.5. : Scanning electron micrograph of catalyst M4 in the fresh condition, the metal oxide completely covered the gehlenite wash-coat

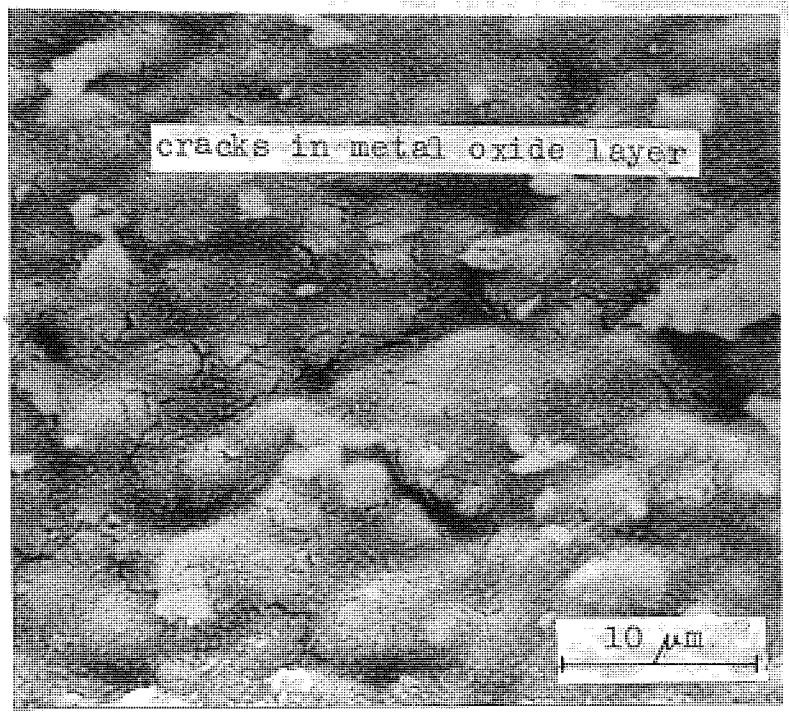

Figure 6.6. : Scanning electron micrograph of sample M4 after ageing in an engine dynamometer rig for the equivalent of 8000 km(5000 miles)

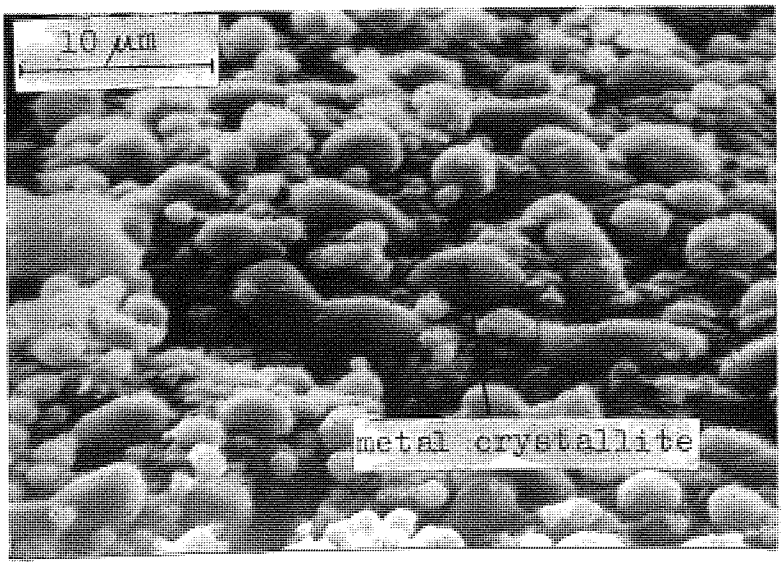

Figure 6.7. : Scanning elctron micrograph of catalyst M4 after ageing for 24 hrs at 900°C in the standard synthetic exhaust gas

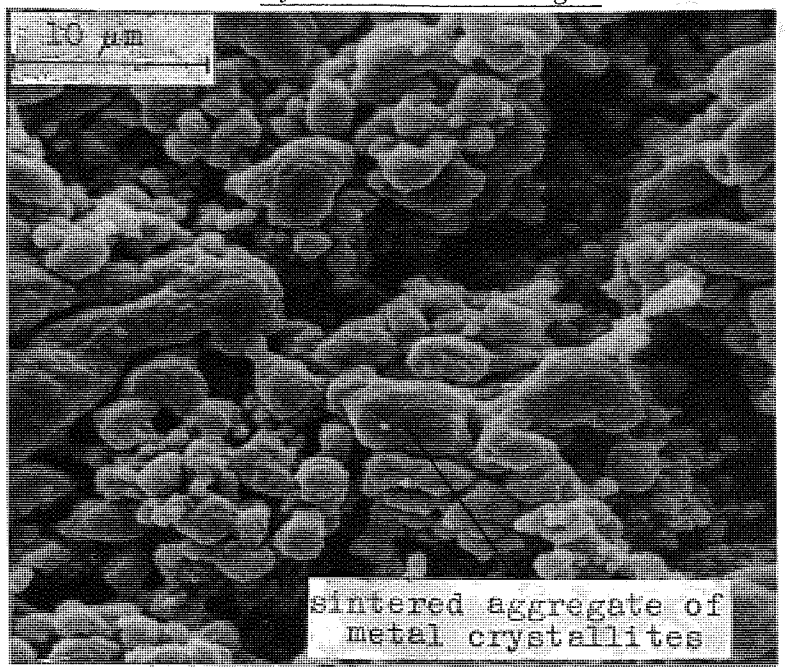

Figure 6.8. : Scanning electron micrograph of catalyst M2 after ageing in an engine dynamometer rig for the equivalent of 5000 miles. The wash-coat has been lost leaving only debris on the surface of the matrix wall

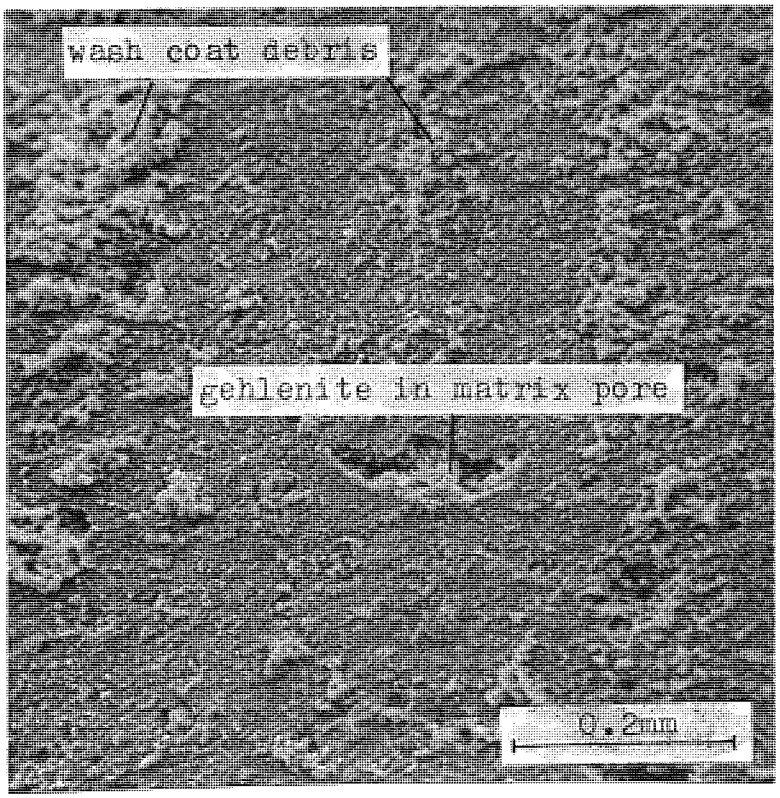

the conversion results after 4000 and 8000 km for the same lead concentrations suggested that the fractional loss of coating and active species was highly significant. Consideration of neither the

Table 6.2. : Lead concentration (% of catalyst) on the engine tested catalysts

Treatment	M2	M3	M4	M5	M6
4000 km (2500 miles)	.12	.20	.18	.07	.14
8000 km (5000 miles)	.05	.37	.02	.39	.14

metal crystallite size, possible reactions of the active species with the wash-coat, nor other poisons offered any alternative explananation. Nevertheless, it was not possible to show any direct correlation between the loss of wash-coat and deactivation. The loss of wash-coat was calculated from chemical analyses of the concentration of calcium and is shown in Table 6.3. The inability to show any correlation with deactivation was thought to be due to a combination of factors. The first was that the sample size was necessarily small. Secondly, the loss of material in the early stages would be primarily from the corners of the channels with little effect on catalytic activity. finally, the initial wash-coat loading varied from 4.7 to 8%, with metal concentrations in the coating of from 40 to 75%, and it is uncertain what effect this would have,

6.3. The Deactivation of Catalyst Samples M2-M6

The five catalysts were each subjected to five different ageing treatments : two involved testing in an engine dynamometer rig whilst

Figure 6.9. : Deactivation after engine testing as a function of lead concentration

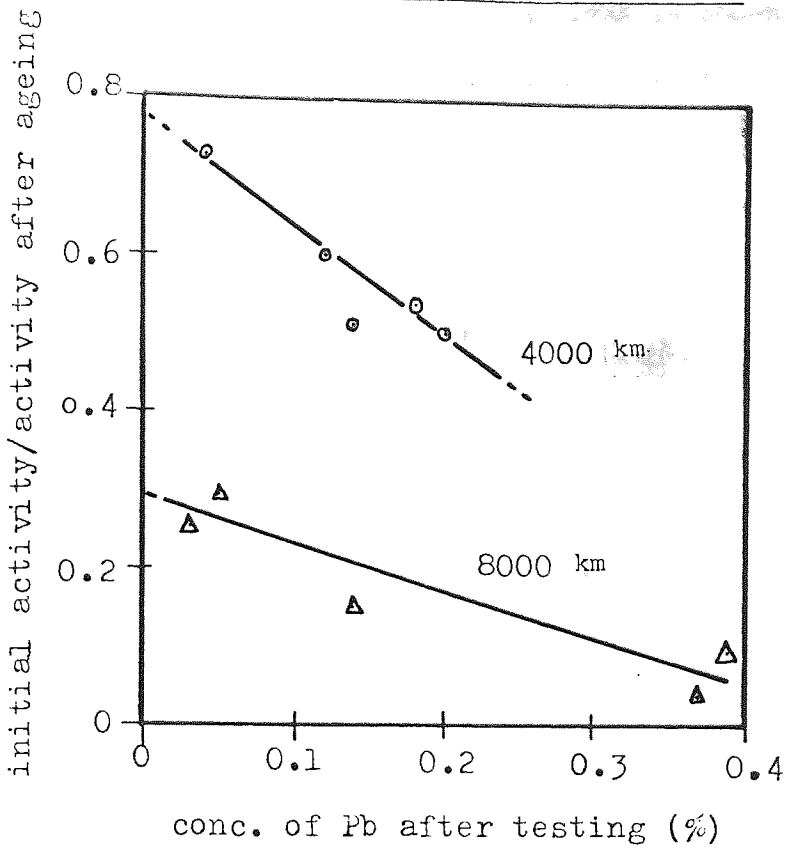

Table 6.3. : The fractional loss of wash-coat and active species from the six samples as a function of test duration

treatment	fractional loss of wash-coat (%)					
	M1	M2	M3	M4	M5	M6
4000 km 2500 miles	1	38	35	20	6	33
8000 km 5000 miles	1.6	47	45	32	23	36

the others were thermal ageing. A summary of the reduction of nitric oxide obtained from temperature-activity scans is shown in Figure 6.10 for high temperatures (650°C) and in Figure 6.11 for low temperatures (500°C).

Figure 6.10. : Comparison of the reduction of nitric oxide at 650°C for catalysts M2-6 after various ageing treatments

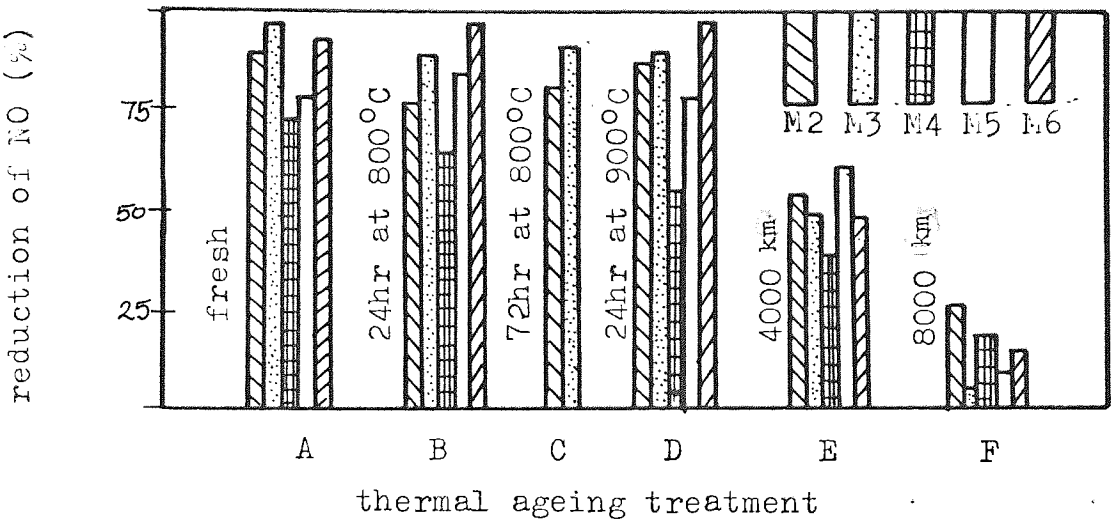

It can be seen that, as in the case of the granular catalysts, pure thermal ageing has little effect on nitric oxide reduction when tested at temperatures well above the "light-off" temperature since the temperature-activity curve was simply shifted to the right, i.e. to higher temperatures. Engine testing, however, showed a further effect : the maximum conversion efficiency was effectively reduced within the temperature limits of the temperature-activity scan as shown by E and F in Figure 6.10. It is obvious from Figure 6.10 that the differences between the catalysts were small ($\pm$10%) compared to the differences between the ageing treatments, particularly when one also considers the results shown in Figure 6.11. It is possible, therefore, to

Figure 6.11. : Comparison of the reduction of nitric oxide at 500°C for catalysts M2-6 after various ageing treatments

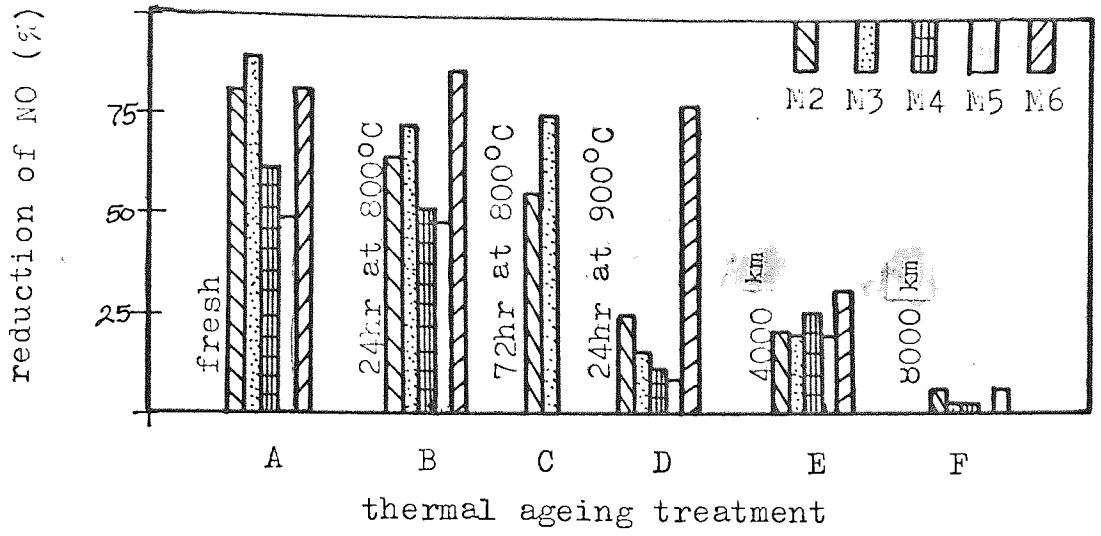

group the catalysts and determine the mean reduction of nitric oxide for each treatment as in Table 6.4. It can be seen that in-engine ageing causes a greater deactivation of the catalysts than pure thermal ageing, as would be expected since all three major deactivation mechanisms will operate. It is interesting to note in Figures 6.12 to 6.16 that the temperature activity curves for the samples aged for 24 hrs at 900°C and those aged for the equivalent of 2500 miles in the

Table 6.4. : The mean percentage conversions of nitric oxide for catalysts M2-6 as a function of the ageing treatment. The conversions were measured in the standard synthetic exhaust

Temp (°C)	Mean conversion (%) after each treatment				
	Standard synthetic exhaust gas			Engine dynamometer	
	Fresh	24hrs at 800°C	24hrs at 900°C	4000 km (2500miles)	8000 km (5000miles)
650	87	82	80	50	14
500	72	64	15*	24	3

* omit M6

engine dynamometer rig intersect, emphasising the danger of comparing catalysts under one set of experimental conditions. The complete activity data for catalysts M2-M6 is shown plotted according to the Arrhenius relationship in Figures 6.12 to 6.16. The "knee" in the curves was again obvious except for those samples aged in the engine dynamometer rig. It was assumed that these were in kinetic control regime because of their low inherent activity. The activation energies in the kinetic control regimes were calculated and are shown in Table 6.5. As in the case of the granules, very low values were obtained

Figure 6.12. : Arrhenius plot of the activity results for M2 after various ageing treatments

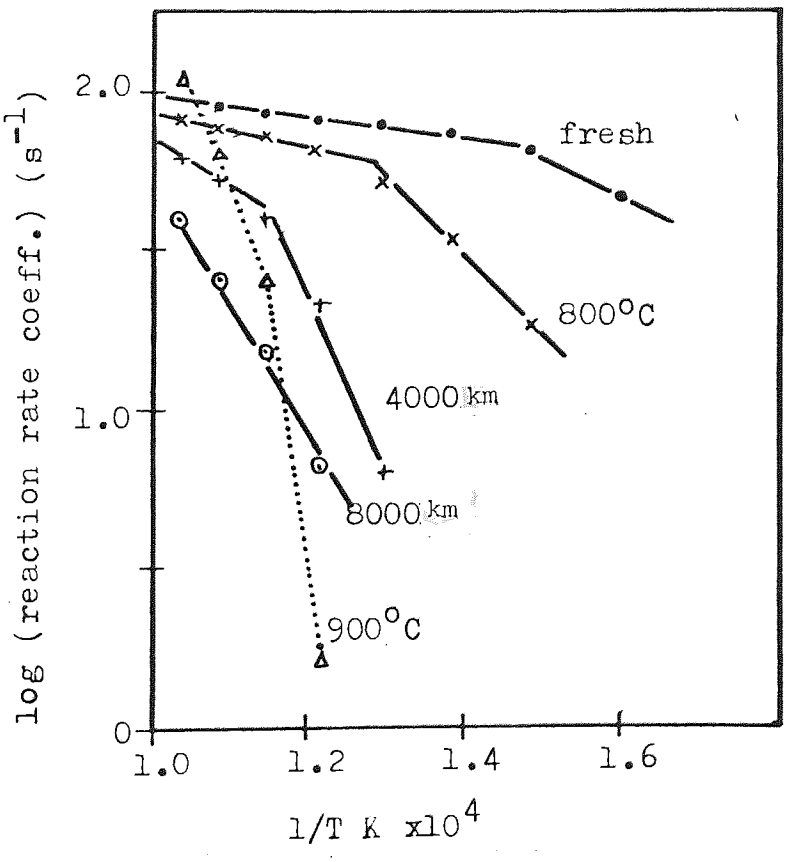

for the activation energies of the fresh catalysts and were increased by ageing. There was no correlation between the active metal content and the activity or the activation energy for this series of catalysts.

Figure 6.13. : Arrhenius plots of activity results for catalyst M3 after various ageing treatments

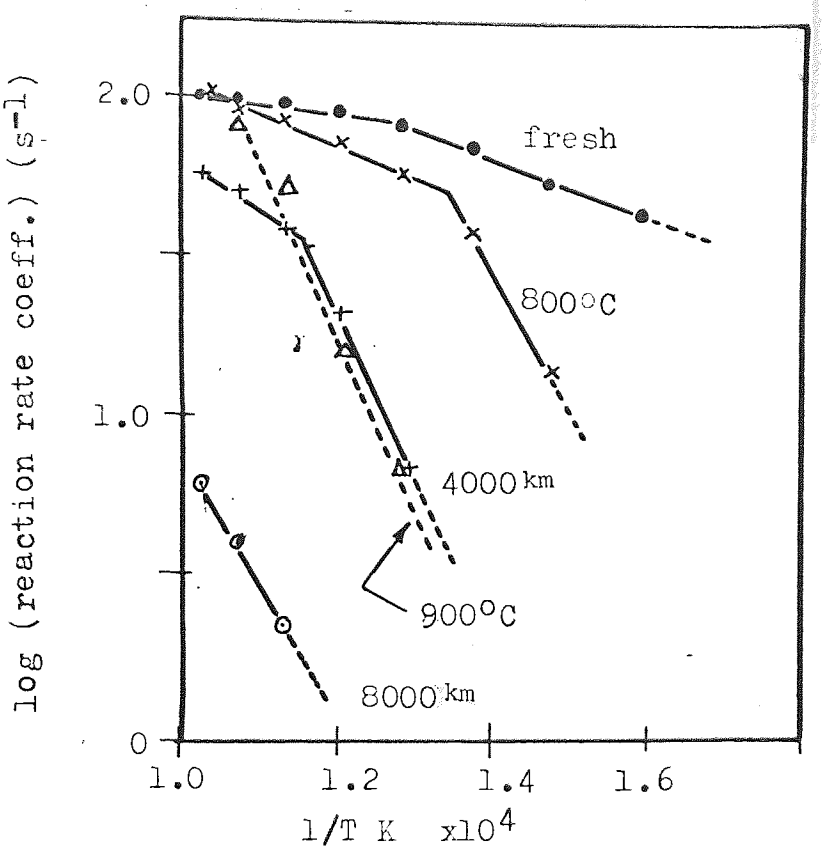

Figure 6.14. : Arrhenius plots of the activity results for M4 after various ageing treatments

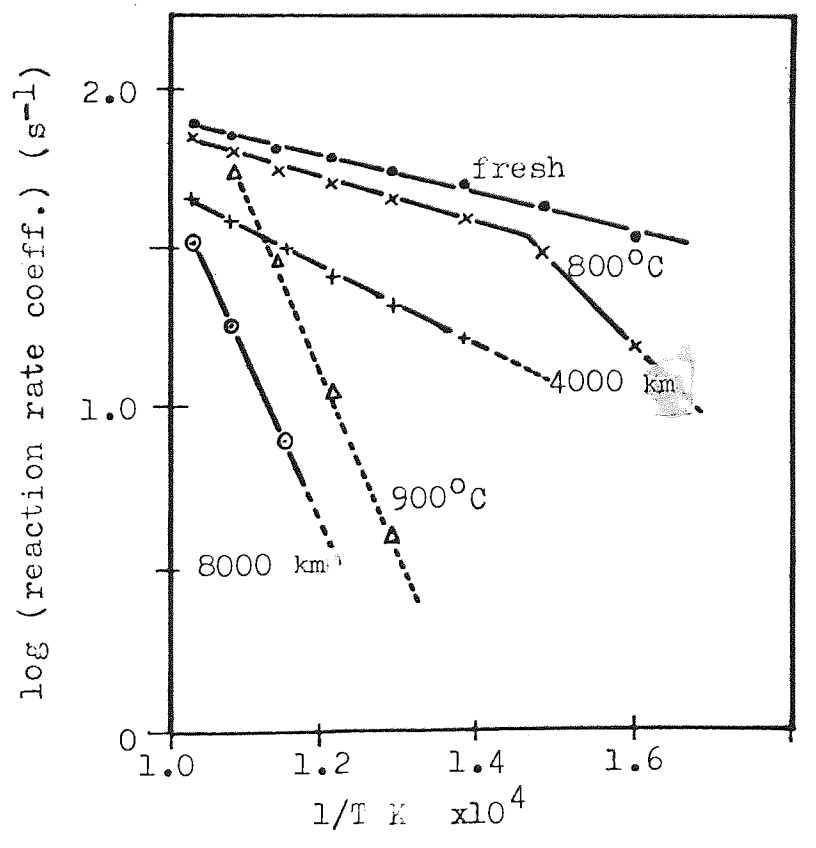

Figure 6.15. : Arrhenius plots of the activity results for M5 after various ageing treatments

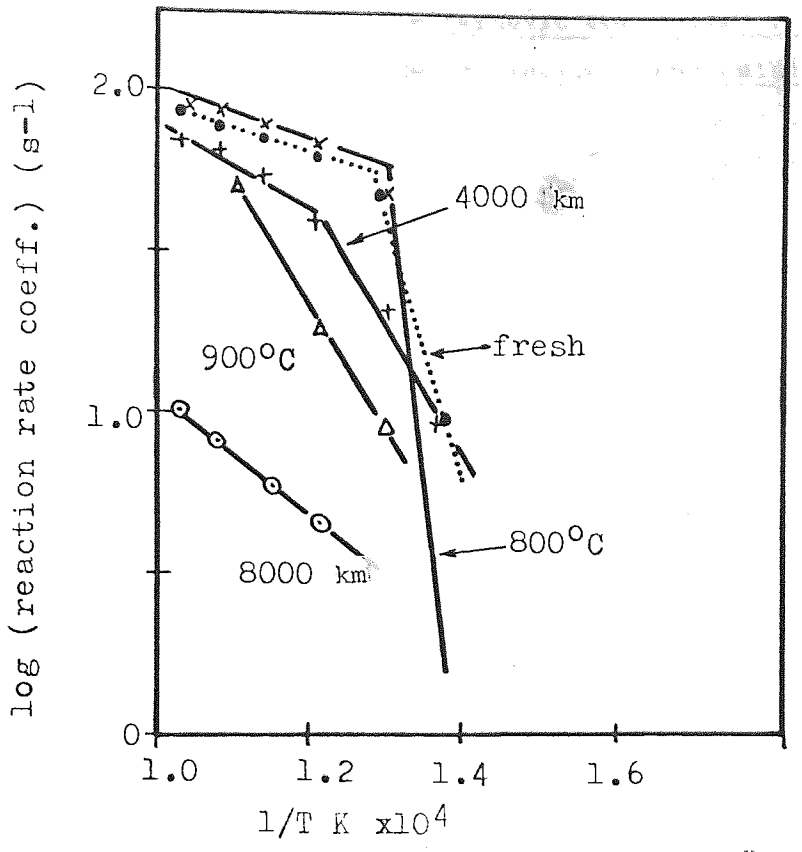

Figure 6.16. : Arrhenius plots of activity results for M6 after various ageing treatments

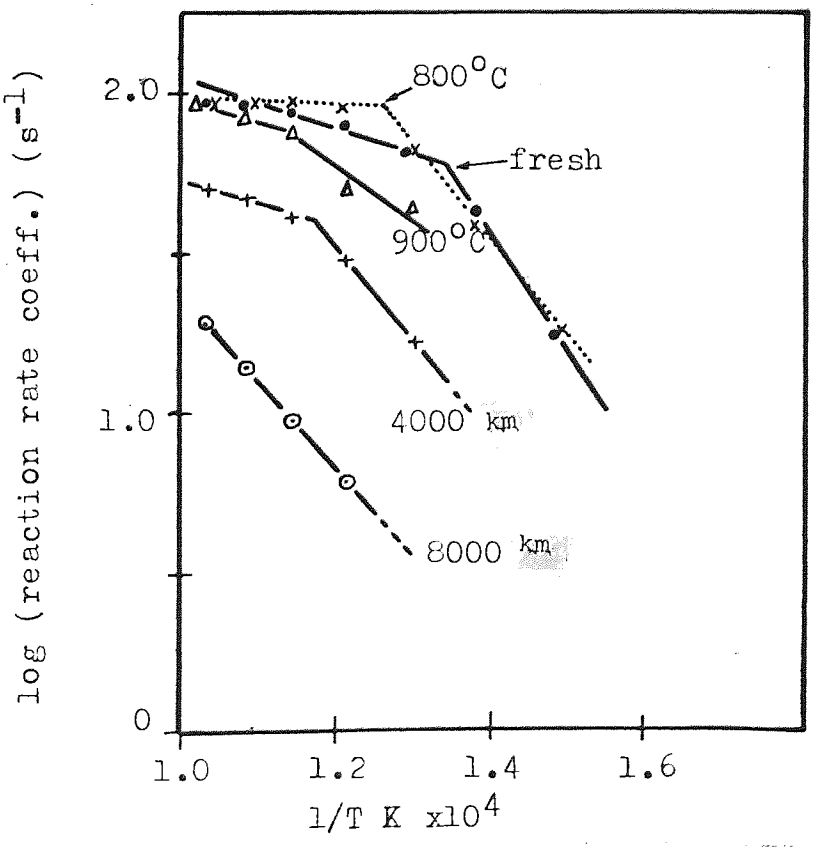

Table 6.5. : Activation energy ($kcals.mol^{-1}$) calculated from Figures 6.12 to 6.16 (kinetic controlled region) as a function of ageing treatment and catalyst

Catalyst	Activation energy ($kcals.mol^{-1}$)				
	Fresh	Thermal ageing		engine dynamometer	
		24hrs at 800°C	24hrs at 900°C	4000 km (2500miles)	8000 km (5000miles)
M2	0.7	5	30	11	9
M3	0.5	9	11	10	8
M4	1.2	4	11	5	10
M5	1.5	40	4	9	4
M6	1.6	8	3	6	6

It was not possible to draw any firm conclusions regarding the correct formulation of the catalysts from the observations recorded in this chapter. However, one factor does stand out, that the loss of wash-coat and active species was of concern and should be investigated further.

6.4. Relative Contributions to Deactivation by the Major Mechanisms

Although catalyst poisoning was not considered experimentally in this project, it cannot be separated from the other major deactivation mechanisms, particularly when considering engine tested catalysts where poisoning effects on activity are inseparable from the other mechanisms. It is possible to carry out a non-rigorous analysis of the approximate relative contributions to deactivation for each mechanism. Although the theoretical basis is open to question, it does indicate trends that agree with results of endurance tests carried out by BL Cars, Air Pollution Control Laboratory. As mentioned in

Chapter 2, endurance runs on nickel-based catalysts up to 80,000 km (50000 miles) have been carried out, and in all cases the deactivation was initially rapid up to 8000 km (5000 miles), and thereafter, the rate of deactivation was very slow. These tests were carried out with unleaded fuel with lead contents of less than 0.013g.L^{-1} (0.05g.gal^{-1}).

The analysis is shown in Figures 6.17 and 6.18, and the following conclusions are drawn from it. The loss of activity due to poisoning has relatively more significance at 650°C than 500°C and after 4000 km (2500 miles) than after 8000 km (5000 miles), as summarised in Table 6.6. The latter effect was assumed to be due to the exposure of fresh surfaces free from lead as the coating was broken up and lost down the exhaust pipe, coupled with the increased loss of activity due to the loss of coating and the active species itself at 8000 km (5000 miles). There is a large decrease in activity due to loss of wash-coat and active species from 4000 km to 8000 km (2500 to 5000 miles) despite the relatively small difference in the loss of active species itself. This was attributed to the fact that initially much of the loss was from the heavy build-up of coating at the cell wall corners, and

Table 6.6. : The relative loss in activity (expressed as a percentage of the conversion of NOx in the fresh catalysts) of the three major mechanisms of deactivation after engine testing

Activity test temp. (°C)	Life (miles)	Relative loss in activity due to :		
		Crystallite aggregation (%)	Loss of active species (%)	Poisoning (%)
650	2500	5	7	25
650	5000	5	52	16
500	2500	8	37	3
500	5000	8	59	2

a simple weight percentage loss gives a disproportionate figure for loss of available surface area of active species since a depth of only a few microns of the coating were actually involved in the catalytic processes.

Figure 6.17. : A simplified analysis of the relative contribution of crystallite aggregation, loss of wash-coat and active species and poisoning to the deactivation of the matrix catalysts in M1-M6 at 650°C

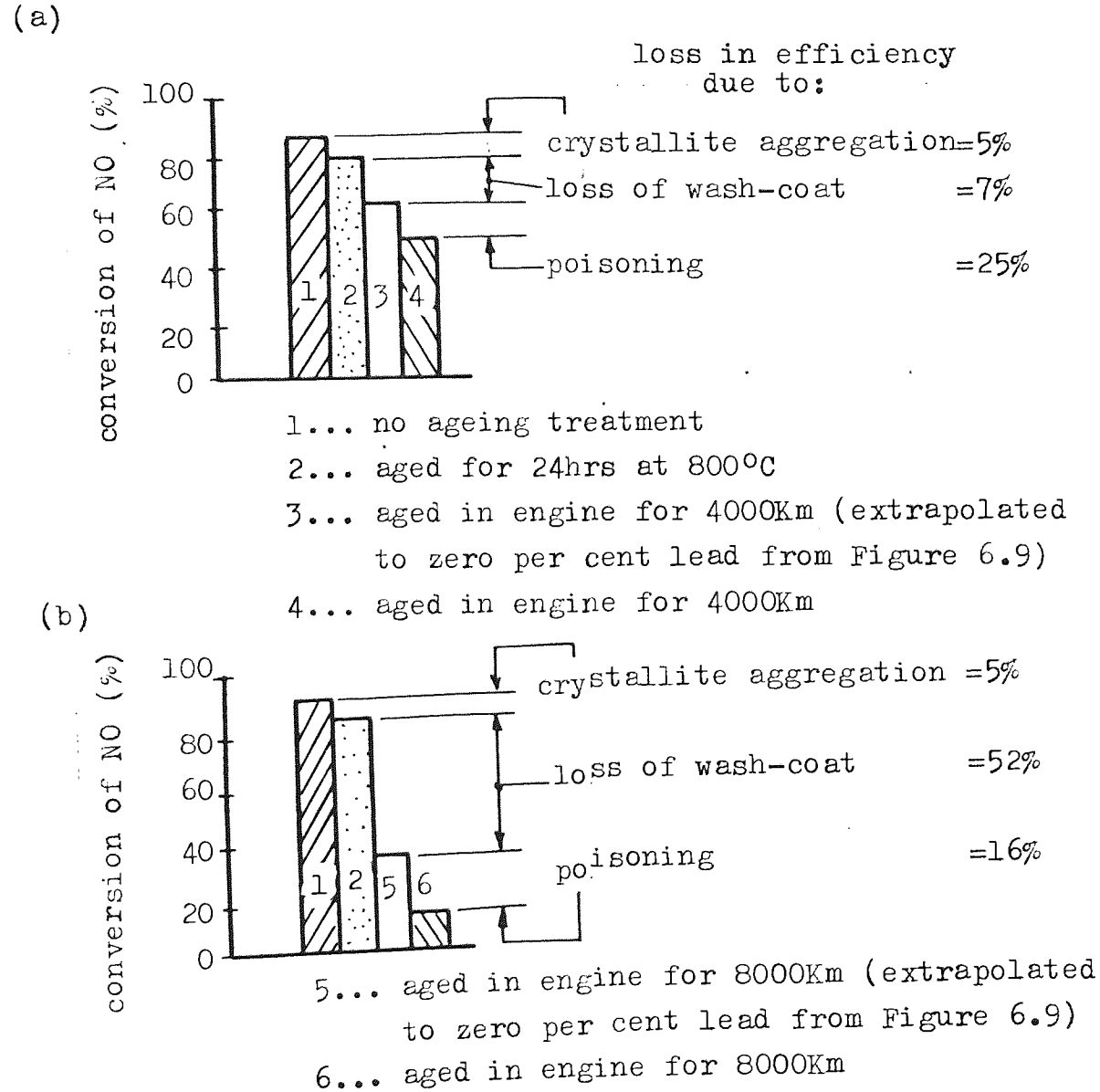

Figure 6.18. : A simplified analysis of the relative contribution of crystallite aggregation, loss of wash-coat and active species and poisoning to deactivation of the matrix catalysts M1-M6 at 500°C

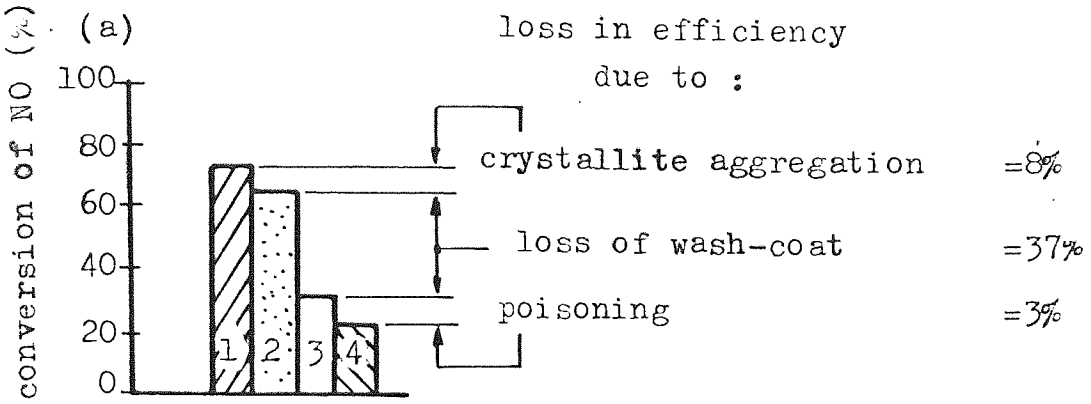

1... no ageing treatment

2... aged for 24hrs at 800°C

3... aged in engine for 4000Km (extrapolated to zero per cent lead from Figure 6.9)

4... aged in engine for 4000Km

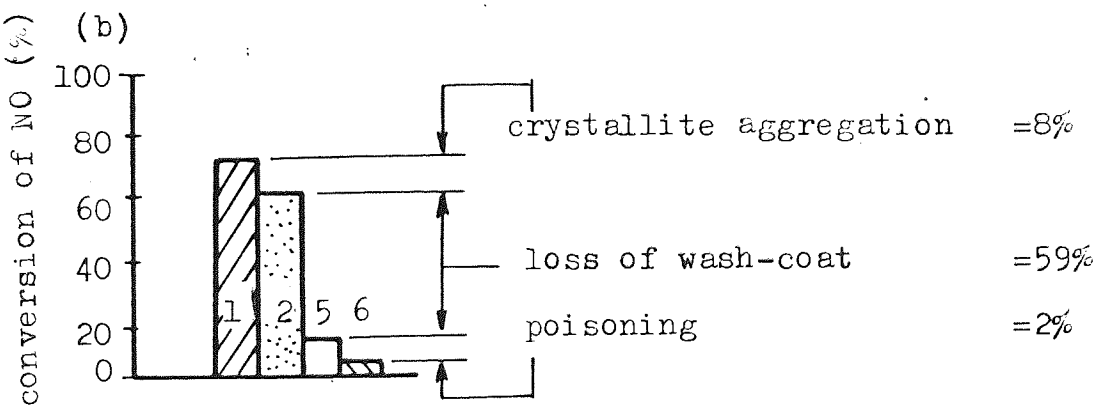

5... aged in engine for 8000Km (extrapolated to zero per cent lead from Figure 6.9

6... aged in engine for 8000Km

The loss of activity due to crystallite aggregation is apparently quite low at 650°C ; intuitively, we may suppose that the distribution of the active species will affect the rate of poisoning and as discussed above, large aggregations contribute to the break-up of the coating. This

deactivation mechanism cannot, therefore, be lightly dismissed. The overall conclusion must be that the loss of wash-coat and the associated active species is the single most significant factor in the deactivation of these base-metal catalysts, followed closely by poisoning (at a lead level of $0.013 g.L^{-1}$) and crystallite aggregation.

7. SUGGESTED IMPROVEMENTS TO THE WASH-COAT

7.1. Improved Mechanical Keying

The difference in thermal expansion coefficient (α) between the cordierite matrix (α = 1.5 x 10^{-6} per ^{o}C) and the gehlenite wash-coat (α = 8 x 10^{-6} per ^{o}C) was thought to be at least partly responsible for the high loss of material during engine-dynamometer testing. If this were so, then better mechanical keying should result in a lower rate of loss. Two ways of improving the mechanical keying are as follows : the first is to etch the surface of the matrix material and the second is to deposit a prior wash-coat of cordierite. The second alternative was considered the most attractive and ICI made up a catalyst to their standard specification except that a pre-coat of cordierite was applied before the gehlenite coating. This was then tested for 4000Km (2500 miles) in an engine-dynamometer rig along with sample which had a regular wash-coat. The results of a subsequent chemical analysis are shown in Table 7.1.

Table 7.1. : Loss of wash-coat and active species calculated from chemical analysis of matrix catalysts M8-M13

Catalyst	Type	Mean loss of active species (%)	Mean loss of wash-coat(%)
M8	+pre-coat	42	75
M9	+ " "	33	88
M10-M13	Standard	54	58

It can be seen that for the pre-coated catalysts the loss of gehlenite was far higher than the loss of active species. This was because the

active species had been impregnated uniformly throughout the double-layered wash-coat and the active species in the cordierite had not been lost. This was not the desired effect since cordierite is said to react relatively readily with nickel and copper oxides[126][127]. However, activity of these catalysts was no worse than the standard catalysts as seen in Table 7.2, and was possibly better, although the significance of the differences between results is not statistically very high because of the small number of samples.

Table 7.2. : Comparison of catalytic activity of pre-coated and standard catalysts after ageing for the equivalent of 4000Km (2500 miles) in an engine-dynamometer. Percentage conversions measured at 650°C in the standard synthetic exhaust gas

Temperature (°C)	Double-layer catalysts (mean of 4 samples)	Standard catalysts (mean of 7 samples)
650	68	50
500	26	24

7.2. An Alternative Method of Applying the Wash-Coat

Cracks have been shown to be present in the wash-coat even in the fresh condition. These cracks were formed during the drying of the aqueous slurry from which the wash-coat was deposited. In order to obtain a slurry with a suitably low viscosity, the ceramic particles would have to be completely separated from each other and encased in fluid, usually water. When this fluid was later evaporated, the shrinkage of the deposited material could give rise to tensile stresses causing the coating to rupture, thereby producing a network of cracks. These crack systems appear to be propagated by thermal

ageing as shown in Chapter 5.

The discrete "islands" formed by the crack network weakened the wash-coat considerably so that during engine testing, much of the coating, including whole "islands", was lost. By careful control of humidity and temperature the crack formation may be minimised, in fact, the controlled drying is an important part of ceramic forming processes.

A novel method of wash-coat deposition which virtually eliminated the problem of "drying" cracks was developed during the investigation. An example of the coating achieved by this method is shown in Figure 7.1. Several catalyst samples were prepared for testing by this experimental procedure[134][135][136] and subsequently tested for 4000Km (2500 miles) in an engine dynamometer. The technique was based

Figure 7.1. : Optical micrograph (with an oil immersion objective) of a polished cross-section of a catalyst prepared by the technique developed during the investigation

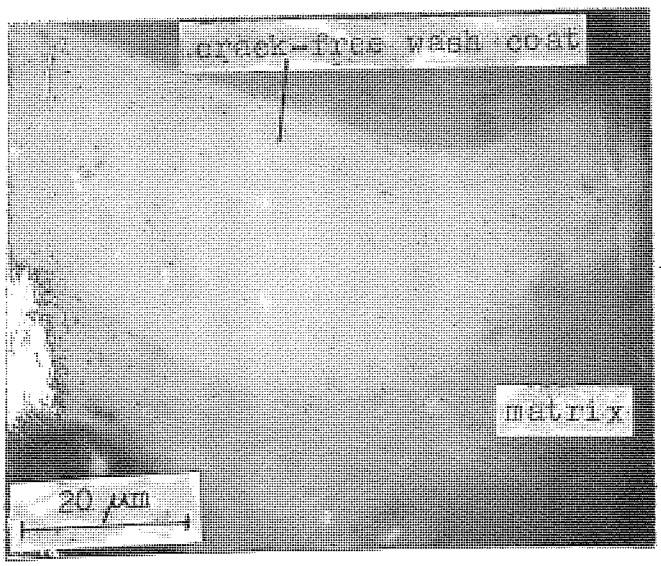

on a method of preparing thin ceramic sheet[137]. It essentially consisted of dipping the catalyst matrix into a "paint" into which the coating material is mixed as a filler. The paint was prepared by dissolving a polymer (polyvinyl butyral) with a plasticiser (di-n-butyl phthalate) in a suitable solvent (butanone) to form a pre-mix. The ratio of polyvinyl butyral to butyl phthalate was critical since this appeared to control the incidence of drying cracks. The pre-mix and wash-coat materials were then mixed and diluted with further additions of butanone, the proportions being chosen to give a viscosity of about $0.2 Ns.m^{2}$ after the addition of the filler material. The effect of "paint" composition on viscosity is shown in Figure 7.2. It can be seen that a wide choice of powder contents were possible for a given viscosity. This enabled the selection of a "paint" which would give the required deposition of wash-coat, whilst the viscosity was maintained for ease of application. The effect of paint composition on wash-coat deposition is shown in Figure 7.3, and this in turn was translated into a coating thickness by the relationship shown in Figure 7.4, which may be expressed as :

$$y = C(W/\rho) \qquad \text{.....7.1.}$$

where y is the coating thickness (μm)

W is the weight gain on deposition (%) or the wash-coat loading

ρ is the density of the coating material ($Kg.m^{-3}$)

and C is a constant dependent on the wash-coating procedure, and the geometry of the catalyst matrix.

The constant C was found to be 3.2 for the data presented in Figure 7.4 but a different, larger sample (33 specimens) gave a value of 2.6 for a number of cordierite, gehlenite and alumina coated specimens where the density of the coating material was 2.7, 3.0 and $3.9 Kg.m^{-3}$ respectively. C calculated from M1-6 was approximately 4.6. Three

Figure 7.2. : Viscosity of the "paint" mix as a function of its composition, 0.25Ns.m^{-2} is the preferred value for ease of application

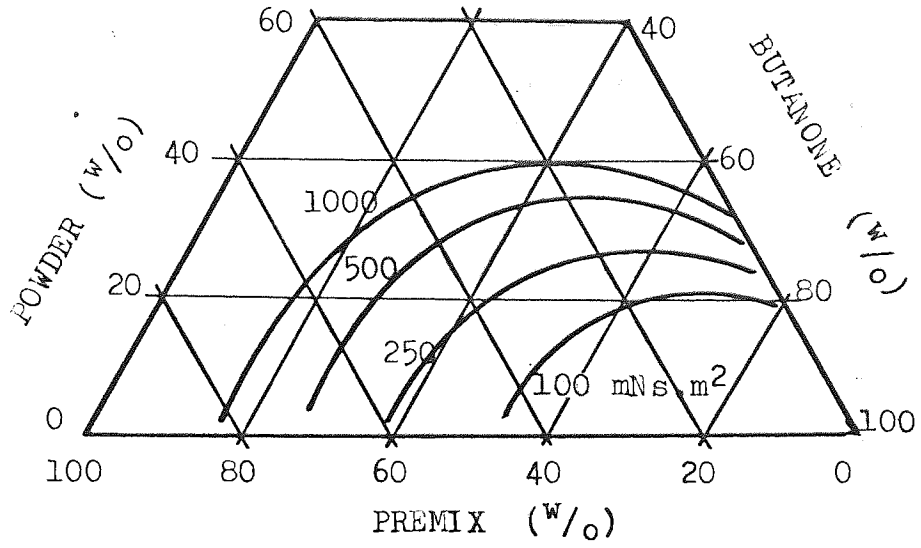

catalysts were prepared to the specifications given in Table 7.3 and nickel and copper oxides in the ratio of three to one were deposited into the wash-coat by impregnation in a 3-molar solution of their nitrates, followed by calcination in air at 500^{o}C to constant weight. The catalysts were tested in an engine dynamometer rig with promising results, as shown in Table 7.4.

Table 7.3. : The catalysts prepared using the technique for deposition of the wash-coat developed during the investigation

Catalyst	Coating material	Wash-coat loading	Thickness (μm) of coating	Concentration of active species in coating (%)
M21	Cordierite	8	10.1	51
M22	"	15	13.2	53
M23	Gehlenite	10	10.3	49

Figure 7.3. : Deposition of wash-coat as a function of the paint composition. The curves represent lines of equal wash-coat loading for a given support geometry

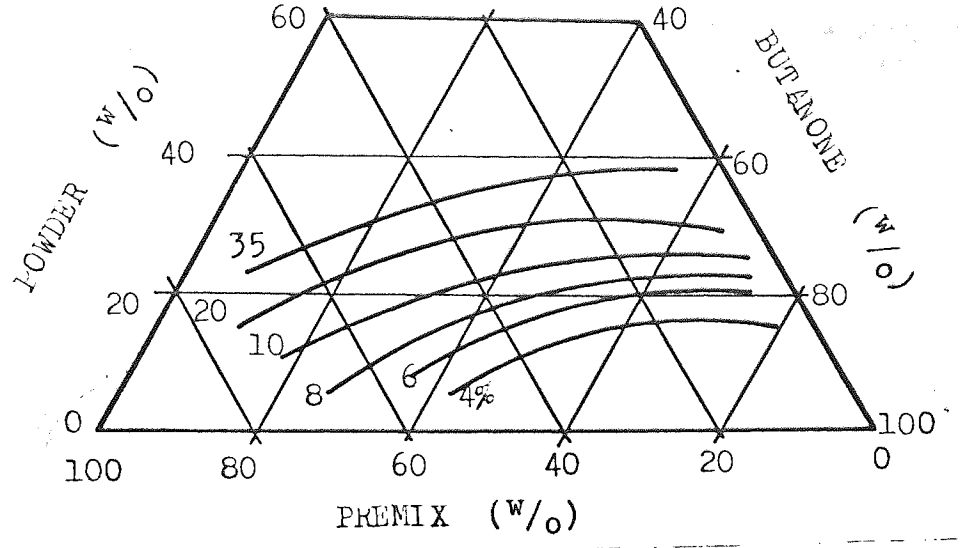

Figure 7.4. : The thickness of the wash-coat as a function of the wash-coat loading for samples prepared by the method developed during this investigation

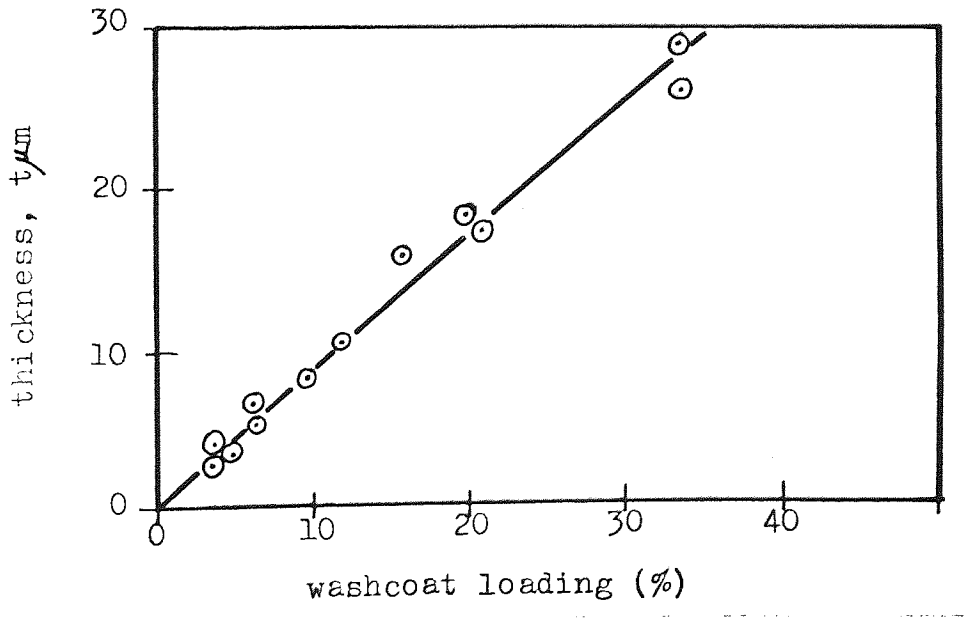

Table 7.4. : Fractional loss of wash-coat after 4000Km (2500miles) in an engine dynamometer and the fractional conversion of NO measured in the standard synthetic exhaust gas

Catalyst	Fractional loss of wash-coat and active species at inlet face(%)	Fractional conversion of NO at 650°C (%)
M21	6	72
M22	14	76
M23	8	62

The loss of wash-coat was low compared to catalysts M2-6 after 4000Km (2500 miles) in engine. However, direct comparisons are not possible because the amount of coating on M21-23 was high compared with M2-6, whilst the concentration of metal in the wash-coat was slightly low. Another feature of this deposition technique was that very little build-up of wash-coat at the matrix cell-wall corners occurred and this must have contributed to the lower observed loss of active species. Also, although M21-23 appear to have retained a higher activity, chemical analysis showed that only 0.05% of lead had been deposited during engine testing. At that level of lead, the reduction of nitric oxide extrapolated from Figure 6.9. for M2-6 was approximately 65%. This still suggests that M21-23 are slightly better especially when it is appreciated that the initial activities at 650°C of M21-23 were, on average, 7% less than the ICI catalysts. It is interesting to note that the catalysts with cordierite wash-coats retained a higher activity than those samples with a gehlenite wash-coat in view of the reported reactivity of cordierite and the metal oxides[126]. However, the cordierite powder used did have a specific surface area of $2.9 m^2.g^{-1}$ compared to $1.9 m^2.g^{-1}$ for the gehlenite.

7.3. A Mechanism for the Loss of Wash-Coat

The loss of wash-coat was proportional to the wash-coat thickness, and apparently independent of the thermal expansion coefficient suggesting that the difference in thermal expansion between wash-coat and matrix was not a major factor loading to loss. The volume change of approximately 15% that occurs with the transformation of nickel (density = 8.9Kg.m^{-3}) to nickel oxides (density = 6.7Kg.m^{-3}) has been suggested as the dominant factor leading to loss of coating, and it has been shown above that no loss occurs with zero metal loading. Consider the situation shown in Figure 7.5, the freshly sintered wash-coat is badly cracked, particularly where the coating is thickest at the cell-wall corners. In the experimental work that led up to the preparation of M21-23, it was found that no cracks were formed in the coating during sintering, even under very exacting conditions. It was inferred that they occurred in the ICI catalysts during the drying stage as mentioned above. Where the coating is relatively thin, and

Figure 7.5. : Schematic representation of a fresh wash-coat deposited from an aqueous slurry; containing drying cracks

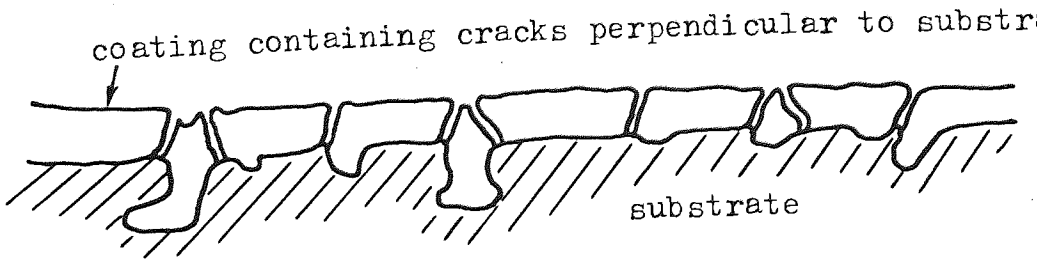

where the tensile stresses are not large enough to cause cracking, or where cracks exist, subsequent conversion of the metal to its oxide accompanied by a volume increase of 15% causes further cracks to develop. It is easily envisaged that a metal particle in a strategic position could lead to initiation of cracks in a brittle, ceramic coating. This leads to the observed development of the original crack systems.

Figure 7.6. : Optical micrograph (with an oil immersion objective) of a polished cross-section of catalyst M22 after 4000Km (2500 miles) in an engine dynamometer rig

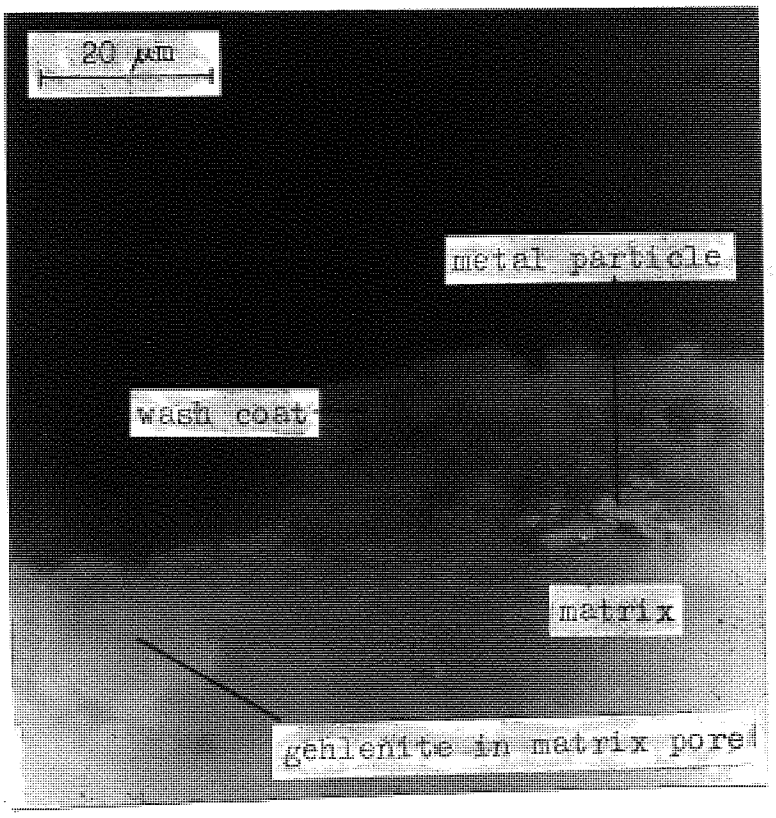

In M21-23 no cracks were observed prior to engine testing, but a different type of crack system was observed after testing. The cracks were parallel to the substrate and were often seen in association

with large metal crystallites or clusters of crystallites as shown in Figure 7.6. If it was assumed that these also occurred in catalysts M2-6, then the situation shown in Figure 7.7. would arise. These secondary cracks would interact with the original crack-system and large sections of the coating would be lost. Also, many of the discrete islands would have no mechanical keying with the substrate and be shaken loose during testing. This would leave some of the coating and some debris on the substrate as shown in Figure 7.8, which would leave the catalyst with a certain residual activity.

Figure 7.7. : Schematic representation of the interaction of the two crack systems

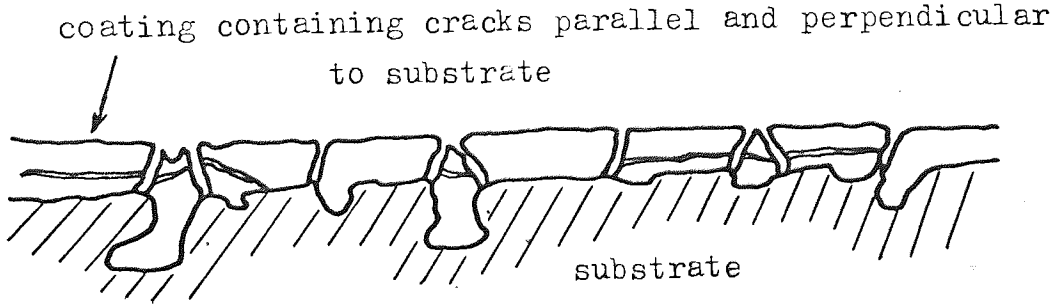

Figure 7.8. : Schematic representation of the situation after break-up of the coating

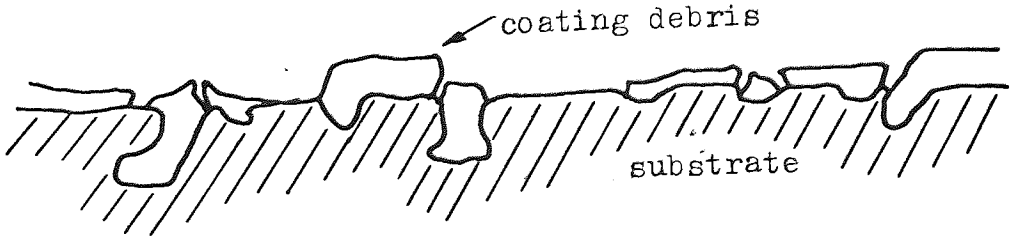

As mentioned above, the initial activities of M21-23 were probably not at their optimum, and they should be capable of improvement. One possible approach is suggested by considering the factor C in equation 7.1 for M21-23 and M2-6. The values given above were derived using the density of the coating material, whereas a better parameter would be the density of the coating itself, C should then be constant and not dependent on the method of manufacture. The coatings of M2-M6 were thicker than those on M21-23 for equivalent wash-coat loadings, as would be expected from the surface areas of the respective materials. For M2-6 the gehlenite had a surface area of $> 1 m^2.g^{-1}$, whereas for M21-23, the surface area of the gehlenite was approximately $0.5 m^2.g^{-1}$. The settling volume of a powder is proportional to its surface area, so the coating on M2-6 has a greater pore volume than that of M21-23, and should accept a greater volume percentage of active species, which was found to be so during the preparation of M21-23. The highest weight percentage of active material that could be impregnated onto M21-23 after repeated immersions in the solution of nitrates was found to be approximately 50% compared to 60-70% for the ICI-prepared catalysts.

Using techniques such as fluid-energy milling [138] it would be possible to increase the surface area of the gehlenite by at least an order of magnitude, and even incorporate the active metal oxides into a mixture with the gehlenite before coating. Ultra-fine powders are, however, susceptible to sintering and the optimum particle size must be determined experimentally, and would be a compromise between high surface area for activity and a lower surface area for stability at high temperatures.

7.4. Analysis of the Loss of Coating and Active Species

The broad scope of the project has resulted in a limited amount of experimental data, particularly concerning the coatings from the "butvar paint" mixes. The samples on one engine test were, unfortunately, completely destroyed by melting, possibly due to a mis-fire, which left only twenty-four samples, eight each of three different catalysts (M21-23) but only two of each at the inlet face of the carrier block. A photograph of the failed test is shown in Figure 7.9. Comparison of the loss of coating and active species between these and M1-6 could not, therefore, be rigorous. However, by inspection in a binocular optical microscope, M21-23 had retained more of their coating.

Analysis of the limited data by multiple regression suggested an empirical relationship of the form :

$$\text{Log } L = GM(\text{Log}W) \qquad \ldots\ldots\ldots 7.2.$$

where L is the functional loss of active species (%)
W is the wash-coat loading (%)
M is the concentration of metal in the wash-coat (%)
G is the material loss coefficient, dependent on coating technique.

The constant G for M1-6 after 4000 and 8000Km (2500 and 5000 miles) and for M21-23 after 4000Km (2500 miles) is given in Table 7.5. The thickness of the coating should be used in preference to its weight percentage, but the amount of data available does not warrant any further refinement of the analysis. The difficulty arises because the coating builds up at the cell-wall corners to an extent, dependent

Figure 7.9. : The molten remains of the catalyst samples after a mis-fire during engine testing

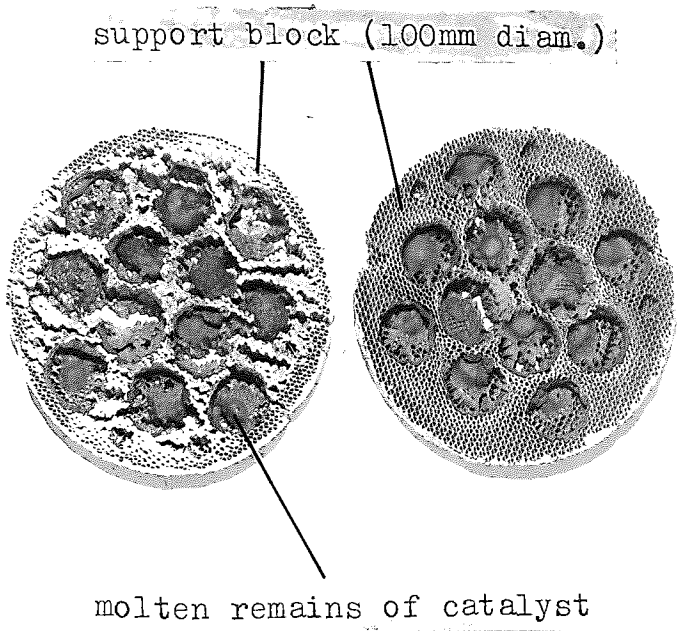

upon the coating process. Thus two parameters are accounted for by the constant G in conjunction with the weight per cent of the coating. Equation 7.2 was then used to construct the curves in Figures 7.10 and 7.11 where the experimental values are included for comparison.

Table 7.5. : The value of the material loss coefficient, G, for the available data

Data set	G
M1-6 (4000Km)	0.028
M1-6 (8000Km)	0.029
M21-23 (4000Km)	0.018

Since little indication of experimental error was available, the fit of equation 7.2 to the data was accepted, and values of loss of active species for catalysts based on the formulation of M21-23 were calculated, using G = 0.028, and these are shown in Table 7.6 together with the experimental and predicted results (G = 0.018).

Table 7.6. : Comparison of the fractional loss of active species from M21-23 (M = 50%) with the loss predicted for similar samples based on the data from M1-6

Wash-coat loading (%)	Observed fractional loss of wash-coat (%)	Predicted loss (%), G= 0.018	Predicted loss (%), G= 0.028
8	6	6.7	18
10	8	8.3	25
15	14	12	44

Figure 7.10 : The relationship between the initial amount of wash-coat (or thickness) and loss of active species after 4000Km (2500 miles) as indicated by equation 7.2.

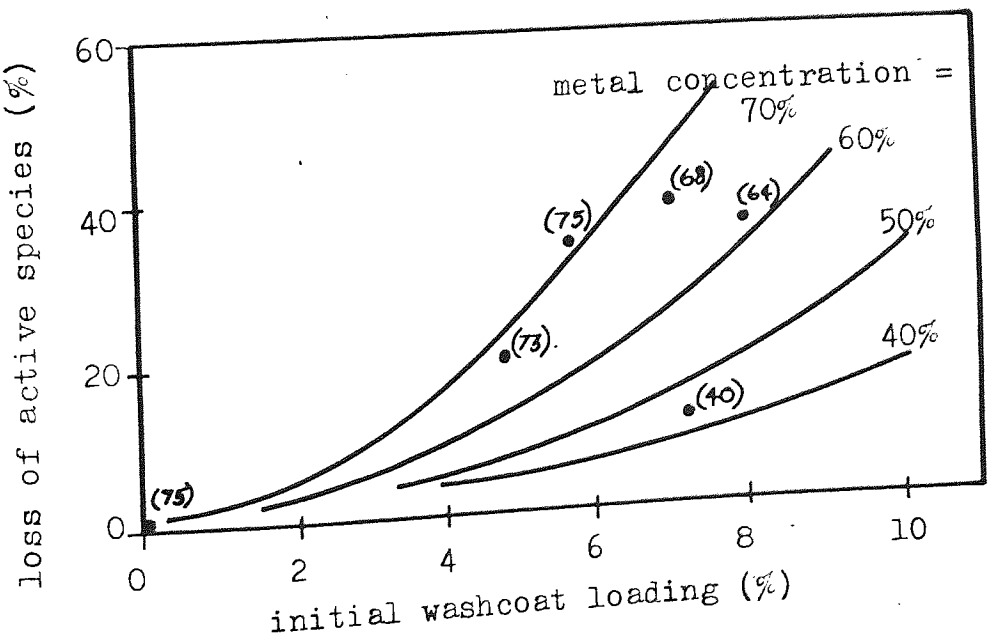

Figure 7.11. : The relationship between the initial amount of wash-coat (or thickness) and loss of active species after 8000Km (5000 miles) as indicated by equation 7.2.

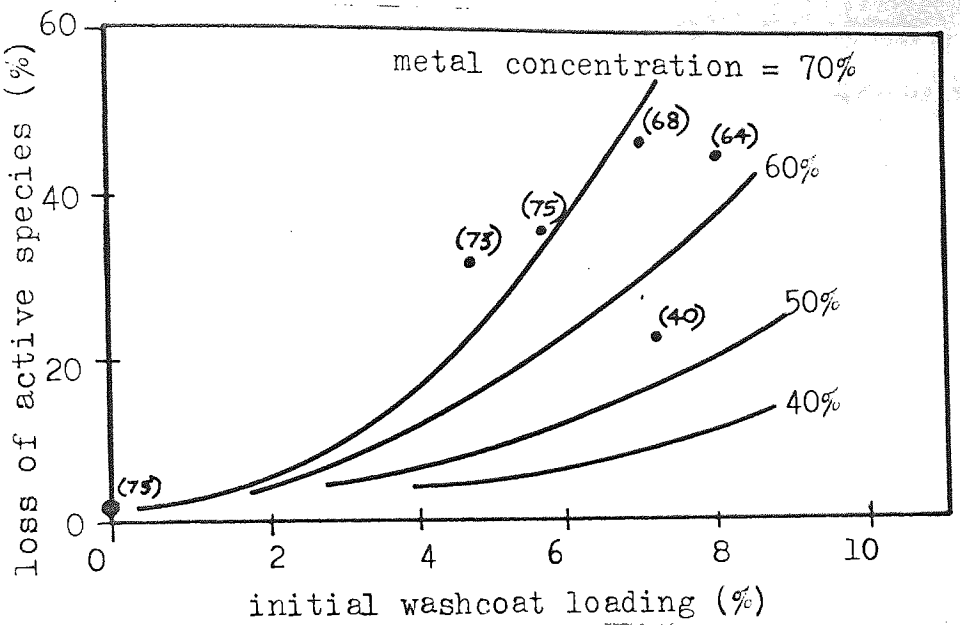

The relationship in equation 7.2. may be used to predict the loss from M21-23 accurately. The predicted loss for similar catalysts prepared by the aqueous technique was three times that observed for M21-23 which, it is suggested, is a significant difference. It was therefore concluded that the process developed produces a wash-coat which is more resistant to mechanical failure and subsequent loss of active species than the accepted technique.

8. CONCLUSIONS

The chief cause of the deactivation of these nickel-copper supported catalysts has been found to be the loss of the wash-coat and the associated active species. For example, after 8000Km (5000 miles) it was found to account for a decrease of more than one-half of the initial activity of the catalyst. This was approximately three times greater than the decrease attributable to all the other main contributory factors such as poisoning and metal crystallite aggregation.

The loss of wash-coat was found to occur by a combination of factors. The original coating was under a tensile stress due to shrinkage during the drying stage in manufacture, and this led to the formation of a system of cracks which separated the coating into many discrete islands, as shown in Chapers 2 and 6. Some of these islands were not mechanically keyed to the substrate and so were readily removed by the exhaust gases. In other islands, aggregation of the metal crystallites was followed by re-oxidation upon cooling, with an accompanying volume change of approximately 15% ; this led to a further system of cracks developing and many of these cracks were in a plane at right-angles to the cracks produced during manufacture. Thus, large sections of the coating were lost where these crack systems intersected. The relationship between the loss of wash-coat (L), the wash-coat loading (W) and the concentration of active metal in the wash-coat (M) was described by the empirical formula :

$$\text{Log } L = GM(\text{Log } W)$$

In the opinion of the author, these drying cracks could be eliminated by depositing the wash-coat from an organic "paint-mix", with the powdered coating material as a filler in the paint. This was shown in Chapter 7 to produce essentially crack-free coatings, and also to avoid the heavy build-up of material at the corners of the cell walls in the substrate. The thickness of the coating may easily be controlled by this technique by varying the concentration of powder to organic material, and the technique will work with a range of materials and particle sizes.

Encouraging results from initial engine tests suggest that improved catalysts can be prepared by optimising parameters such as the specific surface area of the coating and the distribution of the active species to increase the initial efficiency of the catalysts.

By using sophisticated comminution techniques such as fluid-energy milling, very fine powders or mixtures of powders could be produced, and therefore it would be possible to put down the wash-coat and active species in one operation since the nitrates, or other precursors, would be insoluble in the organic solvents.

Crystallite aggregation does not itself contribute greatly to the reduction in efficiency of these catalysts during service, but their tolerance to poisoning by fuel additives would depend, to an as yet undetermined degree, on the available catalytically active surface area, in other words, the metal surface area. Crystallite aggregation of supported nickel-copper catalysts was, as expected, found to be

dependent upon temperature and, to a lesser extent, time, and the relationship was shown in Chapter 4 to be described by the empirical relationship :

$$D^n - D_o^n = K_1 t$$

where n is in some way related to the diffusion mechanism and K_1 is dependent on temperature. The rate of aggregation was not affected by the ratio of nickel to copper, or by the concentration of total metal species over the range of from 5% to 50% by weight in the coating.

REFERENCES

1. Haagen-Smit, A.J. Ind. Eng. Chem. 44 (6), 1342 (1952).

2. Patterson, D.J. and Henein, N.A. (Ch.1), Emissions from Combustion Engines and their Control. Ann Arbor Science Pub. Inc. (1972).

3. Pitts, J.M., J. Air Polltn. Control Assoc. 19,658 (1969).

4. Williamson, S.J. (Ch.10), Fundamentals of Air Pollution, Addison-Wesley (1972).

5. Eyzat, P. and Guibet, J.C., S.A.E. Preprint 680124 (1968).

6. Schuck, E.A. and Stephens, E.R. in Advances in Environmental Sciences, vol.1, p.73. Ed. Pitts, J.N. and Metcalf, R.L. New York : Wiley Interscience (1969).

7. Hottel, H.C. and Eberhardt, J.E., 2nd. Symposium on Combustion, 1937, The Combustion Institute, p.235.

8. Fennimore, C.P., 13th. Symposium (International) on Combustion, Salt Lake City (1970).

9. Newhall, H.K. and Shahed, S.M. 13th. Symposium (International) on Combustion, Salt Lake City (1970).

10. Lavoie, F.A., Heywood, J.B. and Keck, J.C., Combust. Sci. Technol. 1, 313, (1970).

11. Newhall, H.K. and Starkman, E.S., S.A.E. Publication PT-14, 214, (1967-70).

12. Obert, E.F., Internal Combustion Engines, 3rd. ed. (Scranton,Pa : International Textbook Co, 1968) p.204.

13. Schuck, E.A. and Stephens, E.R., Oxides of Nitrogen, in Advances in Environmental Sciences, vol.1, Ed. Pitts, J.N. and Metcalf, R.L., New York : Wiley Interscience, 1969 p. 73.

14. Haagen-Smit, A.J., Reactions in the Atmosphere, in Air Pollution, vol.1, Ed. Stern, A.C., New York : Academic Press,1962.

15. Renzetti, N.A. and Doyle, D.J. Intern. J. Air Poll. (London), 2, 327, 1960.

16. Caplan, J.D., S.A.E. Journal 73 (12), 62, (1965).

17. Goldsmith, J.R., Effects of Air Pollution on Human Health, p.547 in Air Pollution, vol.1, Ed. Stern, A.C., New York : Academic Press, 1968.

18. Stokinger, H.E. and Coffin, D.L., Biological Effects of Air Pollutants, p.446 in Air Pollution, vol.1, Ed. Stern, A.C., New York : Academic Press, 1968.

19. Romanovsky, J.C., J. Air Polltn. Control Assoc., 17 (7), 454 (1967).

20. Agnew, W.G., Proc. Royal Soc., 307A, 153 (1968).

21. Barth, D.S., Romanovsky, J.C., Schuck, E.A. and Cernansky, N.P., J. Air Polltn. Control Assoc., 20 (8), 519 (1970).

22. U.S. Federal Register, 35, (214) (1970).

23. Houdry, E.J., Advances in Catalysis, 9, 499 (1957).

24. U.S. Federal Register, 41, (250) (1976).

25. E.C.E. Regulation 15/03, Exhaust Emissions, Petrol Engined Vehicles, 1 October 1979.

26. Californian Institute, Jet Propulsion Laboratory, Tech. Report No. JPL/SP/43-17, March 1976.

27. Nicholls, J.E., S.A.E. Preprint, 690018 (1969).

28. Benson, J.D., S.A.E. Preprint, 690019 (1969).

29. Rudham, R. and Sanders, M.K., in Chemisorption and Catalysis, Ed. Hepple, P., p.58, Inst. of Petroleum, (1970).

30. Winter, E.R.S., J. Catalysis, 22, 158 (1971).

31. Amirazmi, A. Benson, J.E. and Boudart, M.,J. Catalysis 30, 55 (1) (1973).

32. Baker, K.A. and Doerr, R.C., J. Air Polltn. Control Assoc. 14, 409 (1964).

33. Ayen, R.F. and Ng, Y.S., Int. J. Air Water Poll., 10, 1, (1966).

34. Meguerian, G.H., Rakowsky, F.W., Hirshberg, E.H., Lang, C.R. and Schock, D.N., S.A.E. Preprint, 720480, (1972).

35. Bernhardt, W.E. and Hoffman, E., S.A.E. Preprint, 720481, (1972).

36. Sourirajan, S., and Blumenthal, J.L., Int.J. Air Water Poll. (Oxford), 5, 24, (1961).

37. Meguerian, G.H. and Lang, C.R., S.A.E. Preprint, 710291, (1971).

38. Bentley, D.R. and Schweibold, D.J., S.A.E. Preprint, 730227,(1973).

39. Meguerian, G.H. and Roakowsky, F.W., S.A.E. Preprint, 750417, (1975).

40. Goodell, P.D., Kane, R.H. and Tufnell, G.W., S.A.E. Preprint, 760318, (1976).

41. Zechnall, R., Banmann, G. and Eisele, H., S.A.E. Preprint, 730566, (1973).

42. Tien, T.Y., Stadler, H.L., Gibbon, E.F. and Zachmanidis, P.J., Ceramic Bulletin, 54 (3), 280 (1975).

43. Dreker, H., Friese, R. and Haeker, W., S.A.E. Preprint, 750223, (1975).

44. Harned, J.L. and Montgomery, D.L., S.A.E. Preprint, 730561, (1973).

45. Briggs, W.S. and Graham, J.R., S.A.E. Preprint, 730275 (1973).

46. Bagley, R.D., Doman, R.C., Duke, D.A. and McNally, R.N., S.A.E. Reprint, 730274, (1973).

47. Bernstein, L.S., Lang, R.J., Lunt, R.S. and Musser, G.S., S.A.E. Preprint, 730567, (1973).

48. Taylor, K.C. and Klimish, R.L., J. Catalysis, 30, 478 (1973).

49. Shelef, M., Catalysis Reviews in Science and Engineering, 11 (1), 1-40, (1975).

50. Shelef, M. and Ganghi, H.S., Ind. Eng. Chem. Prod. Res. Devel., 11, 2, (1972).

51. Andrew, S.P.S., Trans. Inst. Chem. Eng., 54, 196, (1976).

52. Klimish, R.L. and Barnes, G.J., Envir.Sci. Technol. 6, 543, (1972).

53. Shelef, M. and Gandhi, H.S. Ind.Eng.Chem.Prod.Res. Devel. 13, 18, (1974).

54. Klimish, R.L. and Taylor, K.C., Envir.Sci. Techol. 7, 127, (1973).

55. Kobylinski, R.P. and Taylor, B.W., J. Catalysis, 31, 450 (1973).

56. Haseba, S. Shimose, T., Kubo, N. and Kitagawa, T., Chem. Eng. Progr. 62, 92, (1966).

57. Shelef, M. and Gandhi, H.S., Ind.Eng.Chem.Prod.Res.Devel., 11, 393, (1972).

58. Otto, K. and Shelef, M., J.Phy.Chem. 85, 308, (1973).

59. Otto, K. and Shelef, M., J. Phy.Chem. 74, 2690, (1970).

60. Otto, K. and Shelef, M., J. Phy.Chem. 76, 37, (1972).

61. Unland, M.L., J. Phy.Chem. 77 (16), 1952 (1973).

62. Unland, M.L., Science, 179, 567, (1973).

63. Voorhoeve, R.J.H., J. Catalysis, 45, 297, (1976).

64. Bell, W.E. and Tagami, M., J. Phy.Chem., 67, 2432, (1963).

65. Shelef, M. and Gandhi, H.S., Plat. Metals Review, 18, 2, (1974).

66. Kobylinski, T.P., Taylor, B.W. and Young, J.E., S.A.E.Preprint, 740250, (1974).

67. Kingery, W.D., Introduction to Ceramics, John Wiley & Sons Inc. (1960), p.118.

68. Voorhoeve, R.J.H., Remeika, J.P. and Trimble, L.E., Mater. Res. Bull., 9, 1393, (1974).

69. Clauser, C.A., and Good,, M.L., J. Catalysis, 46, 58 (1977).

70, Bauerle, G.L., Pinkerton, J.D. and Nobe, K., Atm. Envir., 8. 217, (1974).

71. Libby, W.F., Science, 171, 499, (1971).

72. Meadowcroft, D.M., Nature, 226, 847, (1970).

73. Chien, M.W., Pearson, M. and Nobe, K., Ind.Eng.Chem.Prod. Res. Devel., 14, (2), 131, (1975).

74. Bauerle, G.L. and Nobe, K., Final report proj. ARB No. 2-009-1, Report No. ARB-R-PCA 189-73-02, (1973), UCLA - ENG-7371 School Eng. App. Sci. UCLA.

75. Shoup, R.D., Hoekstra, K.E., andFarrauto, R.J., Ceramic Bulletin, 54, (6), 565, (1975).

76. Kibby, C.L., J. Catalysis, 42, (3), 350, (1976).

77, Shelef, M. and Kummer, J.T., Proc. 62nd. Annual Meeting, A.I.Ch.E. Washington, 1967.

78. Meguerian, G.H., and Lang, C.R., S.A.E.Preprint, 710291, (1971).

79. Meguerian, G.H., Rakowsky, F.W., Hirschberg, E.H. and Lang, C.R. S.A.E.Preprint, 720840, (1972).

80. Lunt, R.S.,Bernstein, L.S., Hansel, J.G. and Holt, E.L., S.A.E. Preprint, 720209 (1972).

81. Movikawa, K., Shivasaki, T. and Okada, M., Adv. in Catalysis, 20, 97-133, (1969).

82. Bernstein, L.S., Kearby, K.K., Raman, A.K.S., Vardi, J. and Wigg, E.E., S.A.E.Preprint, 710014, (1974).

83. Bauerle, G.L., Sorenson, L.L.C., and Nobe, K., Ind.Eng.Chem.Prod. Res.Devel., 13, (1), 61, (1974).

84. Bauerle, G.L. and Nobe, K., Ind.Eng.Chem.Prod.Res.Devel., 13, (3), 185 (1974).

85. Davies, P., Internal Report, ICI Ltd. RD/CC 177/A (Oct.1972).

86. Davies, P., Internal Report, ICI Ltd. RD/CC 173/A (Nov.1973).

87. Ponec, S.K., Catal.Rev.Sci.Eng., 11 (1), 41, (1975).

88. Federal Register, 37, (36), Feb.23 (1972).

89. Bomback, J.L., Wheeler, M.A., Tabock, J. and Janowski, J.D., Envir.Sci. Technol., 9 (2), 139, (1975).

90. Ashmead, D.R., Summary of ICI internal report sent to BL, 1973.

91. Jackson, H.R., McArthur, D.P., and Simpson, H.D., S.A.E. Reprint, 730568, (1973).

92. Ashmead, D.R., Campbell, J.S., Davies, P. and Farmery, K., S.A.E. Preprint, 740249, (1974).

93. Roth, J.F., Ind.Eng.Chem.Prod.Res.Devel., 10, 381, (1971).

94. Ries, H.E., Advan. Catal. 4, 87, (1952).

95. Williams, A., Butler, G.A. and Hammonds, J., J. Catalysis, 24, 352, (1972).

96. Carlson, D.W., Morgan, C.R., and Voltz, S.E., S.A.E.Preprint, 730569, (1973).

97. Liedermann, D., Voltz, S.E. and Snyder, P.W., Ind.Eng.Chem.Prod. Res.Devel., 13, 166 (1974).

98. Dalla Betta, R.A. and McCune, R.C., Ind.Eng.Chem.Prod.Res.Devel. 15, 169 (1976).

99. Wanke, S.E. and Flynn, P.C., Catal.Rev.Sci.Eng., 12 (1), 93,(1975)

100. Baker, R.T.K., and France, J.A., J. Catalysis, 39, 481 (1975).

101. Huang, F.H. and Li, C., Sci. Metall. 7, 1239, (1973).

102. Gruber, H.L., J.Phy.Chem. 66, 48 (1962).

103. Gruber, H.L., Anal.Chem. 34, 1828 (1962).

104. Flynn, P.C. and Wanke, S.E., J. Catal. 37, 432, (1975).

105. Hughes, T.R., Houston, R.J. and Sieg, R.P., Ind.Eng.Chem.Prod. Res.Devel. 1, 96, (1962).

106. Van Hardeveld, R. and Van Montfort, A., Surface Sci., 4, 396 (1966).

107. Carter, J.L., Cusumano, J.A. and Sinfelt, J.H., J.Phy.Chem. 70, 2257, (1968).

108. Williams, A., Butler, G.A., Hammond, J., J. Catal. 24, 352 (1972)

109. Shephard, F.E., J. Catal. 14, 148, (1969).

110. Robertson, J. Catal. 39, 234, (1975).

111. Allred, V.D., Buxton, S.R. and McBride, J.P., J. Phy.Chem., 61, 117 (1957).

112. Anderson, P.J. and Morgan, P.L., Trans.Far.Soc., 60, 930, (1964).

113. Chakraverty, B.K., J. Phy.Chem. Solids, 28, 2401, (1967).

114. Wynblatt, P. and Gjostein, N.A., Scr.Metall., 7, 969, (1973).

115. Reckenstein, E., and Pulvermacher, B., A.I.Ch.E. J. 19, 356, (1973).

116. Ruckenstein, E. and Pulvermacher, B., J. Catal. 29, 224 (1973).

117. Flynn, P.C. and Wanke, S.E., J. Catal. 34, 390 (1974).

118. Flynn, P.C. and Wanke, S.E., J. Catal. 34, 400, (1974).

119. Ruckenstein, E. and Malhotra, M.L., J. Catal. 41, 303 (1976).

120. Granquist, C.G. and Buhrmann, R.A., App. Phy. Lett., 27, 693, (1976).

121. Granquist, C.G. and Buhrmann, R.A., J. Catal. 42, 477 (1976).

122. Wanke, S.E., J. Catal. 46, 234, (1977).

123. Lean, J.P.M. and Haynes, C.D., Internal Report, BL Cars, Advanced Technology, No. ETR 3022 (Nov. 1975).

124. Haynes, C.D. and Lean, J.P.M., Internal Report, BL Cars, Advanced Technology, No. ETR 3043 (Aug. 1976).

125. Davies, P., Personal communication, (March 1975).

126. Confidential reports to ICI Ltd. of work carried out by British Ceramic Research Assoc. (1973).

127. Henney, J.W. and Wilkes, R.S., G198, Confidential Report to ICI Ltd. of work carried out at Materials Dev. Div., UKAEA, AERE, Harwell, (1973).

128. Pilliar, R.M. and Nutting, J., Phil. Mag. 16, 181 (1967).

129. Davis, J.E., Carrithers, V.G. and Watson, D.R., Bull. Amer. Cer. Soc. 50, 906-912, (1971).

130. Dyhouse, J.R. and Winfield, P.H., BL Cars, Adv.Tech. Internal Report no. ETR 3084 (MG/R-118) (Oct. 1977).

131. Selwood, P.M., Adler, S. and Phillips, J., J. Amer.Chem.Soc., 77, 1462, (1955).

132. Roman, A., and Delmon, B., J. Catal. 30, 333 (1973).

133. Wheeler, A., Advanced Catal., 3, 249, (1951).

134. Dyhouse, J.R. and Vas, M., BL Cars, Adv. Tach. Int. Report no. ETR 3088 (MG/R-118) (Nov. 1977).

135. Dyhouse, J.R. and Sayed, A.T., BL Cars Adv.Tech. Int. Report no. ETR 3089 (MG/R-119) (Nov. 1977).

136. Dyhouse, J.R. and Sayed, A.T., BL Cars Adv.Tech.Int. Report no. ETR 3120 (MG/R-136) (March 1978).

137. Brit. Pat. Spec.,no. 12, 8551 (July, 1971).

138. Dobson, B. and Rothwell, E., Powder Tech., 3, 213, (1969).